Fyn-mediated phosphorylation of Menin disrupts telomere maintenance in stem cells

Souren Paul[1*], Preston M. McCourt[1], Le Thi My Le[1], Joohyun Ryu[1], Wioletta Czaja[1,2], Ann M.

Bode[1], Rafael Contreras-Galindo[1,2*], Zigang Dong[3*]

[1]The Hormel Institute, University of Minnesota, 801 16th Avenue NE, Austin, MN 55912, USA

[2]Department of Genetics, University of Alabama, Birmingham, AL 35294, USA.

[3]Department of Pathophysiology, School of Basic Medical Sciences, College of Medicine, Zhengzhou University, Henan, China 450001

***Correspondence to:**

Souren Paul

The Hormel Institute

University of Minnesota, Austin, MN, 55912, USA

Tel#: (507) 355-5241

Fax#: (507) 437-9606

E-mail: paulx215@umn.edu

Rafael Contreras-Galindo

The Hormel Institute

University of Minnesota, Austin, MN, 55912, USA

Tel#: (507) 437-9641

Fax#: (507) 437-9606

E-mail: rcontrer@umn.edu

Zigang Dong

Zhengzhou University, Zhengzhou, Henan, 450001, China.

Phone: 371-6665-8803; Fax: 507-437-9606.

E-mail: dongzg@zzu.edu.cn

Abstract

Telomeres protect chromosome ends and determine the replication potential of dividing cells. The canonical telomere sequence TTAGGG is synthesized by telomerase holoenzyme, which maintains telomere length in proliferative stem cells. Although the core components of telomerase are well-defined, mechanisms of telomerase regulation are still under investigation. We report a novel role for the Src family kinase Fyn, which disrupts telomere maintenance in stem cells by phosphorylating the scaffold protein Menin. Fyn phosphorylates Menin at tyrosine 603 (Y603), which increases Menin's SUMO1 modification, C-terminal stability, and importantly, its association with the telomerase RNA component (TR). We show that SUMO1-Menin decreases TR's association with telomerase subunit Dyskerin, suggesting that Fyn's phosphorylation of Menin induces telomerase subunit mislocalization and may compromise telomerase function at telomeres. Importantly, we find that Fyn inhibition reduces accelerated telomere shortening in human iPSCs harboring mutations for dyskeratosis congenita.

Key Words:

Fyn; Telomere; Menin; Stem cells; Dyskeratosis Congenita

Introduction

Telomeres, regions of TTAGGG repeats at the ends of the chromosomes, shrink in somatic cells during cell replication [1]. Telomere shortening can be counteracted by telomerase holoenzyme, a ribonucleoprotein that maintains telomere length by synthesizing telomeric DNA [2]. Although telomerase activity is greatly reduced in somatic cells, it is upregulated in stem cells that undergo rapid expansion [3]. In telomere biology disorders (TBD) such as dyskeratosis congenita, telomere maintenance is defective, which often causes bone marrow failure due to accelerated telomere shortening in hematopoietic stem cells [4]. Aberrant telomere maintenance in dyskeratosis congenita is most frequently a consequence of mutations in telomerase holoenzyme or shelterin complex components [5]. Currently, there is no specific treatment for TBD and transplantation comes with great risk and poses a number of challenges [6].

Endogenous telomere maintenance is modulated by many methods, including transcriptional regulation of the telomerase RNA component (TR) and telomerase reverse transcriptase (TERT), post-translational regulation of TERT, and telomerase recruitment and assembly [7]. Little is known about the role that kinases play in telomere maintenance, although previous studies showed that ATM and ATR are positive regulators of telomere length [8, 9].

Fyn is a non-receptor Src family tyrosine protein kinase that phosphorylates multiple substrates and regulates many critical biological processes, including cell growth and survival [10, 11]. Previous studies showed that Src family kinase inhibition prevents stem cell differentiation [12, 13]. Here, we describe a critical role for Fyn, which negatively regulates telomere length in mammalian stem cells. We determined that genetic or pharmacological suppression of Fyn stabilizes telomere length in mouse and human stem cells. We also found that

post-translational modifications of Menin, a novel Fyn phosphorylation substrate, play crucial roles in Fyn-mediated telomere erosion. Named for its role in multiple endocrine neoplasia type 1 (MEN1) syndrome, Menin is a scaffold protein that regulates gene expression, interacts with multiple signaling pathways, and can act as a cancer suppressor or promoter depending on the context [14]. A previous study found that Menin localizes to telomeres in meiotic cells but does not directly interfere with telomerase activity in carcinoid cells [15]. Here we show that Fyn promotes Menin localization to telomeres in mouse embryonic stem cells (mESCs) and that Fyn does not modulate telomerase activity using *in vitro* assays. We also show that Menin is phosphorylated by Fyn at Y603 promoting phosphorylation-dependent SUMO1 modification at its C-terminal region. Importantly, we demonstrate that SUMO1-modified Menin has greater stability and increased affinity for TR, which disrupts TR's association with the telomerase subunit Dyskerin likely after telomerase assembly. These results suggest that SUMO1-modified Menin induces telomerase subunit mislocalization and may compromise telomerase activity. Thus, Fyn may act as a negative regulator of telomere maintenance by phosphorylating and promoting stable SUMO1-modification of Menin. We further demonstrate that Fyn knockout prevents accelerated telomere erosion in DC patient iPSCs that harbour a mutation in DKC1. Our findings indicate that Fyn inhibitors may be a viable therapeutic intervention for patients with TBD.

Results

Fyn inhibition slows telomere erosion in mice and stem cells

We previously found that Fyn$^{-/-}$ mice produced larger and greater number of tumors after induction of skin carcinogenesis [10]. Other studies have focused on the role of Fyn in stem cell differentiation, finding that Src family kinase inhibition prevented stem cell differentiation [12,13]. Given that telomere maintenance is a critical component of both cancer and stem cell proliferation, we were curious to see how the absence of Fyn affected telomere length in Fyn$^{-/-}$ mouse tissue and stem cells. In a pilot study, we found that 43-week-old Fyn$^{-/-}$ female mice (n=4) exhibited greater telomere length in colon, liver, and skin tissues compared to WT mice, while centromere length was unchanged (Figs. EV1-EV6). We previously demonstrated that centromere size does not change with cell passaging [16]. Therefore, we used centromere Q-FISH as a baseline control. Representative Q-FISH images (Figs. EV1, EV3, EV5) and frequency distribution of mean fluorescence with detailed statistics (Figs. EV2A, B; EV4A, B; EV6A, B) from these images show longer telomere length in Fyn$^{-/-}$ mouse colon, liver, and skin tissues compared to WT. Statistical analysis showed a significantly higher telomere mean fluorescence (Figs. EV2C, EV4C, EV6C), but no significant difference was noted when centromere mean fluorescence was compared (Figs. EV2D, EV4D, EV6D) between WT and Fyn$^{-/-}$ mouse tissues. The telomere/centromere mean fluorescence ratio was also significantly higher in Fyn$^{-/-}$ mouse compared to WT (Figs. EV2E, EV4E, EV6E) in colon, liver, and skin. As previous reports showed that skin and gastrointestinal tract tissues are excellent sources of stem cells [17,18], we hypothesized that Fyn may negatively regulate telomere length in stem cells.

We tested this hypothesis in mESCs obtained from WT and Fyn$^{-/-}$ blastocysts (Fig. 1A, C, and Figs. EV7A- EV7G). Fyn knockout was confirmed by western blot (Fig. 1C). Q-FISH analysis showed that telomeres in Fyn$^{-/-}$ stem cells are indeed longer than telomeres in WT stem cell metaphase spreads (Fig. 1A) or interphase nuclei (Figs. EV7E-EV7F) at passage 12. We also

performed Fyn knockdown in ES-E14TG2a (E14) mESCs using sh-RNA and confirmed knockdown by western blot (Fig. 1D). Sh-Fyn cells showed greater telomere length compared to sh-Mock cells (Fig. 1B, and Figs. EV7E, EV7G) at passage 18.

We used qRT-PCR and Flow-FISH to further confirm that $Fyn^{-/-}$ ES cells and Fyn knockdown E14 cells have greater telomere length (Figs. EV8A-EV8D). The mean telomere fluorescence value was higher in Fyn-deficient ES cells than WT ES cells or mock-infected cells as determined by Flow-FISH (Figs. EV8A and EV8C). A significantly higher telomere to single copy gene ratio (T/S) was observed in $Fyn^{-/-}$ ES cells (Fig. EV8B) and Fyn knockdown E14 cells (Fig. EV8D) compared to WT ES cells and sh-mock cells, respectively. Notably, stable overexpression of the *Fyn* gene in sh-Fyn E14 cells (Figs. EV8E-EV8H) significantly reduced telomere FISH signals as compared to sh-Fyn cells (Figs. EV8E, EV8H), suggesting that the level of active Fyn imposes a negative impact on telomeres.

We also investigated whether $Fyn^{-/-}$ mice had longer telomeres than WT mice at old age. Genotyping, IHC analysis and quantification of IHC confirmed Fyn knockout in colon and skin tissues of 97-week-old $Fyn^{-/-}$ mice (Figs. EV9A-EV9F). Q-FISH analysis showed that telomere length in $Fyn^{-/-}$ mice was significantly greater in both male and female mice compared to WT mice (Fig. 1E, F).

Moreover, Telomere Molecular Combing Assay (TMCA) results strengthen our observation that Fyn inhibition promotes telomere maintenance in stem cells (Fig. 2). The TMCA shows that $Fyn^{-/-}$ mESCs DNA fibers have greater telomere length compared to WT mESCs DNA fibers (Fig. 2A, B, C). Detailed statistical analysis from the telomere signals shows that mean and median telomere sizes were 39.0811 kb and 43.8300 kb, respectively, in $Fyn^{-/-}$ mESCs compared to WT mESCs, which shows that mean and median telomere sizes were

27.8796 kb and 23.8800 kb, respectively (Fig. 2A, B). A comparative statistical analysis shows significantly longer absolute telomere length in Fyn$^{-/-}$ mESCs compared to WT mESCs (Fig. 2C). Similarly, Sh-Fyn stable E14 stem cells show mean and median telomere sizes of 61.2999 kb and 33.6950 kb, respectively, compared to Sh-Mock, which shows mean and median telomere sizes of 50.4590 kb and 12.0150 kb, respectively (Fig. 2D, E). Comparative statistical analysis also shows significantly greater absolute telomere length in Sh-Fyn cells compared to Sh-Mock cells (Fig. 2F). Taken together, these results indicate that Fyn is a negative regulator of mammalian telomere length in stem cells.

Fyn does not inhibit telomerase activity *in vitro*

To elucidate the molecular mechanism of Fyn-mediated telomere erosion, we measured telomerase reverse transcriptase (TERT) expression and found no difference between Fyn$^{-/-}$ and WT stem cells or between Fyn knockdown and sh-mock stem cells (Fig. EV10A-B). Therefore, the greater telomere length found in Fyn$^{-/-}$ and Fyn knockdown stem cells does not appear to be the result of a change in TERT expression. To evaluate whether Fyn directly interferes with telomerase activity, we performed telomere repeat amplification protocol (TRAP) [19]. There was no significant difference in telomerase activity between Fyn$^{-/-}$ and WT mESCs (Fig. EV10C), Sh-Fyn and Sh-Mock E14 cells (Fig. EV10D), or colon lysates of Fyn$^{+/+}$ and Fyn$^{-/-}$ mice (Fig. EV10E) and in Sh-Mock vs Sh-Fyn HEK293T cells (Fig. EV10F). The TRAP assay is helpful for measuring telomerase activity, but cannot detect improper localization of telomerase subunits [20, 21]. Thus, Fyn might not directly interfere with TERT expression or telomerase activity. Rather, these data suggest that Fyn may interfere with endogenous telomere maintenance indirectly.

Fyn phosphorylates Menin at tyrosine 603

After discovering that Fyn does not directly interfere with TERT expression or telomerase activity, we began to screen a candidate list of transcriptional modulators related to telomere maintenance (Table EV1) [22]. We included the transcriptional repressor Menin that is known to bind to telomeres [15, 22] . We performed Fyn immunoprecipitation with WT mESCs lysates using an anti-Fyn antibody and blotted against the candidate proteins. Of the candidate proteins, only the scaffold protein Menin showed significant interaction with Fyn (Fig. EV11). We later found that Menin is involved in telomere maintenance through interaction with TR and/or telomeres (see below). Endogenous Menin was detected in anti-Fyn-precipitated protein complexes in both E14 cells (Fig. 3A) and WT mESCs isolated from mice (Fig. 3B). We performed the previously described *in vitro* kinase assay with full-length recombinant human Menin purified from wheat germ expression system and found that Fyn does indeed phosphorylate Menin (Fig. 3C). Tandem mass spectrometry analysis identified Menin Y603 as the site of Fyn phosphorylation (Fig. EV12).

We performed a radioactive *in vitro* kinase assay with active Fyn to compare WT and mutant Menin that cannot be phosphorylated at Y603 (Menin Y603F). These WT and mutant Menin proteins were purified using an *E. coli* expression system. The assay showed that phosphorylation of Menin Y603F is greatly decreased (Figs. 3D-E), confirming that Y603 serves as the site of Fyn phosphorylation.

We also performed a non-radioactive *in vitro* kinase assay with Fyn and WT or Y603F-Menin protein purified using an *E.coli* expression system. A custom-synthesized pY603-Menin

antibody showed that phosphorylation of Menin Y603F is greatly decreased compared to WT Menin (Fig. 3F). To validate specificity of phospho-specific antibody, lambda phosphatase was used to eliminate phospho-signal. pY603-Menin signal was nearly abolished in the lambda phosphatase treated sample, but the signal was recovered by phosphatase inhibitor treatment (Fig. 3F).

In addition, we evaluated whether Fyn phosphorylates Menin at Y603 endogenously (*in vivo* kinase assay). We transfected HEK 293T cells with Xpress-tagged Menin to compare the amount of pY603-Menin in Xpress-Menin immunoprecipitation samples with or without Fyn over-expression. When co-expressed with Fyn, Xpress-tagged Menin showed pY603 signal that was not present in the sample without Fyn (Fig. 3G). Consistent with our previous observation, the pY603 signal was abolished in the lambda phosphatase-treated sample and recovered in the phosphatase inhibitor-treated sample. Furthermore, we found that endogenous Menin is indeed phosphorylated at Y603 (Fig. 3H). The pY603 signal was also abolished in the lambda phosphatase-treated sample and recovered in the phosphatase inhibitor-treated sample. Together, these data suggest that Y603 serves as the site of Fyn phosphorylation and the custom synthesized antibody against pY603-Menin is specific to the site.

Menin does not affect TERT transcription in mESCs

A previous study described Menin as a cell-type specific negative regulator of TERT transcription, but overexpression of Menin did not significantly reduce *in vitro* telomerase activity [23]. Although we found that Fyn deletion or inhibition did not affect TERT expression or *in vitro* telomerase activity (Figs. EV10A-F), we evaluated whether Fyn's phosphorylation of

Menin is involved with TERT transcription in stem cells. We performed a chromatin-immunoprecipitation assay using anti-Menin antibody in Sh-Mock vs Sh-Fyn E14 stem cells to evaluate whether Fyn-mediated phosphorylation of Menin affects its binding at TERT promoter. qPCR of the TERT promoter showed no significant difference in Menin occupancy between sh-Mock vs sh-Fyn E14 nuclear lysates (Fig. EV13A). These data suggest that Fyn-mediated phosphorylation of Menin does not regulate TERT transcription in stem cells. We also tested whether Menin binds to TERT. Immunoprecipitation results showed that Menin appears not to be a binding partner with TERT (Fig. EV13B).

Fyn promotes Menin localization to telomeres

A previous study found that Menin localizes to telomeres in mouse spermatocytes during meiosis [15]. We proceeded to investigate whether Menin localizes to telomeres in stem cells by performing IF-FISH in unsynchronized mESCs with anti-Menin antibody and telomere FISH probe. We found that Menin does indeed co-localize with telomeres (Fig. 4A). Strikingly, Fyn$^{-/-}$ mESCs showed a significant decrease in telomere/Menin co-localization compared to WT mESCs. These IF-FISH results suggest that Fyn-mediated phosphorylation of Menin promotes Menin localization to telomeres. It is not clear from these results whether Menin directly interferes with telomerase recruitment or activity at the site of telomere elongation.

Menin is associated with TR *in vitro* and its association with TR is modulated by Fyn

We next investigated whether Menin interacts with the telomerase RNA component (TR) using an *in vitro* RNA pulldown assay with *in vitro* transcribed biotinylated TR and nuclear lysates

from mESCs. Western blotting from two independent experiments revealed that Menin was present in the TR pulldown complex. Interestingly, Menin showed greater association with TR in WT mESCs vs Fyn$^{-/-}$ mESCs (Fig. 4B). We also performed Menin immunoprecipitation to compare TR expression in WT mESCs vs Fyn$^{-/-}$ mESCs. TR expression was significantly decreased in the Menin immunoprecipitation sample from Fyn$^{-/-}$ mESCs (Fig. 4C). These results show that Menin is a TR-associated protein and suggest that Fyn increases Menin's association with TR. We performed IF-FISH with anti-Menin antibody and TR FISH probes in unsynchronized cells. The Pearson coefficient (*r*) of co-localization for TR and Menin was significantly higher in WT cells compared to Fyn$^{-/-}$ cells (Fig. 4D), confirming that Fyn increases Menin's association with TR. We also evaluated co-localization of TR and Coilin, a cajal body marker, in WT and Fyn$^{-/-}$ mESCs (Fig. 4E). Although cajal bodies are not essential for telomerase biogenesis or activity [24, 25], they are involved in telomerase trafficking and TR accumulates at cajal bodies in fixed cells [26-28].

Interestingly, there was no difference in TR/Coilin co-localization between WT and Fyn$^{-/-}$ mESCs (Fig. 4E). These results show that Fyn's phosphorylation of Menin does not interfere with TR accumulation in cajal bodies and, taken together with TRAP assay results (Figs. S10C-F), suggest that phospho-Menin does not interfere with telomerase assembly.

Phosphorylation of Menin at Y603 promotes SUMO1 modification

Considering that many studies have demonstrated telomerase function and its subunits are modified by small ubiquitin-like modifier (SUMO) proteins [29-33], we were curious to see if Menin and phospho-Menin are modified by SUMO proteins, which is known to affect stability

and localization [34]. Interestingly, a phosphorylation-dependent SUMO modification consensus motif has previously been reported [35]. Another report showed SUMO modification of Menin at K591 and suggested that Menin contains multiple SUMOylation sites [36]. To further study Menin SUMOylation, we used GPS-SUMO (http://sumosp.biocuckoo.org/) to identify additional SUMOylation sites [37]. We selected lysine residues with the lowest p-values, 609 (K609) as possible SUMO-modification site (Fig. EV14A) and proceeded to investigate whether Fyn's phosphorylation of Menin at Y603 regulates its SUMOylation. We performed immunoprecipitation with anti-Menin antibody and blotted against SUMO1 and SUMO2/3/4. Results showed that endogenous Menin interacted with SUMO1 in Sh-Mock cells, but the interaction was greatly reduced in Sh-Fyn cells (Fig. 5A-B), suggesting that Fyn-mediated phosphorylation of Menin is important for SUMO1 interaction with Menin. We did not observe an interaction between endogenous Menin and endogenous SUMO2/3/4 (Fig. EV14B). We also used an ELISA SUMOylation assay that specifically detects SUMO1 to measure Menin SUMO1 modification in nuclear lysates from mESCs. We observed a reduced SUMOylation intensity in Fyn-knockout cells vs. WT cells. Moreover, SUMOylation intensity was also reduced in Sh-Fyn compared to Sh-Mock mESCs (Fig. EV14C).

To gain insight into the mechanism of Fyn-mediated Menin SUMOylation, we transfected HEK 293T cells with Xpress-tagged pcDNA-WT-Menin *(*WT-Menin*),* pcDNA-Y603F-Menin (Y603F-Menin), and pcDNA-Y603D-Menin (Y603D-Menin*)* with or without pcDNA-HA-SUMO1 (SUMO1). Menin Y603D served as a phosphomimetic mutant. We performed Xpress immunoprecipitation followed by western blot with anti-HA antibody. No SUMO1-Menin band was observed in cells transfected with WT-Menin only (Fig. 5C, upper blot). SUMO1-Menin was observed in both WT-Menin+SUMO1 and Y603D-Menin+SUMO1-transfected cells, but

SUMO1-Menin was reduced significantly in Y603F-Menin+SUMO1-transfected cells (Fig. 5C-D). The significantly reduced SUMO1-Menin band in Y603F-Menin+SUMO1-transfected cells suggests that SUMOylation modification of Menin is phosphorylation-dependent (Fig. 5C-D). Interestingly, K609R-Menin+SUMO1-transfected cells show greater SUMO1-Menin signal than Y603F-Menin+SUMO1-transfected cells, indicating that Y603 phosphorylation may affect SUMO1 modification at additional residues. Surprisingly, anti-Xpress reblotting of Xpress IP membrane with Xpress antibody shows a very strong Xpress-Menin band in Y603D-Menin+SUMO1 transfected cells compared to WT-Menin+SUMO1 and other mutants (Fig. 5C). However, reblotting of the same membrane with Menin antibody did not show any difference between Y603D-Menin+SUMO1, Y603F-Menin+SUMO1 and K609R-Menin+SUMO1 (Fig. 5C). These results suggested that the C-terminal region of Xpress-Menin, which contains the Xpress tag and mutation sites, may be subject to degradation and that phosphorylation at 603 prevents C-terminal degradation. Later we explore this mechanism in more detail (see Fig. 6 and Fig. EV15).

In a similar experimental model, we performed Menin pulldown using anti-Menin antibody with lysates from WT+SUMO1 or mutant Menin+SUMO1 co-transfected HEK 293T cells. Fig. 5E (upper blot) shows more HA-SUMO1 band in Y603D-Menin+SUMO1-transfected cells compared to Y603F-Menin+SUMO1 and K609R-Menin+SUMO1 transfected cells. In an additional experimental model, we pulled down HA-SUMO1 with HA antibody using the same cell lysates that were used in previous co-transfection experiments. The anti-Xpress immunoblot in Fig. 5F shows increased Xpress-Menin in HA pulldown from Y603D-Menin+SUMO1-transfected cells compared to HA pulldowns from WT+SUMO1, Y603F-Menin+SUMO1, and

K609R-Menin+SUMO1-transfected cells. Taken together, these immunoprecipitation results suggest that phosphorylation of Menin at Y603 promotes SUMO1 modification.

Phosphorylation-dependent SUMO1 modification of Menin promotes Menin's association with TR by increasing Menin stability

In order to determine if SUMO1 modification of Menin affects Menin/TR association, we performed TR pulldown assays with HEK 293T lysates co-overexpressing WT or mutant Menin with or without SUMO1. Interestingly, we detected significantly higher Xpress-Menin in TR pulldown complexes of Y603D-Menin+SUMO1-transfected cells (Fig. 6A). The Y603D-Menin without SUMO1 sample showed Xpress-Menin/TR association, but to a lesser extent than Y603D-Menin+SUMO1 sample (Fig. 6A). Y603F-Menin and K609R-Menin samples show negligible or no binding with TR irrespective of SUMO1 transfection (Fig. 6A). These results suggest that phosphorylation and SUMOylation of Menin at the C-terminal domain promote its association with TR. Conversely, reblotting with an anti-Menin antibody that recognizes the center region of Menin, showed no change between WT and mutant Menin with or without SUMO1 (Fig. 6A). Taken together, the seemingly contradictory results of anti-Xpress and anti-Menin blots suggest that there are at least two distinct domains of Menin associated with TR. To further investigate the strong binding affinity between TR and Y603D-Menin+SUMO1 lysates, we performed a modified TR-pulldown experiment, where 50-fold less Y603D-Menin+SUMO1 input was used compared to Y603F-Menin+SUMO1 and K609R-Menin+SUMO1 input. The input lanes show that Xpress-Menin expression is near equal between the samples, while β-actin expression shows a 50-fold difference (Fig. EV15A). In TR-IP lanes, even 50-fold less input

from Y603D-Menin+SUMO1 sample shows increased TR binding affinity compared to Y603F-Menin+SUMO1 and K609R-Menin+SUMO1.

We assessed Menin subcellular expression and localization comparing WT, Y603F, and Y603D Menin with or without SUMO1 in cytoplasmic and nuclear extracts. The ratio of cytoplasmic to nuclear Menin expression did not change between WT and mutant Menin (Fig. 6B). These results indicate that phosphorylation-dependent SUMOylation of Menin promotes its stability, but does not affect subcellular localization.

To further explore how the C-terminal phosphorylation and SUMO1 modification affect Menin stability, we performed a Cyclohexamide (CHX) Chase Assay in Y603F-Menin and Y603D-Menin with or without SUMO1. The Xpress-Menin shows a time dependent degradation in both Y603F-Menin and Y603D-Menin, but the protein turnover was much slower in Y603D-Menin, likely due to increased stability at the C-terminal region (Fig. 6C, Fig. EV15B). The anti-Menin antibody that recognizes the central region shows that stability of Y603D-Menin was slightly higher in the presence of SUMO1 compared to Y603F-Menin+SUMO1 (Fig. 6C, Fig. EV15B). The stability of both Y603F-Menin and Y603D-Menin was higher in the presence of SUMO1, indicating that SUMO1-modification increases Menin stability. In order to directly compare Menin stability between Y603D and Y603F, we performed western blotting with CHX assay lysates on the same membrane. A time dependent exposure of western blot membrane showed no Xpress-Menin in Y603F-Menin lysates after 1 minute, while Xpress Menin showed significant expression in Y603D-Menin lysates. Xpress-Menin was only visible in the Y603F-Menin lysates after a 10-minute exposure (Fig. EV15B). Detection of the central region of Menin shows Menin expression at 1 min or 10 min of exposure in both Y603F-Menin and Y603D-Menin lysates (Fig. EV15C). However, Menin shows much greater stability in Y603D-Menin

lysates compared to Y603F-Menin lysates. Altogether, these results suggest that phosphorylation and SUMOylation at the C-terminal region of Menin increase its stability and/or promote resistance to C-terminal degradation, ultimately promoting Menin's association with TR.

Overexpressed, SUMO1-modified Menin inhibits TR association with Dyskerin and GAR1

We performed tandem mass spectrometric analysis of TR pull-down complex from Y603F-Menin+SUMO1 and Y603D-Menin+SUMO1 co-transfected HEK 293T nuclear lysates. The results indicated that 54 human proteins were associated with TR in Y603F-Menin-transfected cells. The number of proteins was reduced dramatically in Y603D-Menin+SUMO1 co-transfected cells (Fig. 7A and Table EV2). Importantly, Y603D-Menin transfection inhibited TR association with telomerase subunits Dyskerin and GAR1 (Fig. 7B and Table EV2).

We corroborated mass spectrometry results by performing TR-IP followed by Western blot using Y603F-Menin+SUMO1 and Y603D-Menin+SUMO1 co-transfected HEK 293T lysates. Whole cell lysates showed that Dyskerin and GAR1 levels were not reduced, suggesting that Menin does not affect Dyskerin or GAR1 expression (Fig. 7C). However, Dyskerin and GAR1 binding were reduced in TR-IP of Y603D-Menin+SUMO1 transfected cells, confirming the TR mass spectrometry results (Fig. 7C). Coilin/TR binding was not changed between these two groups (Fig. 7C). We also compared Dyskerin and GAR1 expression in TR-IP of whole cell lysates of 293T cells transfected with Y603D-Menin+SUMO1 or K609R-Menin+SUMO1. We found that cells transfected with SUMO-deficient Menin (K609R), showed greater Dyskerin and GAR1 binding in TR-IP (Fig. 7D). Xpress-tagged Menin binding was also reduced in the K609R

sample, further supporting that SUMO1 modification of Menin at K609 promotes its association with TR, Menin blot did not show any changes further confirming our previous results (Fig. 7D).

We also performed IF-FISH experiments with DKC1 antibody and TR FISH probe to evaluate co-localization of Dyskerin and TR after Menin and SUMO1 overexpression. IF-FISH analysis showed significantly more Dyskerin and TR co-localization in Y603F-Menin+SUMO1 and K609R-Menin+SUMO1 compared to Y603D-Menin+SUMO1 transfected 293T cells (Fig. 7E, F). Transfection of Menin mutants did not affect the binding of Coilin to TR (Fig. EV16). Collectively, these results suggest that association of SUMO1-modified Menin with TR restricts Dyskerin's association with TR.

Menin knockdown promotes telomerase localization to telomeres and slows telomere erosion

We performed Menin knockdown in HEK 293T cells to evaluate whether Menin expression affects telomerase assembly, telomerase localization to telomeres, and telomere length. Western blotting analysis in Sh-Mock vs Sh-Menin 293T cells confirmed efficient Menin knockdown (Fig. 8A). IF staining of Dyskerin and Coilin alongside FISH with TR probes showed no significant difference in either Coilin-Dyskerin co-localization or Coilin-TR co-localization (Fig. 8B-D) between Sh-Mock cells and Sh-Menin cells. These results further support that Menin does not interfere with telomerase assembly in Cajal bodies. Analysis of Dyskerin IF and telomere FISH showed that co-localization of Dyskerin and telomeres was increased in Sh-Menin 293T cells compared to Sh-Mock cells (Fig. 8E-F). These results suggest that Menin inhibition significantly increased Dyskerin localization to telomeres. A significantly higher Dyskerin/TR

co-localization was also noted in Sh-Menin cells than Sh-Mock (Fig. 8G). Telomere length analysis by qRT-PCR showed significantly higher telomere to *Alu* sequence ratio (T/S) in Sh-Menin cells compared to Sh-Mock cells at both passages 5 and 10 (Fig. 8H). These studies indicate that Menin knockdown slows telomere erosion in a manner similar to Fyn Knockdown.

Fyn knockdown in Human DC iPSCs slows telomere shortening

We next investigated Fyn inhibition in iPSCs from a DC patient that exhibit accelerated telomere erosion and telomerase deficiency due to a mutation in DKC1. We first used DC fibroblasts to generate DC iPSCs. iPSC generation was confirmed by the expression of SSEA-4, Tra-1-60, KLF4 and Nanong (Fig. EV17A-B). Next, we created DC iPSCs with Fyn KO using CRISPR-Cas9. A mock CRISPR-Cas9 plasmid was used as negative control. CRISPR-Cas9 transduction generated a population of iPSCs with significantly decreased Fyn expression, although expression was not completely abolished in the whole iPSC population (Fig. 9A). Therefore, we used the term Fyn knockdown (Fyn^{KD}) to describe these iPSCs instead of Fyn knockout (Fyn^{KO}). CRISPR-Cas9-mediated Fyn^{KD} reduced both Fyn and pY603-Menin expression in DC iPSCs (Fig. 9A-C). iPSCs showed no significant difference in telomere length after 3 passages (Fig. 9D-E). However, at passage 12, Fyn^{KD} iPSCs showed significantly longer telomeres than mock iPSCs as determined by Q-FISH (Fig. 9D, F). Consistent with these results, Flow-FISH and qRT-PCR results showed that Fyn^{KD} DC iPSCs exhibited significantly higher telomere signals compared to control DC iPSC after 12 passages (Fig. 9G and H, respectively).

Moreover, TMCA results also show that Fyn knockdown slows telomere erosion in DC iPSCs. DNA fibres from Fyn^{KD} iPSC show significantly longer telomeres than Mock iPSC (Fig.

9I-K). Detail statistical analysis from the telomere signals shows that mean and median telomere sizes were 15.4599 kb and 18.3200 kb, respectively, in Fyn^{KD} cells compared to Mock cells, which shows that mean and median telomere sizes were 13.5937 kb and 15.990 kb, respectively (Fig. 9I-K). A comparative statistical analysis shows significantly longer absolute telomere length in Fyn^{KD} cells compared to Mock cells (Fig. 9K).

Discussion

This work uncovers a new mechanism of telomere maintenance in mammalian stem cells. We demonstrate that Fyn, an Src family kinase, is a negative regulator of mammalian telomere length. We first discovered that inhibition or deletion of Fyn stabilizes telomere length. However, we found that Fyn does not affect TERT expression and does not interfere with telomerase activity using *in vitro* assays. Rather, our results suggest Fyn negatively regulates telomere length by phosphorylating the scaffold protein Menin at Y603, promoting telomerase subunit mislocalization, and may compromise telomerase activity *in vivo*.

Phosphorylation of Menin at Y603 promotes phosphorylation-dependent SUMOylation at K609, which increases Menin's C-terminal stability and association with TR. Importantly, phospho-site mutant Y603F and SUMO-site mutant K609R Menin showed decreased SUMOylation and stability, thereby reducing its association with TR. We found that SUMO1-modified Menin associates much more strongly with TR, decreasing TR's association with telomerase subunits Dyskerin and GAR1.

Telomerase stability, assembly, and recruitment to telomeres are essential steps during telomere elongation [38]. Our results strongly suggest that knockdown of Fyn or Menin does not

affect telomerase assembly, but rather, impairs telomerase holoenzyme function. One possible mechanism is that binding of Menin to TR promotes the dissociation of Dyskerin and GAR1 from telomerase RNPs en route to telomeres. An elegant study by Schmidt *et al* used live cell imaging to reveal that more than 85 % of telomerase RNPs are freely diffusing throughout the nucleus [28]. Our results point to the possibility that SUMO1-Menin compromises telomerase function by binding to TR in a portion of the telomerase RNP population, rather than the telomerase RNP accumulated in cajal bodies. Another possibility is that SUMO1-Menin compromises telomerase function by associating with TR at telomeres.

Defective telomere maintenance may result in a TBD such as DC [6, 39, 40]. We saw that CRISPR-Cas9-mediated Fyn inhibition in mutant DKC1 human DC iPSCs stabilized telomeres concurrent with a decline in pY603-menin expression. There are conflicting findings of telomere shortening in DC iPSCs. Agarwal *et. al.,* 2010 showed that DC iPSCs increased telomere length over time [41]. However, Batista et. al., Woo et al., and Fernandez et al observed telomere shortening in DC iPSCs over time. Consistent with the latter publications, we found telomere shortening in later passages of DC iPSCs accompanied by spontaneous differentiation [42-44]. It is tempting to speculate that endogenous Fyn exacerbates telomere shortening in these telomerase-defective human iPSCs by phosphorylating Menin and further compromising *in vivo* telomerase holoenzyme function. Indeed, our human DC iPSC data suggests that endogenous Fyn negatively regulates telomere maintenance even in the presence of defective telomerase.

In conclusion, our results demonstrate that Fyn-mediated phosphorylation and subsequent SUMO1-modification of Menin disrupt telomere maintenance in proliferating stem cells. We found that Fyn inhibition promotes telomere maintenance, even in telomerase-defective stem

cells. Fyn inhibitors may be a viable treatment option for DC or other TBDs, although the development of specific inhibitors is needed.

Materials and Methods

The antibodies, primers, kits, and chemicals used in this study are in Tables EV3-8.

Plasmid Men1-pDNR-Dual (Cat. no: HsCD00000838) was purchased from DNASU. pcDNA3-HA-Sumo1 was a gift from Junying Yuan (Addgene plasmid # 21154) [45].

Fyn $^{-/-}$ animal model

Fyn$^{-/-}$ mice (B6.129S7-Fyntm1Sor/J) were purchased from The Jackson laboratory [46] and bred, propagated, and maintained at The Hormel Institute, University of Minnesota. Mice were maintained following the guidelines established by the University of Minnesota Institutional Animal Care and Use Committee. Fyn genotyping was performed by PCR using a protocol as recommended by The Jackson Laboratory. Representative genotyping characterization is shown in Fig. EV9A. For this study, age-matched wildtype (WT) and Fyn$^{-/-}$ mice (n = 12 males + 12 females) were maintained for 97 weeks. Some mice needed to be euthanized based on the veterinary advice. This study was completed with 13 WT and Fyn $^{-/-}$ mice (6 males + 7 females).

Generation of mouse embryonic stem cells (mESCs) from WT and Fyn$^{-/-}$ mice

mESCs were obtained from the inner cell mass of blastocysts isolated from 3.5 days post coitum mice [47]. Briefly, a feeder layer of mouse embryonic fibroblasts (MEFs, $1x10^6$) was plated in tissue culture dishes two days before blastocyst isolation and treated with mitomycin C (10

μg/mL) for 2 h. Isolated blastocysts were washed with KnockOut™ Dulbecco's Modified Eagle Medium (DMEM), transferred aseptically to the feeder layer, and cultured with KnockOut™ DMEM supplemented with 20 % knockout serum replacement and 1000 U/mL Leukemia Inducing Factor (LIF). After 48 h the medium was replaced, and the blastocysts were left to hatch for 7-10 days. Cells released from hatched blastocysts were transferred to a new feeder layer. Colonies generated from the previous step were transferred onto a new feeder layer. Pluripotency was confirmed through alkaline phosphatase (AP) staining and immunofluorescence of Sox2 and KLF4 (Fig. EV7A-D).

Alkaline phosphatase (AP) staining

To perform AP staining, mESCs were fixed with 4 % paraformaldehyde in phosphate buffered saline (PBS) for 2 min at room temperature. AP staining was performed using an Alkaline Phosphatase Detection Kit following the manufacturer's protocol (MilliporeSigma).

mESCs culture

The mESCs E14Tg2a line was maintained in DMEM supplemented with 15 % heat-inactivated fetal bovine serum (FBS), 0.055 mM β-mercaptoethanol, 2 mM L-glutamine, 0.1 mM minimum essential medium non-essential amino acids, and 1,000 U/mL LIF.

RNA interference of Fyn

To generate Fyn knockdown cells, pLKO.1-sh-Fyn or pLKO.1-mock lentivirus plasmids were co-transfected with packaging vectors psPAX2 and pMD2.0G into HEK 293T cells using the iMFectin transfection reagent (GenDepot). The mouse lentiviral sh RNA vector sequence for

Fyn was designed and confirmed in the University of Minnesota Genomic Center. Viral particles containing 4 μg/mL polybrene were transduced into E14TG2a cells at 24 h and 48 h time points. After transduction, cells were selected in the presence of 1 μg/mL puromycin for 7-10 days.

Telomeric repeat amplification protocol (TRAP) assay

TRAP assay was used to determine telomerase activity according to the manufacturer's recommendation (TRAPEZE® RT Telomerase Detection Kit S7710, MilliporeSigma). Briefly, cell lysates were resuspended into CHAPS lysis buffer at a concentration of 500 ng/μL. Relative telomerase activity was determined using a TSR8 standard curve following the protocol described by the manufacturer.

Quantitative Fluorescent In Situ Hybridization (Q-FISH) and flow cytometry-FISH (Flow-FISH) assays

Q-FISH of metaphase chromosomes, interphase nuclei, and mouse tissues, was performed as previously described [48]. Briefly, cells were treated with 1 μg/mL colcemid (Cayman Chemicals) for 1 hour, hypotonically swelled with 75 mM KCl solution, and fixed with Carnoy's solution. Embedded tissue samples were cut in 5 μM sections and deparaffinized using standard protocols. Telomere and centromere Q-FISH staining was performed using a TelC-Alexa-488, or TelG-Cy3 PNA telomere probe together with a CENPB-Cy3 centromere probe (PNA Bio Inc). Slides were counterstained with DAPI (Electron Microscopy Sci.) and visualized using a Nikon or a Zeiss LSM 900 confocal microscope. Telomere length was measured using an open-source software (Telometer; http://demarzolab.pathology.jhmi.edu/telometer/), as previously described [49].

Flow-FISH analysis was performed as previously described [50] with slight modifications. Briefly, 0.5 x 10^6 cells were washed with PBS containing 0.1 % BSA and resuspended in 300 µL of hybridization buffer (70 % formamide, 20 mM Tris-HCl, pH 7.0, 1 % blocking reagent, and 1 µg/mL PNA probe) and incubated for 2 h at RT. Cells were washed twice with fixation buffer (60 % formamide, 10 mM Tris-HCl, pH 7.0, 0.1 % blocking reagent, 0.1 % Tween 20) at 40 °C, resuspended in PBS containing 0.1 % BSA and 0.05 µg/mL propidium iodide (PI) and analyzed using a BD-FACS (BD Aria III). TelC-Alexa-488 PNA probe and PI nuclear staining was used in all flow-FISH analysis. CRISPR-Cas9 transfected cells were stained with the TelG-Cy3 PNA probe and counterstained with DAPI.

TeloSizer® assay

Telomere length was evaluated using the TeloSizer® assay (Genomic Vision, Bagneux, France) based on molecular combing technology. This assay measures physical telomere lengths in kilobase (kb), but also differentiates TTS (true telomere sequence) and ITS (interstitial telomere sequence).

Briefly, cells were harvested and embedded into agarose plugs using the Genomic Vision FiberPrep® kit (Genomic Vision, Bagneux, France). DNA extraction and combing were performed according to the EasyComb procedure (Genomic Vision, Bagneux, France). Coverslips were hybridized with a telomere-specific probe G-rich PNA probe Cy3-(TTAGGG)3 (Panagene, Daejeon, South Korea) followed by counterstaining with YOYO™-1 Iodide (Thermo Scientific, Bordeaux, France) according to the TeloSizer® assay procedure. Coverslips were scanned using the FiberVision® scanner. Telomere signals were automatically detected and measured using the FiberStudio® Easyscan software. TeloSizer® assay is based on molecular

combing and has been shown to provide accurate telomere length measurements comparable to other telomere length analysis techniques [51].

Generation of DC-iPSCs from fibroblasts

DC fibroblasts were purchased from The Coriell Cell Repositories and maintained in MEM supplemented with 15 % FBS and 1 % non-essential amino acids. Induced pluripotent stem cells (iPSCs) were generated from DC fibroblasts by lentiviral transduction with polycistronic STEMCCA vector containing transfecting Yamanaka transcription factors Oct4, Klf4, Sox2, and c-Myc according to the manufacturer's protocol (MilliporeSigma). Briefly, 1 x10^6 DC fibroblasts were seeded onto gelatin-coated dishes and transduced with the STEMCCA lentivirus. Transduced cells were transferred to a plate containing 1 x 10^5 feeder cells. iPSC colonies were picked 25–30 days post-transduction and maintained in feeder-free E8 media (StemCell Technologies) on a Matrigel (Corning). Pluripotency was confirmed by immunofluorescence and Western blotting using human iPSC specific markers (Figs. S17A-B).

q-PCR assay for telomere length measurement

Average telomere length was measured using a qPCR method previously described [52]. The single-copy genes *m36B4* and *h36B4,* and the multicopy gene *hAlu* were used as normalization references. A 20 µL PCR reaction contained 10 µL of 2X SYBR Green mix, 0.5 µL of each 10 µM forward and reverse primers (Table EV5), 4 µL DNase/RNase free water, and 5 µL genomic DNA at a concentration of 8 ng/µL. The qPCR was carried out in a Bio-Rad thermocycler (CFX96) with reaction conditions of 95 °C for 10 min followed by 40 cycles of denaturation at

95 °C for 15 s, 60 °C annealing for 30 s, 72 °C extension and data collection for 30 sec. The CFX manager software was used to generate standard curves. The average telomere length is expressed as the telomere to single copy gene (T/S) ratio.

Protein extraction, Western blotting, and Immunohistochemistry (IHC)

Cells were lysed with NP-40 lysis buffer (50 mM Tris-HCl, pH 7.6, 150 mM NaCl, 5 mM EDTA, 1 % Nonidet P-40 with a protease inhibitor cocktail). Nuclear and Cytoplasmic fractions were obtained using the NE-PER cytoplasmic and nuclear protein extraction kit (ThermoFisher Scientific). A phosphatase inhibitor cocktail was used for phosphoprotein analysis, and N-ethylmaleimide (NEM) was used for SUMO-protein analysis. Proteins were resolved in SDS-PAGE and transferred to polyvinylidene difluoride (PVDF) membranes. The membranes were blocked with 5 % milk, and target proteins were detected with specific antibodies and visualized by chemiluminescence.

IHC was performed using a standard protocol. Paraffin-embedded tissues were subjected to deparaffination and antibody retrieval. Tissue sections were blocked with 10 % goat-serum followed by overnight incubation with a primary antibody at 4 °C. Slides were incubated with a secondary antibody and stained with 3,3′-Diaminobenzidine (DAB). For IF, a fluorochrome-conjugated secondary antibody was used. Images were quantified using ImageJ2 software [53].

Immunoprecipitation

A total amount of 1 mg of cell lysates in a volume of 500 µL were immunoprecipitated with 2 µg of target antibody and samples were rotated overnight at 4 °C. 40 µL of protein A/G Sepharose

beads (GenDepot) were added to each sample and rotated 1 h at 4 °C. Beads were washed 3 times with lysis buffer, and the supernatant fraction was analyzed by Western blotting.

Chromatin immunoprecipitation assay

Stable sh-mock and sh-Fyn E14 cells were seeded in 10 cm^2 plates. Chromatin immunoprecipitation (ChIP) was performed using the One-Day Chromatin Immunoprecipitation Kit (Magna ChIP G, MilliporeSigma) according to the manufacturer's protocol. Chromatin samples were immunoprecipitated with anti-Menin antibody overnight at 4 °C. The DNA fractions for TERT promoter was analyzed by qPCR.

Protein expression, purification, and in vitro kinase assay

WT and mutant *MEN1* (Y603F) were cloned into a pGEX-5X1 vector upstream a C-terminal 6×His tag. Menin WT and mutant proteins were expressed in *E. coli* BL21(DE3) pLysS cells (Promega). Cells were grown in Lysogeny broth to an OD 600 of 0.5-0.7 and protein expression was induced with 0.5 mM IPTG for 20 h at 16 °C. Cells suspended in 200 mL were pelleted at 6000 × g and resuspended in 10 mL lysis buffer (50 mM HEPES pH 8.0, 500 mM NaCl, 20 mM imidazole, 10 % glycerol, 2 mM TCEP, 1 % Tween-20, and 1X protease inhibitor). Cell suspensions were incubated with lysozyme for 30 min and disrupted by sonication for 10 min. Cells were centrifuged for 30 min at 20000 × g, and lysates were equilibrated with Ni-NTA agarose beads (ThermoFisher Scientific) for 2 h at 4 °C. Samples were centrifuged at 120 × g for 3 min to remove the supernatant fraction. Beads were washed with 10 mL buffer 1 (50 mM HEPES pH 8.0, 500 mM NaCl, 30 mM imidazole, 10 % glycerol, 0.5 % Tween-20, and 2 mM DTT), and 2X with 10 mL buffer 2 (50 mM HEPES pH 8.0, 500 mM NaCl, 40 mM imidazole,

10 % glycerol, 0.5 % Tween-20, and 2 mM DTT). Proteins were eluted with three washes of 0.1 mL elution buffer (50 mM HEPES pH 8.0, 150 mM NaCl, and 300 mM imidazole) and transferred to a kinase buffer (50 mM Tris pH 8.0, and 100 mM NaCl) using Zeba Spin Desalting columns (ThermoFisher Scientific). Proteins were separated by SDS-PAGE and stained with Coomassie blue. The protein concentrations were quantified using a Nanodrop (ThermoFisher Scientific).

For radioactive *in vitro* kinase assay, 100 ng of Fyn protein (MilliporeSigma, Cat # 14-441) was incubated with or without 1 µg of recombinant Menin protein, either commercially purchased (Novus Biologicals, Cat # H00004221-P01) or produced in the laboratory. WT or mutant Menin were incubated for 30 min in a 30 °C water bath. Proteins were incubated with 10 µCi [$^{\gamma 32}$P] ATP in kinase buffer (20 mM HEPES (pH 7.4), 1 mM dithiothreitol, 10 mM $MgCl_2$, and 10 mM $MnCl_2$). The incorporated radioactivity was measured by autoradiography.

For the non-radioactive kinase assay, 100 ng of commercially purchased Fyn protein (MilliporeSigma) was incubated with or without in house synthesized 1 µg Menin recombinant protein (WT or mutant Menin) for 30 min in a 30 °C water bath. Proteins were incubated in the presence of 200 µM ATP in kinase buffer (20 mM HEPES (pH 7.4), 1 mM dithiothreitol, 10 mM $MgCl_2$, and 10 mM $MnCl_2$). Immunoblots measured the incorporated ATP phosphorylation to Menin using a pY603-Menin antibody. Lambda protein phosphatase was used to validate the specificity of the pY603-Menin antibody. To stop the Fyn kinase activity, the *in vitro* kinase assay reaction mix was incubated for 30 min in a 30 °C water bath with 400 U of Lambda protein phosphatase in the presence of 10 mM $MnCl_2$ in 1x NEBuffer for Protein MetalloPhosphatases. To counteract the effect of Lambda protein phosphatase, we added a 1X phosphatase inhibitor cocktail to the reaction mix to recover the phospho signal. The *in vitro*

kinase assay reaction mixtures were separated into 8 % polyacrylamide gels and blotted against a pY603-Menin. Membranes were stripped and reblotted with Menin and Fyn antibodies.

For *in vivo* kinase assay, Xpress-Menin and HA-Fyn were over-expressed in 293T cells. Xpress-Menin was immunoprecipitated with Xpress antibodies and the Lambda phosphatase assay was performed with or without 1× phosphatase inhibitors as previously described. Reaction mixtures were separated into 8 % PAGE and blotted with pY603-Menin, Menin or Fyn antibodies. *In vivo* kinase assays were also performed in endogenously expressed Menin protein. Briefly, endogenous Menin was immunoprecipitated with an anti-Menin antibody (Invitrogen) and Lambda phosphatase assay was performed as previously described. Reaction mixtures were separated into 8 % polyacrylamide gels and blotted against a pY603-Menin or Menin antibody.

Site-directed mutagenesis

Site-directed mutagenesis was performed using QuikChange II Site-Directed Mutagenesis Kit (Agilent) according to the manufacturer's protocol. Primers for mutagenesis were designed using online tools provided by Agilent. WT MEN1 plasmid was used as a template. The mutations were confirmed by sequencing.

Identification of phosphorylation sites on Fyn-phosphorylated Menin

An in vitro kinase assay was performed as discussed above, replacing [$^{\gamma 32}$P]ATP with unlabelled 200 µM ATP. The ABSciex TripleTOF 5600 system (SCIEX) coupled with Eksigent 1D+ Nano LC system (SCIEX) was used to identify Menin's phosphorylated sites. Nano LC of enzymatic peptides was performed with the Eksigent 1D+ Nano LC equipped with the cHiPLC nanoflex system (SCIEX). Peptides were loaded onto the column and then eluted with a linear gradient of

5 - 40 % binary solvent B1 for 30 min at a flow rate of 0.3 mL/min. Mass spectrometry analysis of peptides was performed using the ABSciex TripleTOF 5600 system. Analysis was performed using the NanoSpray III source (SCIEX). The mass spectrometry was calibrated by the acquisition of [Glu1] fibrinopeptide (25 pmol/mL). The raw data were processed and searched with ProteinPilot™ software (version 4.0) using the Paragon algorithm. Proteins were identified by searching the UniProtKB human database and filtered at an R95 % confidence cut-off. Peptides for phosphorylated Men1 were identified at a 1 % false discovery rate.

Small ubiquitin-like modifier (SUMOylation) assay

We performed an *in vitro* SUMOylation assay with endogenously-expressed or overexpressed proteins. Briefly, HEK 293T cells were transfected with pcDNA3.1-Xpress-*MEN1* (WT or Y603F, Y603D, K493R, K609R mutants) and pcDNA3-HA-*SUMO-1* using iMFectin. 24 h after transfection, cells were lysed in NP-40 buffer. SUMOylated-Menin proteins were immunoprecipitated with Dynabeads™ Protein A beads (Invitrogen) coupled to Xpress tags or Protein A/G-Agarose (GenDEPOT) coupled to a Menin antibody and visualized with HA or SUMO1 antibodies. In other experiments we also pulldown Dynabeads™ Protein A beads (Invitrogen) coupled to HA or Menin antibody and visualized Menin-SUMOylation by blotting against Xpress and HA respectively. We analyzed SUMOylation of Menin by using the EpiQuik™ In Vivo Universal Protein Sumoylation Assay Kit (EPIGENTEK). Briefly, nuclear lysates from mESCs were prepared using the NE-PER cytoplasmic and nuclear protein extraction kit (ThermoFisher Scientific). SUMOylated proteins were pulldown using Dynabeads™ Protein A beads and 10 μg of pulldown protein was used for the assay.

SUMOylation intensity was calculated against a standard curve prepared from recombinant SUMO protein according to the manufacturer's protocol.

RNA-immunoprecipitation (RNA-IP) and RNP-immunoprecipitation (RNP-IP)

RNA-IP was performed according to Tang *et al*., 2018 [54]. Briefly, cDNA was used as a template to amplify hTR or mTR. The 5′ primers contained the T7 promoter sequence 5′-CCAAGCTTCTAATACGACTCACTATAGGGAGA-3′. PCR-amplified DNA was used as a template to transcribe biotinylated RNA using T7 RNA polymerase and biotinylated-UTP. One μg of purified biotinylated transcripts was incubated with 200 μg of nuclear extracts for 60 min at 4 °C. Complexes were isolated with streptavidin-conjugated agarose beads (MilliporeSigma), and the pull-down material was analyzed by Western blotting.

For RNP IP assays, cells were exposed to UVC (400 mJ/cm^2), and lysates were prepared in IP buffer (10 mM Hepes, pH 7.4, 50 mM β-glycerophosphate, 1 % Triton X-100, 10 % glycerol, 2 mM EDTA, 2 mM EGTA, 10 mM NaF, 1 mM DTT, protease inhibitor cocktail, NEM, RNase inhibitor) and immunoprecipitated with anti-Menin or anti-Xpress antibodies overnight. The complexes were washed twice with stringent buffer (100 mM Tris-HCl, pH 7.4, 500 mM LiCl, 0.1 % Triton X-100, and 1 mM DTT, protease inhibitor cocktail, N-ethylmaleimide, and RNase inhibitor) and twice with IP buffer. The RNA in RNP IP was assessed by qRT-PCR analysis and normalized with the copy number of the *U6* gene [54].

Mass spectrometry analysis of RNA-IP

A proteome-based approach was used for determining the protein targets associated with TR after transfection with *SUMO1* and *MEN1* Y603F or Y603D. First, HEK 293T cells were

transfected with *MEN1* mutants (Y603F or Y603D) and HA-tagged *SUMO-1* for 24 h. Nuclear lysates from the transfected cells were subjected to RNA-IP with TR. Differential protein expression across the samples was screened by conducting MS/MSALL with SWATHTM acquisition. The raw data were collected through Information Dependent Acquisition (IDA) and SWATHTM acquisition using ABSciex TripleTOF™ 5600 with Eksigent 1D+ nano LC (nanoLC-MS/MS instrument). Protein identification, MS peak extraction, and statistical analysis were performed with ProeinPilot™ (version 4.5), PeakView™ (version 2.2) and MarkerView™ (version 1.2), respectively. Bioinformatics analyses were conducted with the BioVenn program and displayed in a Venn-diagram of differential expressed proteins [55]. Protein classification was performed using the String software (https://string-db.org) and Graphpad prism 8.0 was used to make the pie diagram.

Cycloheximide Chase Assay

Cycloheximide (CHX) chase assay was performed in transfected HEK 293T cells using treatment of 50 µg/mL CHX (Cayman Chemical) at different time points. Briefly, $5x10^5$ cells were plated in a 6 well plate and transfected with Y603F-*MEN1* and Y603D-*MEN1* with or without *SUMO1*. Transfected media was replaced by fresh media containing 50 µg/mL CHX and treated for 0, 4 and 8 h. Lysate were prepared using M-PER™ mammalian protein isolation buffer (ThermoScientific).

Generation of Fyn knockout DC-iPS cells by CRISPR-Cas9

CRISPR-Cas9-mediated genome editing was performed transfecting DC fibroblasts with Fyn and control Double Nickase human Plasmids (Santa Cruz Biotechnology, Table EV6). according to the manufacturer's protocol. Immunoblots confirmed gene knockdown efficiency.

pY603-Menin antibody validation

The specificity of custom purified pTyr603-menin (pY603-menin) rabbit polyclonal antibody (Abclonal) was confirmed using a Lambda phosphatase assay (New England BioLabs).

Immunofluorescence-FISH (IF-FISH)

Unsynchronized cells were fixed on culture slides with 4 % paraformaldehyde at room temperature for 10 min, followed by permeabilization with 0.05 % Triton-X100 for 10 min. Slides were blocked in 5 % serum for 1 h, incubated overnight with a primary antibody, and incubated with a fluorochrome-tagged secondary antibody for 1 h. The same slides were subjected to FISH assay using telomeric PNA probes as described above.

FISH of TR was performed using the Single-Molecule Inexpensive FISH (smiFISH) method with slight modifications [56]. Briefly, FLAP oligos were annealed to 15 human telomeric RNA (hTR) probes (Table EV7) using a PCR machine with a denaturation step at 85 °C for 3 mins, and annealing at 65 °C for 3 mins and 25 °C for 5 mins. The probes used in this experiment recognize human TR RNA as well as mouse TR RNA due to high sequence similarity. About, 1×10^3 cells were grown onto 0.5 % gelatin-coated 4/8 well glass chambered slides (MilliporeSigma). Cells were fixed with 4 % paraformaldehyde for 20 min, rinsed twice with PBS, and permeabilized with 0.5 % Triton-X-100 in PBS for 5 min. After permeabilization, cells were washed twice with PBS followed by one wash with 1x SSC 15 % formamide buffer,

and incubated with the same buffer for an additional 15 min. Cells were then covered with smiFISH hybridization buffer (1x SSC, 15 % formamide, 4.5 mg/mL BSA, 10.6 % dextran sulfate, 2 mM VRC, 0.425 mg/mL tRNA, 0.08 µM FLAP-annealed probe set) and incubated at 37 °C overnight in a humidified chamber protected from light.

Slides were washed twice with 1X SSC, 15 % formamide at 37 °C for 30 mins, followed by rinsing twice in PBS. The slides were then blocked with IF antibody buffer (0.1 % Triton-X-100 and 2 % BSA in PBS) for 2 h and incubated with the primary antibody dissolved in the same buffer at 4 °C overnight. Slides were washed three times with 0.1 % Triton-X-100 in PBS and twice with the IF antibody buffer. Slides were incubated with Alexa fluor secondary antibodies resuspended in the IF antibody buffer for 1 h at room temperature. Slides were washed twice with IF antibody buffer and three times with 0.1 % Triton-X-100 in PBS and covered with DAPI with antifade.

For IF double FISH, TR FISH was performed followed by telomere FISH using a PNA probe as we previously described. IF was performed on the same slides.

Statistical analysis

Data were analyzed either by student's t-test or by one-way analysis of variance (ANOVA) followed by Tukey multiple comparisons test using the GraphPad Prism software (Ver 9.0). The frequency of distribution and detailed statistical analysis was performed using SPSS software (Ver 29.0). PCR data were obtained in at least three replicates. Western blot and ELISA quantitation was performed with at least three independent experiments. Immunofluorescent and FISH data were analyzed in at least 10 micrographs, unless it is indicated otherwise. Each

experiment was performed at least 3 times unless otherwise indicated. A probability of $p < 0.05$ was considered statistically significant. $^{*}p \leq 0.05$, $^{**}p \leq 0.01$, and $^{***}p \leq 0.001$

Acknowledgements

The authors thank Genomic Vision's 'TeloSizer® Triathlon Program' (Genomic Vision, Bagneux, France) and their help for Molecular Combing Assay. The authors are grateful to Tara Adams and Teri Bishop Johnson for their help to handle animal colonies, and Josh Monte and Todd Schuster for their help in Flow-FISH analysis. NIH grant R01-GM-143428 supported R.C-G. and W.C. An NIH/NCI grant R21-CA259630 and the National Scleroderma Foundation supported R.C-G. This work was supported by The Hormel Foundation.

Conflict of Interests

The authors have declared that no conflict of interest exists.

References

1. Shay, J. W. & Wright, W. E. Hallmarks of telomeres in ageing research. *J. Pathol*. **211**, 114–123 (2007).

2. Shay, J. W. Telomeres and aging. *Curr. Opin. Cell Biol.* **52,** 1–7 (2018).

3. Hiyama, E. & Hiyama, K. Telomere and telomerase in stem cells. *Br. J. Cancer.* **96**, 1020–1024 (2007).

4. Kirwan, M. & Dokal, I. Dyskeratosis congenita, stem cells and telomeres. *Biochim. Biophys. Acta Mol. Basis Dis.* **1792**, 371-379 (2009).

5. Mason, P. J. & Bessler, M. The genetics of dyskeratosis congenita. *Cancer Genet.* **204,** 635-645 (2011).

6. Kam, M. L. W., Nguyen, T. T. T. & Ngeow, J. Y. Y. Telomere biology disorders. *NPJ Genom Med.* **6**, 36 (2021).

7. Cifuentes-rojas, C. & Shippen, D. E. Telomerase regulation. *Mutat. Res.* **730**, 20–27 (2012).

8. Lee, S. S., Bohrson, C., Pike, A. M., Wheelan, S. J. & Greider, C. W. ATM Kinase Is Required for Telomere Elongation in Mouse and Human Cells. *Cell Rep.* **13**, 1623–1632 (2015).

9. Tong, A. S. et al. ATM and ATR Signaling Regulate the Recruitment of Human Telomerase to Telomeres. *Cell Rep.* **13**, 1633–1646 (2015).

10. Kim, J. E. et al. Fyn is a redox sensor involved in solar ultraviolet light-induced signal transduction in skin carcinogenesis. *Oncogene* **35**, 4091–4101 (2016).

11. Saito, Y. D., Jensen, A. R., Salgia, R. & Posadas, E. M. Fyn: A novel molecular target in cancer. *Cancer* **116,** 1629–1637 (2010).

12. Meyn, M. A., Schreiner, S. J., Dumitrescu, T. P., Nau, G. J. & Smithgall, T. E. Src family kinase activity is required for murine embryonic stem cell growth and differentiation. *Mol. Pharmacol.* **68**, 1320–1330 (2005).

13. Zhang, X., Simerly, C., Hartnett, C., Schatten, G. & Smithgall, T. E. Src-family tyrosine kinase activities are essential for differentiation of human embryonic stem cells. *Stem Cell Res.* **13**, 379–389 (2014).

14. Katona, B. W., Glynn, R. A., Hojnacki, T. A. & Hua, X. Menin: Expanding and dichotomous roles in cancer. *Oncoscience* **6**, 368-370 (2019).

15. Suphapeetiporn, K., Greally, J. M., Walpita, D., Ashley, T. & Bale, A. E. MEN1 tumor-suppressor protein localizes to telomeres during meiosis. *Genes Chromosom. Cancer* **35**, 81-85 (2002).

16. Paul, S. et al. Centromere defects, chromosome instability, and cGAS-STING activation in systemic sclerosis. *Nat. Commun.* **13,** 7074 (2022).

17. Blanpain, C. & Fuchs, E. Epidermal Stem Cells of the Skin. *Annu. Rev. Cell Dev. Biol*. **22**, 339-373 (2006).

18. Andersson-Rolf, A., Zilbauer, M., Koo, B. K. & Clevers, H. Stem cells in repair of gastrointestinal epithelia. *Physiology* **32**, 278–289 (2017).

19. Skvortsov, D. A., Zvereva, M. E., Shpanchenko, O. V & Dontsova, O. A. Assays for Detection of Telomerase Activity. *Acta Naturae* **3**, 48-68 (2011).

20. Podlevsky, J. D. & Chen, J. J. L. It all comes together at the ends: Telomerase structure, function, and biogenesis. *Mutat. Res*. **730**, 3-11 (2012).

21. Liu Y et al. Shwachman-Diamond Syndrome Protein SBDS Maintains Human Telomeres by Regulating Telomerase Recruitment. *Cell Rep.* 13 1849-1860 (2018).

22. Ramlee, M. K., Wang, J., Toh, W. X. & Li, S. Transcription regulation of the human telomerase reverse transcriptase (hTERT) gene. *Genes (Basel)* **7**, 50 (2016).

23. Hashimoto, M. et al. Role of menin in the regulation of telomerase activity in normal and cancer cells. *Int. J. Oncol.* **33**, 333–340 (2008).

24. Chen, Y. et al. Human cells lacking coilin and Cajal bodies are proficient in telomerase assembly, trafficking and telomere maintenance. *Nucleic Acids Res*. **43**, 385-395 (2015).

25. Vogan, J. M. et al. Minimized human telomerase maintains telomeres and resolves endogenous roles of H/ACA proteins, TCAB1, and Cajal bodies. *Elife* **5**, e18221 (2016).

26. Zhu, Y., Tomlinson, R. L., Lukowiak, A. A., Terns, R. M. & Terns, M. P. Telomerase RNA Accumulates in Cajal Bodies in Human Cancer Cells. *Mol. Biol. Cell* **15**, 81-90 (2004).

27. Schmidt, J. C. & Cech, T. R. Human telomerase: Biogenesis, trafficking, recruitment, and activation. *Genes and Dev*. **29**, 1095-1105 (2015).

28. Schmidt, J. C., Zaug, A. J. & Cech, T. R. Live Cell Imaging Reveals the Dynamics of Telomerase Recruitment to Telomeres. *Cell* **166**, 1188-1197 (2016).

29. Brault, M. E., Lauzon, C. & Autexier, C. Dyskeratosis congenita mutations in dyskerin SUMOylation consensus sites lead to impaired telomerase RNA accumulation and telomere defects. *Hum. Mol. Genet*. **22**, 3498-3507 (2013).

30. MacNeil, D. E. et al. SUMOylation- and GAR1-Dependent Regulation of Dyskerin Nuclear and Subnuclear Localization. *Mol. Cell. Biol.* **41**, e00464-20 (2021).

31. Sanyal, S., Mondal, P., Sen, S., Sengupta, S. & Das, C. SUMO E3 ligase CBX4 regulates hTERT-mediated transcription of CDH1 and promotes breast cancer cell migration and invasion. *Biochem. J*. **477**, 3803-3818 (2020).

32. Kim, J. H. et al. Roles of sumoylation of a reptin chromatin-remodelling complex in cancer metastasis. *Nat. Cell Biol*. **8**, 631-639 (2006).

33. Jung, H. K. et al. SUMOylation of pontin chromatin-remodeling complex reveals a signal integration code in prostate cancer cells. *Proc. Natl. Acad. Sci. U. S. A.* **104**, 20793–20798 (2007).

34. Geiss-Friedlander, R. & Melchior, F. Concepts in sumoylation: A decade on. *Nat. Rev. Mol. Cell Biol.* **8,** 947-956 (2007).

35. Hietakangas, V. et al. PDSM, a motif for phosphorylation-dependent SUMO modification. *Proc. Natl. Acad. Sci. U. S. A.* **103**, 45-50 (2006).

36. Feng, Z.-J., Gurung, B., Jin, G.-H., Yang, X.-L. & Hua, X.-X. SUMO modification of menin. *Am. J. Cancer Res*. **3,** 96-106 (2013).

37. Zhao, Q. et al. GPS-SUMO: A tool for the prediction of sumoylation sites and SUMO-interaction motifs. *Nucleic Acids Res*. **42**, W325-30 (2014).

38. Roake, C. M. & Artandi, S. E. Regulation of human telomerase in homeostasis and disease. *Nat. Rev. Mol. Cell Biol*. **21**, 384–397 (2020).

39. Mitchell, J. R., Wood, E. & Collins, K. A telomerase component is defective in the human disease dyskeratosis congenita. *Nature* **402**, 551-555 (1999).

40. Ayas, M. & Ahmed, S. O. Dyskeratosis Congenita. *Congenital and Acquired Bone Marrow Failure* **Chapter 18**, 225–233 (2017).

41. Agarwal, S. et al. Telomere elongation in induced pluripotent stem cells from dyskeratosis congenita patients. *Nature* **464**, 292–296 (2010).

42. Batista, L. F. Z. et al. Telomere shortening and loss of self-renewal in dyskeratosis congenita induced pluripotent stem cells. *Nature* **474**, 399-402 (2011).

43. Woo, D. H. et al. Enhancing a Wnt-Telomere Feedback Loop Restores Intestinal Stem Cell Function in a Human Organotypic Model of Dyskeratosis Congenita. *Cell Stem Cell* **19**, 397-405 (2016).

44. Fernandez, R. J. et al. GSK3 inhibition rescues growth and telomere dysfunction in dyskeratosis congenita iPSC-derived type II alveolar epithelial cells. *Elife* **11**, 1–28 (2022).

45. Teruit, Y., Saad, N., Jia, S., McKeon, F. & Yuan, J. Dual role of sumoylation in the nuclear localization and transcriptional activation of NFAT1. *J. Biol. Chem*. **279**, 28257–28265 (2004).

46. Stein, P. L., Lee, H. M., Rich, S. & Soriano, P. pp59fyn mutant mice display differential signaling in thymocytes and peripheral T cells. *Cell* **70**, 741-750 (1992).

47. Bryja, V., Bonilla, S. & Arenas, E. Derivation of mouse embryonic stem cells. *Nat. Protoc*. **1**, 2082–2087 (2006).

48. Canela, A. S., Vera, E., Klatt, P. & Blasco, M. A. High-throughput telomere length quantification by FISH and its application to human population studies. *Proc. Natl. Acad.Sci. U. S. A*. **104,** 5300–5305 (2007).

49. Mourkioti, F. et al. Role of telomere dysfunction in cardiac failure in Duchenne muscular dystrophy. *Nat. Cell Biol.* **15**, 895–904 (2013).

50. Schmid, I. & Jamieson, B. D. Assessment of Telomere Length, Phenotype, and DNA Content. *Curr. Protoc. Cytom*. **Chapter 7**, 7.26.1-7.26.13 (2004).

51. Kahl, V. F. S. et al. Telomere Length Measurement by Molecular Combing. *Front. Cell Dev. Biol.* **8**, 493 (2020).

52. Wang, F. et al. Robust measurement of telomere length in single cells. *Proc. Natl. Acad. Sci. U. S. A.* **110**, E1906-12 (2013).

53. Rueden, C. T. et al. ImageJ2: ImageJ for the next generation of scientific image data. *BMC Bioinformatics* **18**, 529 (2017).

54. Tang, H. et al. HuR regulates telomerase activity through TERC methylation. *Nat. Commun.* **9**, 2213 (2018).

55. Hulsen, T., de Vlieg, J. & Alkema, W. BioVenn - A web application for the comparison and visualization of biological lists using area-proportional Venn diagrams. *BMC Genomics* **9**, 488 (2008).

56. Querido, E., Sfeir, A. & Chartrand, P. Imaging of Telomerase RNA by Single-Molecule Inexpensive FISH Combined with Immunofluorescence. *STAR Protoc.* **1**, 100104 (2020).

Figure legends

Fig. 1. Fyn inhibition slows telomere erosion in mESCs and tissue

A. Representative images of Q-FISH telomere analysis in metaphase chromosomes of mESCs isolated from WT and Fyn$^{-/-}$ mice (passage 12). Scale bar is 5 µm.

B. Representative images of Q-FISH telomere analysis in metaphase chromosomes of stable sh-Mock and sh-Fyn E14 cells (passage 18). Scale bar is 5 µm.

C. Fyn and β-actin western blots in WT and Fyn$^{-/-}$ mESCs.

D. Fyn and β-actin western blots in sh-Mock and sh-Fyn E14 cells.

E. Representative images of female and male colon from 97-week-old WT and Fyn$^{-/-}$ mice used in Q-FISH analysis. Scale bar is 20 µm. Arrows indicate telomeres.

F. Representative images of female and male skin from 97-week-old WT and Fyn$^{-/-}$ mice used in Q-FISH analysis. Scale bar is 20 µm. Arrows indicate telomeres.

Data Information: In (A and B), the Mean Telomere Fluorescent Indexes, shown at the right of each figure, was calculated from 400 telomeres in 20 metaphase spreads. In (C and D), β-actin served as a loading control. Protein molecular weights are shown at the right. In (E and F), the Mean Telomere fluorescence indexes shown in a graph plot at the right of the figures were quantitated using the Telometer program (n = 100 nuclei). In (A, B, E, F), data are presented as mean ± SD from a two-tailed t-test (**** = $p < 0.0001$). A probability of $p < 0.05$ was considered statistically significant.

Fig. 2. Molecular Combing Assay shows that Fyn inhibition slows telomere erosion in mESCs

A. Representative images of telomere analysis using Molecular Combing Assays from genomic DNA of mESCs isolated from WT mice (passage 12). The scale bar is 20 µm.

B. Representative images of telomere analysis using Molecular Combing Assays from genomic DNA of mESCs isolated from $Fyn^{-/-}$ (B) mice (passage 12). The scale bar is 20 µm.

C. Absolute Telomere length of WT and $Fyn^{-/-}$ mESCs.

D. Representative images of telomere analysis using Molecular Combing Assays from genomic DNA of stable sh-Mock E14 cells (passage 18). The scale bar is 20 µm.

E. Representative images of telomere analysis using Molecular Combing Assays from genomic DNA of stable sh-Fyn E14 cells (passage 18). The scale bar is 20 µm.

F. Absolute Telomere length of Sh-Mock and Sh-Fyn E14 cells.

Data information: In (A, B, D, E), a detailed statistical analysis and frequency of distribution of telomere sizes in chromatin fibers are shown below sample images. The telomere size was quantified using a telomere probe. Q1, quartile 1; Q2, quartile 2 and Q3, quartile 3. In (C and F), data are presented as means ± SD from a two-tailed t-test (*** = $p < 0.001$, * = $p < 0.1$). A probability of $p < 0.05$ was considered statistically significant.

Fig. 3. Fyn phosphorylates Menin at tyrosine 603

A. Immunoprecipitation using an anti-Fyn antibody followed by Western blotting using an anti-Menin antibody showing the interaction of endogenous Fyn and Menin in E14 ES cells.

B. Immunoprecipitation using an anti-Fyn antibody followed by Western blotting using an anti-Menin antibody showing the interaction of endogenous Fyn and Menin in primary mESCs.

C. Active Fyn and full-length Menin were subjected to an *in vitro* kinase assay with [γ-^{32}P]ATP. Phosphorylated Menin was visualized by autoradiography. β-catenin was used as a positive control. Menin and β-catenin were stained with Coomassie blue as loading controls (lower gel).

D. Fyn phosphorylates Menin at tyrosine 603. *In vitro* kinase assay of Fyn-mediated phosphorylation of full-length His-Menin and mutant His-Y603F-Menin in the presence of [γ-32P]ATP. β-catenin was used as a positive control. Phosphorylated Menin was detected by autoradiography. Increased phosphorylation was detected in WT Menin compared to mutant Y603F Menin. The lower gel matches the key above to show WT Menin, Y603F Menin, and β-catenin stained with Coomassie blue.

E. Quantification of Fyn-mediated phosphorylation of full-length His-Menin and mutant His-Y603F-Menin in the presence of [γ-32P]ATP. Data are presented as mean ± SD from a two-tailed t-test (**** = $p < 0.0001$). A probability of $p < 0.05$ was considered statistically significant.

F. *In vitro* kinase assay of Fyn-mediated phosphorylation of WT His-Menin and mutant Y603F His-Menin in the presence of 200 μM ATP and phosphatase. Phosphorylated Menin was detected by Western blot using a custom-synthesized antibody against (phospho-tyrosine 603-Menin) pY603-Menin. WT-His-Menin shows increased pY603 compared to Y603F His-Menin. Fyn-mediated phosphorylation of Menin was blocked using Lambda phosphatase as indicated in the materials and methods section. The phosphatase effect was reversed using a phosphatase inhibitor (PhI).

G. *In vivo* kinase assay of Xpress-Menin pulldown in HEK 293T cells. Xpress-Menin and HA-Fyn were over-expressed in HEK 293T cells. pY603-Menin was visualized by Western blotting

using a custom-synthesized antibody against pY603-Menin. Lambda phosphatase was used to block Menin phosphorylation. The phosphatase effect was reversed using a PhI. Pulldown of Xpress-tagged Menin and immunoblot against Menin shows the presence of pull-down proteins in all lanes (middle blot). Pulldown of Xpress-tagged Menin and immunoblot against the HA-tagged antibody shows the presence of Fyn in Fyn-positive lanes (lower blot).

H. *In vivo* kinase assay of endogenous Menin pulldown in E14 mESCs. pY603-Menin was visualized by Western blotting using a custom-synthesized antibody against pY603-Menin. Lambda phosphatase was used to block Menin phosphorylation. The phosphatase effect was reversed using a PhI. Anti-Menin immunoblot of endogenous Menin pulldown shows Menin in all samples (bottom blot). IgG serves as the negative control.

Data information: Molecular weight markers are shown at the right of each blot. In (C, D, F, G, H), the black arrow indicates phosphorylated Menin. In (C, D), red arrow indicates β-catenin phosphorylation by Fyn. * indicates nonspecific bands. In (C, D), AP = autophosphorylation. In (E), The phosphorylation band intensities of WT Menin and Y603F Menin from (D) were quantified using ImageJ. In (F), the same membrane was stripped and reprobed using anti-Menin or anti-Fyn antibodies (lower blots).

Fig. 4. Fyn promotes Menin co-localization to telomeres and association with telomerase RNA *in vitro*

A. IF-FISH analysis of unsynchronized interphase cells in WT and $Fyn^{-/-}$ mESCs shows Menin and telomere co-localization. The scale bar is 10 μm. Telomere/Menin co-localization analysis

was performed manually. Totally merged and partially merged Telomere/Menin signals were considered co-localization counts.

B. Western blotting of *in vitro* transcribed Telomerase RNA (TR) pulldown assays using nuclear lysates from WT Fyn and $Fyn^{-/-}$ mESCs shows Menin interaction with TR.

C. RNP pulldown assay with anti-Menin antibody followed by qRT-PCR for TR in WT and $Fyn^{-/-}$ mESCs shows increased TR amplification in WT vs $Fyn^{-/-}$ mESCs.

D. Representative IF-FISH images and quantification of Pearson correlation coefficient (*r*) of colocalization shows significantly higher Menin (IF) and TR (FISH) binding in WT cells compared to $Fyn^{-/-}$ cells. The scale bar is 5µm.

E. Representative of IF-FISH images and quantification of Pearson correlation coefficient (*r*) of colocalization shows no significant difference in Coilin (IF) and TR (FISH) binding in WT cells compared to $Fyn^{-/-}$ cells. The scale bar is 5 µm.

Data information: In (A), data are presented as means of co-localization counts ± SD in 20 nuclei counts. In (B), molecular weight markers are shown at the right. In (D, E), co-localization was analyzed using ImageJ plugin 'Coloc 2'. In (E), Coilin fluorescence is represented by pseudo color yellow instead of magenta. In (A, C, D, E), unpaired student's t-test was used for statistical analysis (ns, non-significant, ** = $p < 0.01$, **** = $p < 0.0001$). A probability of $p < 0.05$ was considered statistically significant.

Fig. 5. Phosphorylation of Menin at Y603 promotes SUMO1 modification at K609

A. Fyn is important for SUMO1 modification of endogenous Menin. Immunoprecipitation of Menin and Western blotting of SUMO1 in sh-Mock and sh-Fyn E14 cells (upper). Menin expression in Menin-immunoprecipitated samples (middle). SUMO1 expression in input (lower).

B. SUMO1-Menin intensity was quantified using ImageJ. Menin densitometry was used to normalize SUMO1-Menin intensity.

C. Mutations at tyrosine 603 and lysine 609 impair SUMO1 modification of Menin as shown by immunoprecipitation of overexpressed WT or mutant Xpress-tagged Menin and immunoblotting of HA-tagged SUMO1 in HEK 293T cells. Phosphodeficient Menin mutant (Y603F) and a SUMO-deficient Menin mutant (K609R) show reduced SUMO1 modification, whereas the phosphomimetic mutant Y603D Menin mutant shows increased SUM1 modification. Black arrow, SUMO1-Menin, red arrow, Menin; FT, flowthrough.

D. Quantification of SUMO1-Menin intensity in (C). Menin densitometry from IP: Xpress, IB: Menin in (C) was used to normalize SUMO1-Menin intensity.

E. Mutations at tyrosine 603 and lysine 609 impair SUMO1 modification of Menin as shown by immunoprecipitation of overexpressed WT or mutant Menin and immunoblotting of HA-tagged SUMO1 in HEK 293T cells. Phosphodeficient Menin mutant (Y603F) and a SUMO-deficient Menin mutant (K609R) show reduced SUMO1 modfication, whereas the phosphomimetic mutant Y603D Menin mutant shows increased SUMO1 modification.

F. Phosphodeficient Menin mutant (Y603F) and a SUMO-deficient Menin mutant (K609R) show reduced SUMO1 modification, whereas the phosphomimetic mutant Y603D Menin mutant showed increased SUMO1 modification as shown by pulldown of HA-tagged SUMO1 and immunoblotting of Xpress-tagged Menin in HEK 293T cells.

Data information: Molecular weight markers are shown at the right of each blot. A probability of $p < 0.05$ was considered statistically significant. In (B), Data are presented as means ± SD from a two-tailed t-test (*** = $p < 0.001$). In (D), Data are presented as means ± SD from a One-way ANOVA followed by Tukey's multiple comparison tests (**** = $p < 0.0001$).

Fig. 6. Menin Phosphorylation and SUMO1 modification promote Menin association with telomerase RNA by increasing protein stability

A. Phosphorylation and SUMO1 modification of Menin promote Menin-TR association. RNA pulldown assay using *in vitro* transcribed TR and overexpressed WT or mutant (Y603F, Y603D, K609R) Menin with *or* without SUMO1. Menin was analyzed with an Xpress antibody that binds the C-terminal Xpress Tag of the protein or a Menin antibody that binds the central region of Menin. The Western blot using Xpress antibody indicates that Y603D Menin with SUMO1 expression is greatly increased in TR pulldown complex compared to WT, Y603F and K609R Menin with or without SUMO1 expression. Y603D-Menin shows less expression in TR pulldown binding than Y603D-Menin+SUMO1. No significant changes were detected with Menin antibody. β-actin served as a loading control.

B. Western blotting of cytoplasmic and nuclear protein extracts shows that phosphomimetic Y603D-MEN1 and SUMO1 promote Menin stability. HEK 293T cells were transfected with Xpress-tagged *MEN1* (WT or Y603F, Y603D) with or without HA-tagged SUMO1. Lamin B served as a loading control.

C. Cycloheximide chase assay showing significantly higher protein degradation in Y603F-Menin with or without SUMO1 compared to Y603D-Menin with or without SUMO1. Y603F and

Y603D *MEN1*-transfected HEK 293T cells co-transfected with *SUMO1* were treated with 50μg/mL cycloheximide for indicated time points. B-actin served as a loading control.

Data information: Molecular weight markers are shown at the right of each blot. The Y603D-Menin+SUMO1 lane in (A) was intentionally loaded with less sample in order to show similar intensities of Xpress-Menin in the Input.

Fig. 7. SUMO1-modified Menin disrupts TR's association with Dyskerin and GAR1

A. A Venn diagram determined by mass spectrometry analysis displays differential proteins recruited to TR after Y603F-*MEN1*+*SUMO1* or Y603D-*MEN1*+*SUMO1* transfection in 293T cells.

B. Pie charts show TR binding proteins in the Y603F-*MEN1*+*SUMO1*-transfected 293T sample, but not in the Y603D-*MEN1*+*SUMO1*-transfected 293Tsample.

C. Western blotting of *in vitro* transcribed TR pulldown assay from whole cell lysates of HEK 293T cells with over-expressed mutant (Y603F, Y603D) Menin and SUMO1 shows decreased Dyskerin and GAR1 binding in Y603D-*MEN1*+*SUMO1*-transfected cells. Coilin binding shows no difference between Y603F vs Y603D. Xpress-tagged Menin shows increased binding in Y603D-Menin compared to Y603F-Menin although Menin expression shows no difference. β-actin was used as a loading control.

D. Western blotting of *in vitro* transcribed TR pulldown assay from whole cell lysates of HEK 293T cells with over-expressed mutant (Y603D, K609R) Menin and SUMO1 shows increased Dyskerin and GAR1 binding in K609R-*MEN1*+SUMO1 transfected cells. Coilin binding shows

no difference between Y603D vs K609R. Xpress-tagged Menin shows increased binding in Y603D-Menin compared to K609R-Menin although Menin expression shows no difference. β-actin was used as a loading control.

E. Quantification of the Pearson correlation coefficient (*r*) of colocalization of Dyskerin and TR from Fig. 7F shows significantly less Dyskerin and TR binding in Y603D-*MEN1*+SUMO1 transfected 293T cells compared to mutant Y603F-*MEN1+SUMO1* and K609R-*MEN1*+SUMO1 transfected cells.

F. Representative IF-FISH images show significantly less Dyskerin and TR binding in Y603D-*MEN1*+SUMO1 transfected 293T cells compared to mutant Y603F-*MEN1+SUMO1* and K609R-*MEN1*+SUMO1 transfected cells. The scale bar is 5 μm.

Data information: In (C, D), molecular weight markers are shown at the right of each blot. In (E), colocalization was analyzed using ImageJ plugin 'Coloc 2'. Data are presented as means ± SD from a one-way ANOVA followed by Tukey's multiple comparison tests (** = $p < 0.01$, *** = $p < 0.001$). A probability of $p < 0.05$ was considered statistically significant.

Fig. 8. Menin knockdown improves Dyskerin localization to telomeres and increases telomere length without affecting Dyskerin accumulation in Cajal bodies

A. Western blotting of Menin in sh-Mock and sh-Menin HEK 293T cells. β-actin served as a loading control.

B. Quantification of the Pearson correlation coefficient (*r*) for Coilin/Dyskerin co-localization analysis obtained by IF of Dyskerin, Coilin, and FISH of TR in Fig. 8D.

C. Quantification of the Pearson correlation coefficient (*r*) for Coilin/TR co-localization analysis obtained by IF of Dyskerin, Coilin, and FISH of TR in Fig. 8D.

D. Representative IF-FISH images of Coilin/Dyskerin and Coilin/TR in Sh-Mock and Sh-Menin 293T cells. The scale bar is 5µm.

E. Representative images of Dyskerin IF and TR/Telomere FISH in Sh-Mock and Sh-Menin 293T cells. The scale bar is 5µm.

F. Quantification of Pearson correlation coefficient (*r*) of colocalization shows significantly more Dyskerin/telomere co-localization in sh-Menin cells compared to sh-Mock HEK 293Tcells.

G. Quantification of Pearson correlation coefficient (*r*) of colocalization shows significantly more Dyskerin/TR co-localization in sh-Menin cells compared to sh-Mock HEK 293Tcells.

H. Telomere length in sh-Menin 293T cells and sh-Mock cells as determined by quantitative PCR at passages 5 and 10. T/S ratios were calculated relative to the single-copy gene *Alu*.

Data information: In (A), Molecular weight markers are shown at the right. In (B, C, F, G), co-localization was analyzed using ImageJ plugin 'Coloc 2'. In (D), Arrows indicate colocalization between Dyskerin and Coilin. Region of interest (ROI) was used to analyze Coilin/Dyskerin co-localization. A pseudo color yellow was used replacing magenta for Coilin. In (E), Arrows indicate colocalization between Dyskerin, telomere and TR. Region of interest (ROI) was used to analyze co-localization. A pseudo color yellow was used replacing magenta for Dyskerin. For (B, C, F, G), Data are presented as means ± SD from an unpaired student's t-test (* = $p < 0.05$, *** = $p < 0.0001$), ns, non-significant. For (H), Data are presented as means ± SD from a one-way ANOVA followed by Tukey's multiple comparison tests (* = $p < 0.05$). A probability of $p < 0.05$ was considered statistically significant.

Fig. 9. Fyn knockdown in Human DC iPSCs slows telomere erosion

A. Western blotting showing *Fyn* gene knockdown efficiency in DC iPSCs using CRISPR-Cas9- and the expression of Menin and pY603-Menin. β-actin served as a loading control.

B. Densitometry by ImageJ shows knockdown of Fyn in Fyn^{KD} DC iPSC vs mock DC-iPSC.

C. Densitometry by ImageJ shows reduced expression of pY603-Menin in Fyn^{KD} DC iPSC vs mock DC-iPSC.

D. Representative images of interphase telomere Q-FISH analysis in Fyn^{KD} DC iPSCs vs mock DC iPSCs at passages 3 and 12. The scale bar is 5µm.

E. Quantification of Q-FISH images reveal no significant differences in telomere length at passages 3 of Fyn^{KD} DC iPSCs vs mock DC iPSCs (n = 50 nuclei).

F. Quantification of Q-FISH images show significant differences in telomere length at passages 12 of Fyn^{KD} DC iPSCs vs mock DC iPSCs (n = 50 nuclei).

G. Flow-FISH analysis showed higher telomeric mean fluorescence in Fyn^{KD} DC iPSCs vs mock-DC-iPSCs at passages 12.

H. qRT-PCR analysis shows a significantly higher T/S ratio in Fyn^{KD} DC iPSCs vs mock-DC-iPSCs at passages 12. The human *Alu* gene was used for normalization.

I. Representative images of telomere analysis using a Molecular Combing assay from genomic DNA fibers isolated from Mock iPSC at passage 12. The scale bar is 20 µm. A detailed statistical analysis and frequency distribution are shown below each sample DNA fiber image.

J. Representative images of telomere analysis using a Molecular Combing assay from genomic DNA fibers isolated from Fyn^{KD} iPSC at passage 12. The scale bar is 20 µm. A detailed statistical analysis and frequency distribution are shown below each sample DNA fiber image.

K. Absolute Telomere length in kb (n= 240 DNA fibers) between mock iPSC vs Fyn^{KD} iPSC at passages 12.

Data information: In (A), Molecular weight markers are shown at the right. In (I, J), Q1, quartile 1; Q2, quartile 2 and Q3, quartile 3. In (B, C, E, F, G, H, K), data are presented as means ± SD from a two-tailed t-test (ns = not significant, * = $p < 0.05$, ** = $p < 0.01$, *** = $p < 0.001$, **** = $p < 0.0001$). A probability of $p < 0.05$ was considered statistically significant.

Extended View Figure Legends

Fig. EV1. Fyn inhibition slows telomere erosion in mouse colon tissue

Representative images (in duplicates) of Q-FISH analysis using telomere and centromere probes on colon tissue of 43-week-old wild type and $Fyn^{-/-}$ female mice, showing that Fyn knockout mice have significantly higher telomere fluorescence (green dots). The scale bar is 20 μm.

Data information: A pseudo color grey was used, replacing blue for nucleus.

Fig. EV2. Fyn inhibition slows telomere erosion in mouse colon tissue

A. Frequency of distribution and detailed statistics of mean telomere fluorescence quantified from Fig. EV1 using Telometer in colon tissue from WT mice (n=1947)

B. Frequency of distribution and detailed statistics of mean telomere fluorescence quantified from Fig. EV1 using Telometer in colon tissue from $Fyn^{-/-}$ mice (n=1805).

C. Differences in mean telomere fluorescence in WT and $Fyn^{-/-}$ mice colon. Centromere FISH signals were used as a staining control.

D. Differences in mean centromere fluorescence in WT and $Fyn^{-/-}$ mice colon.

E. Telomere/centromere fluorescence in WT and $Fyn^{-/-}$ mice colon. Centromere FISH signals were used as a staining control.

Data information: In (A, B), Q1, quartile 1; Q2, Quartile 2; Q3, quartile 3. In (C, D, E), Data are presented as fluorescent means ± SD from a two-tailed t-test (ns=no significant, **** = $p < 0.0001$). A probability of $p < 0.05$ was considered statistically significant.

Fig. EV3. Fyn inhibition slows telomere erosion in mouse liver tissue

Representative images (in duplicates) of Q-FISH analysis using telomere and centromere probes on liver tissue of 43-week-old wild type and $Fyn^{-/-}$ female mice, showing that Fyn knockout mice have significantly higher telomere fluorescence (green dots). The scale bar is 20 μm.

Data information: A pseudo color grey was used, replacing blue for nucleus.

Fig. EV4. Fyn inhibition slows telomere erosion in mouse liver tissue

A. Frequency of distribution and detailed statistics of mean telomere fluorescence quantified from Fig. EV3 using Telometer in liver tissue from WT mice (n=142)

B. Frequency of distribution and detailed statistics of mean telomere fluorescence quantified from Fig. EV3 using Telometer in liver tissue from $Fyn^{-/-}$ mice (n=168).

C. Differences in mean telomere fluorescence in WT and $Fyn^{-/-}$ mice liver. Centromere FISH signals were used as a staining control.

D. Differences in mean centromere fluorescence in WT and $Fyn^{-/-}$ mice liver.

E. Telomere/centromere fluorescence in WT and $Fyn^{-/-}$ mice liver. Centromere FISH signals were used as a staining control.

Data information: In (A, B), Q1, quartile 1; Q2, Quartile 2; Q3, quartile 3. In (C, D, E), Data are presented as fluorescent means ± SD from a two-tailed t-test (ns=no significant, **** = $p < 0.0001$). A probability of $p < 0.05$ was considered statistically significant.

Fig. EV5. Fyn inhibition slows telomere erosion in mouse skin tissue

Representative images (in duplicates) of Q-FISH analysis using telomere and centromere probes on liver tissue of 43-week-old wild type and $Fyn^{-/-}$ female mice, showing that Fyn knockout mice

have significantly higher telomere fluorescence (green dots). The scale bar is 20 μm.

Data information: A pseudo color grey was used, replacing blue for nucleus.

Fig. EV6. Fyn inhibition slows telomere erosion in mouse skin tissue

A. Frequency of distribution and detailed statistics of mean telomere fluorescence quantified from Fig. EV5 using Telometer in skin tissue from WT mice (n=304)

B. Frequency of distribution and detailed statistics of mean telomere fluorescence quantified from Fig. EV5 using Telometer in skin tissue from $Fyn^{-/-}$ mice (n=436).

C. Differences in mean telomere fluorescence in WT and $Fyn^{-/-}$ mice skin. Centromere FISH signals were used as a staining control.

D. Differences in mean centromere fluorescence in WT and $Fyn^{-/-}$ mice skin.

E. Telomere/centromere fluorescence in WT and $Fyn^{-/-}$ mice skin. Centromere FISH signals were used as a staining control.

Data information: In (A, B), Q1, quartile 1; Q2, Quartile 2; Q3, quartile 3. In (C, D, E), Data are presented as fluorescent means ± SD from a two-tailed t-test (ns=no significant, **** = $p < 0.0001$). A probability of $p < 0.05$ was considered statistically significant.

Fig. EV7. Fyn deletion or inhibition slows telomere erosion in mouse embryonic stem cells

A. Representative images of morphology of mESCs isolated from WT and $Fyn^{-/-}$ mice. The scale bar is 50 μm.

B. Representative images of AP staining of mESCs isolated from WT and $Fyn^{-/-}$ mice. The scale bar is 20 μm.

C. IF analysis of stem cell markers KLF4 and SOX2 in mESCs isolated from WT mice. The

scale bar is 10 μm.

D. IF analysis of stem cell markers KLF4 and SOX2 in mESCs isolated from $Fyn^{-/-}$ mice. The scale bar is 10 μm.

E. Representative images of interphase nuclei Q-FISH analysis of wild type vs $Fyn^{-/-}$ mESCs at passage P12 (top) and sh-Mock vs sh-Fyn E14 cells at passage 18 (bottom) The scale bar is 5 μm. F. Quantification of fluorescent signal using the Telometer program in WT vs $Fyn^{-/-}$ mESCs. Showing higher telomere fluorescence intensity in Fyn deficient conditions. n = 20 interphase nuclei.

G. Quantification of fluorescent signal using the Telometer program in sh-Mock vs sh-Fyn E14 cells showing higher telomere fluorescence intensity in Fyn deficient conditions. n = 20 interphase nuclei.

Data information: In (F, G), data are presented as means ± SD from a two-tailed t-test (** = $p < 0.01$, *** = $p < 0.001$). A probability of $p < 0.05$ was considered statistically significant.

Fig. EV8. Fyn deletion or inhibition slows telomere erosion in mouse embryonic? stem cells

A, B. Telomere erosion is stabilized in $Fyn^{-/-}$ vs WT mESCs as determined by telomere measurement by Flow-FISH analysis and T/S ratio calculated by quantitative PCR (qRT-PCR), respectively.

C, D. Telomere erosion is stabilized in sh-Fyn vs sh-Mock-transfected mouse embryonic stem? cells as determined by telomere measurement by Flow-FISH analysis and T/S ratio calculated by qRT-PCR, respectively.

E. Q-FISH analysis of sh-Mock, sh-Fyn and sh-Fyn/Fyn over-expression in E14 cells, showing that overexpression of the *Fyn* gene in sh-Fyn cells promotes telomere erosion.

F. Western blotting analysis confirmed Fyn knockdown. β-actin acts as loading control.

G. Western blotting analysis confirmed the over-expression status of Fyn. Tubulin acts as loading control.

H. Mean telomere fluorescence was calculated using a Telometer program from panel E.

Data information: In (B, D), T/S ratios were calculated relative to the single-copy gene 36B4. Data are presented as means ± SD from a two-tailed t-test (* = $p < 0.05$, ** = $p < 0.01$). In (F, G), Molecular weight markers are shown at the right of each blot. In (H), data are presented as means ± SD from one-way ANOVA followed by Tukey's multiple comparison test (**** =$p < 0.0001$). A probability of $p < 0.05$ was considered statistically significant.

Fig. EV9. Fyn deletion improves telomere length in mouse tissue

A. Representative image of genotyping of wild type $Fyn^{+/+}$, heterozygous $^{-/+}$, and $Fyn^{-/-}$ mice.

B. IHC analysis of Fyn in colon or skin tissue of female and male wild type and $Fyn^{-/-}$ mice. The scale bar is 20 μm.

C, D. Quantitation of IHC images using imageJ shows reduced expression of Fyn in colon and skin tissue of female $Fyn^{-/-}$ mice.

E, F. Quantitation of IHC images using imageJ shows reduced expression of Fyn in colon and skin tissue of male $Fyn^{-/-}$ mice.

Data information: In (C, D, E, F), data are presented as means ± SD. An unpaired student's t-test was used for statistical analysis. A probability of $p < 0.05$ was considered statistically significant (**** = $p < 0.0001$).

Fig. EV10. Fyn does not inhibit telomerase activity *in vitro*

A. Western blotting of Fyn and TERT in WT and Fyn$^{-/-}$ mESCs. β-actin served as a loading control. Densitometry analysis by ImageJ shows no significant difference in TERT expression.

B. Western blotting of Fyn and TERT in sh-Mock and sh-Fyn E14 cells. β-actin served as a loading control. Densitometry analysis by ImageJ shows no significant difference in TERT expression.

C. Telomerase enzyme activity (TRAP assay fold change) was not significantly different between WT and Fyn$^{-/-}$ mESCs.

D, Telomerase enzyme activity was not significantly different between sh-Mock and sh-Fyn E14 cells.

E. Telomerase enzyme activity was not significantly different in colon of 43-weeks-old WT vs Fyn$^{-/-}$ mice.

F. Telomerase enzyme activity was not significantly different in sh-Mock and sh-Fyn 293T cells at passage 10.

Data information: In (A, B), Molecular weight markers are shown at the right. In (A-F), Data are presented as means ± SD from a two-tailed t-test. A probability of $p < 0.05$ was considered statistically significant. ns = not significant.

Fig. EV11. Fyn interacts with Menin

Immunoprecipitation using an anti-Fyn antibody followed by Western blotting using proteins that influence the telomere pathway showing only Menin interacting with Fyn (scattered box). Arrows indicate the respective protein band sizes.

Fig. EV12. Fyn phosphorylates Menin at tyrosine 603

A, B, C. Tandem mass spectrometry spectra of the Menin site phosphorylated by Fyn. The precursor mass (m/z) of 611.7975 was matched to the triply charged peptide, DpYTLSFLKR, indicating that Y603 is phosphorylated. The b2 ion at 359.06 and b3 ion at 460.11 indicate that Y603 is phosphorylated.

Fig. EV13. Menin does not bind to TERT promoter or with TERT in mESCs

A. Menin occupancy at the TERT promoter in sh-Mock and sh-Fyn E14 cells after chromatin immunoprecipitation (ChIP) of Menin with an anti-Menin antibody and amplification of TERT by qPCR.

B. Immunoprecipitation of TERT using an anti-Menin antibody in Sh-Mock and Sh-Fyn E14 cells followed by Western blotting using an anti-Menin antibody shows Menin and TERT are not binding partners.

Data information: In (A), Data are presented as the fold enrichment mean ± SD of the TERT promoter amplification. An unpaired student's t-test was used for statistical analysis. ns = not significant.

Fig. EV14. Menin is not SUMO-modified by SUMO2/3/4. Fyn-deficient cells have decreased Menin-SUMO1 modification

A. Prediction results of Menin SUMOylation sites from the GPS-SUMO open-source program.

B. Immunoprecipitation of endogenous Menin and immunoblot against SUMO2/3/4 in sh-Mock and sh-Fyn transfected E14 cells, showing the lack of interaction between Menin and SUMO2/3/4.

C. Menin SUMO1 modification is decreased in Fyn-deficient cells as shown by ELISA in nuclear lysates of WT and $Fyn^{-/-}$ mESCs or sh-Mock and sh-Fyn E14 cells.

Data information: In (C), data are presented as SUMOylation intensity means ± SD from a two-tailed t-test (*** = $p < 0.001$). A probability of $p < 0.05$ was considered statistically significant.

Fig. EV15. Menin Phosphorylation and SUMOylation promote TR binding through improved protein stability

A. Phosphorylation and SUMOylation at the C-terminal site of Menin contribute for Menin-TR binding. RNA pulldown assay using *in vitro* transcribed TR and overexpressed mutant (Y603F, Y603D, K609R) Menin with SUMO1 indicates that 50 times lesser protein of Y603D Menin with SUMO1 interacts with TR very strongly compared to Y603F and K609R Menin with SUMO1.

B, C. Cycloheximide chase assay showing significantly higher protein degradation in Y603F-Menin with or without SUMO1 compared to Y603D-Menin with or without SUMO1. Y603F and Y603D transfected HEK 293T cells co-transfected with SUMO1 were treated with 50µg/mL cycloheximide for indicated time points.

Data information: In (B, D), Xpress-tagged Menin and endogenous Menin protein expression were analyzed at indicated time points. Differential exposure times show very strong expression of only Xpress-Menin in Y603D and Y603D+SUMO1 transfected cell in 1 min exposure. Y603F and Y603F+SUMO1 were visible after 10 mins. Blotting with anti-Menin antibody shows Menin band at short exposure. Menin was analyzed with an Xpress antibody that binds the C-terminal Xpress Tag of the protein or a Menin antibody that binds the central region

of Menin.

Fig. EV16. SUMO1-modified Menin prevents TR's association with Dyskerin

Representative IF-FISH images show Coilin and TR binding in Y603F-MEN1+SUMO1, K609R-MEN1+SUMO1, and Y603D-MEN1+SUMO1 transfected 293T cells. The scale bar is 5 μm.

Data information: Arrows indicate co-localization. A pseudo color yellow was used, replacing magenta for nucleus.

Fig. EV17. Generation of DC-iPSC from DC- fibroblasts

A. Immunofluorescence analysis of SSEA-4 and TRA-1-60 protein expression, showing positive staining for transduction pluripotency markers in DC iPSCs. The scale bar is 100 μm.

(B) Western blotting analysis of pluripotency markers Nanog and KLF4 showing expression in DC iPSCs, but not in DC fibroblasts. β-actin was used as a loading control.

Data information: In (B), molecular weight markers are shown at the right.

Table S1. Candidate Fyn substrate's list for probable telomere length regulator

Transcription factor	Activator/Repressor	Reference
Stat1	Unknown	
Stat3	Activator	Ref. 19
Stat5	Activator	
c-Myc	Activator	
KLF2	Repressor	
KLF7	Unknown	
KLF15	Unknown	
Menin	Repressor	Ref. 19
E2F1	Repressor	
SP3	Repressor	
WT1	Repressor	
MAD1	Repressor	

Table S2. Differential TERC-bound proteins detected in Mass-spectrometry analysis using RNA-IP products of Y603F-*MEN1+SUMO-1* and Y603D-*MEN1+SUMO-1* transfected 293T cells.

Y603F-Menin+SUMO-1 -TERC binding proteins:	
Accession #	Name
sp|Q00839|HNRPU_HUMAN	Heterogeneous nuclear ribonucleoprotein U
sp|P22626|ROA2_HUMAN	Heterogeneous nuclear ribonucleoproteins A2/B1
sp|Q9NR30|DDX21_HUMAN	Nucleolar RNA helicase 2
sp|O43390|HNRPR_HUMAN	Heterogeneous nuclear ribonucleoprotein R
sp|P16402|H13_HUMAN	Histone H1.3
sp|Q99729-3|ROAA_HUMAN	Isoform 3 of Heterogeneous nuclear ribonucleoprotein A/B
sp|P09874|PARP1_HUMAN	Poly [ADP-ribose] polymerase 1
sp|P07910-2|HNRPC_HUMAN	Isoform C1 of Heterogeneous nuclear ribonucleoproteins C1/C2
sp|P52272|HNRPM_HUMAN	Heterogeneous nuclear ribonucleoprotein M
sp|Q92841|DDX17_HUMAN	Probable ATP-dependent RNA helicase DDX17
sp|O94776|MTA2_HUMAN	Metastasis-associated protein MTA2
sp|Q9Y3I0|RTCB_HUMAN	tRNA-splicing ligase RtcB homolog
sp|P98179|RBM3_HUMAN	RNA-binding protein 3
sp|Q0P5I0|MEN1_BOVIN	Menin
sp|P29692|EF1D_HUMAN	Elongation factor 1-delta
sp|Q8N684|CPSF7_HUMAN	Cleavage and polyadenylation specificity factor subunit 7
sp|P12956|XRCC6_HUMAN	X-ray repair cross-complementing protein 6
sp|Q6ZRS2|SRCAP_HUMAN	Helicase SRCAP
sp|P55265|DSRAD_HUMAN	Double-stranded RNA-specific adenosine deaminase
sp|P26358|DNMT1_HUMAN	DNA (cytosine-5)-methyltransferase 1
sp|Q13263|TIF1B_HUMAN	Transcription intermediary factor 1-beta
sp|Q969G3|SMCE1_HUMAN	SWI/SNF-related matrix-associated actin-dependent regulator of chromatin subfamily E member 1
sp|Q1KMD3|HNRL2_HUMAN	Heterogeneous nuclear ribonucleoprotein U-like protein 2
sp|Q92922|SMRC1_HUMAN	SWI/SNF complex subunit SMARCC1
sp|O00571|DDX3X_HUMAN	ATP-dependent RNA helicase DDX3X
sp|Q9Y3C1|NOP16_HUMAN	Nucleolar protein 16
sp|P24534|EF1B_HUMAN	Elongation factor 1-beta
sp|Q9Y4C8|RBM19_HUMAN	Probable RNA-binding protein 19
sp|P07814|SYEP_HUMAN	Bifunctional glutamate/proline--tRNA ligase
sp|O60506|HNRPQ_HUMAN	Heterogeneous nuclear ribonucleoprotein Q
sp|Q8TAQ2|SMRC2_HUMAN	SWI/SNF complex subunit SMARCC2
sp|Q9BXP5|SRRT_HUMAN	Serrate RNA effector molecule homolog
sp|Q5SRE5|NU188_HUMAN	Nucleoporin NUP188 homolog
sp|Q9H6R4|NOL6_HUMAN	Nucleolar protein 6
sp|Q9NY12|GAR1_HUMAN	H/ACA ribonucleoprotein complex subunit 1

sp|Q9Y2L1|RRP44_HUMAN	Exosome complex exonuclease RRP44
sp|Q9P2I0|CPSF2_HUMAN	Cleavage and polyadenylation specificity factor subunit 2
sp|Q9Y2X3|NOP58_HUMAN	Nucleolar protein 58
sp|Q14980|NUMA1_HUMAN	Nuclear mitotic apparatus protein 1
sp|Q14690|RRP5_HUMAN	Protein RRP5 homolog
sp|Q96I24|FUBP3_HUMAN	Far upstream element-binding protein 3
sp|Q9UMS4|PRP19_HUMAN	Pre-mRNA-processing factor 19
sp|P31942|HNRH3_HUMAN	Heterogeneous nuclear ribonucleoprotein H3
sp|O95983|MBD3_HUMAN	Methyl-CpG-binding domain protein 3
sp|Q9H5H4|ZN768_HUMAN	Zinc finger protein 768
sp|Q86YP4|P66A_HUMAN	Transcriptional repressor p66-alpha
sp|Q13243|SRSF5_HUMAN	Serine/arginine-rich splicing factor 5
sp|Q12906|ILF3_HUMAN	Interleukin enhancer-binding factor 3
sp|O60832|DKC1_HUMAN	H/ACA ribonucleoprotein complex subunit 4
Y603D+ SUMO-1-TERC binding proteins:	
Accession #	Name
sp|Q00839|HNRPU_HUMAN	Heterogeneous nuclear ribonucleoprotein U
sp|O43390|HNRPR_HUMAN	Heterogeneous nuclear ribonucleoprotein R
sp|Q99729-3|ROAA_HUMAN	Isoform 3 of Heterogeneous nuclear ribonucleoprotein A/B
sp|P09874|PARP1_HUMAN	Poly [ADP-ribose] polymerase 1
sp|P52272|HNRPM_HUMAN	Heterogeneous nuclear ribonucleoprotein M
sp|Q9NR30|DDX21_HUMAN	Nucleolar RNA helicase 2
sp|O60506|HNRPQ_HUMAN	Heterogeneous nuclear ribonucleoprotein Q
sp|Q9Y3I0|RTCB_HUMAN	tRNA-splicing ligase RtcB homolog
sp|P29692|EF1D_HUMAN	Elongation factor 1-delta
sp|Q14839|CHD4_HUMAN	Chromodomain-helicase-DNA-binding protein 4
sp|Q99879|H2B1M_HUMAN	Histone H2B type 1-M
sp|O00571|DDX3X_HUMAN	ATP-dependent RNA helicase DDX3X
sp|Q13263|TIF1B_HUMAN	Transcription intermediary factor 1-beta
sp|Q13435|SF3B2_HUMAN	Splicing factor 3B subunit 2
sp|Q0P5I0|MEN1_BOVIN	Menin
sp|Q8N684|CPSF7_HUMAN	Cleavage and polyadenylation specificity factor subunit 7
sp|Q14974|IMB1_HUMAN	Importin subunit beta-1
sp|P98179|RBM3_HUMAN	RNA-binding protein 3
sp|Q92841|DDX17_HUMAN	Probable ATP-dependent RNA helicase DDX17
sp|O95983|MBD3_HUMAN	Methyl-CpG-binding domain protein 3
sp|P07814|SYEP_HUMAN	Bifunctional glutamate/proline--tRNA ligase
sp|Q9BXP5|SRRT_HUMAN	Serrate RNA effector molecule homolog
sp|Q10570|CPSF1_HUMAN	Cleavage and polyadenylation specificity factor subunit 1
sp|Q6ZRS2|SRCAP_HUMAN	Helicase SRCAP
sp|Q8TDD1|DDX54_HUMAN	ATP-dependent RNA helicase DDX54
sp|P12956|XRCC6_HUMAN	X-ray repair cross-complementing protein 6

Table S3. List of primary antibodies used for Western blotting (WB) and immunoprecipitation (IP)

Antigen	WB dilutions	IP dilutions	Antibody name	Catalog number	Company
Fyn	1:1000	1:100	Fyn (15), Mouse	sc-434	Santa Cruz
Fyn	1:1000	——	Fyn, Rabbit	4023	Cell Signaling
β-actin	1:1000	——	β-Actin (C4), Mouse	sc-47778	Santa Cruz
α-Tubulin	1:1000	——	α-Tubulin (6A204), Mouse	sc-69969	Santa Cruz
Lamin B1	1:1000	——	Lamin B1 (B-10), Mouse	sc-374015	Santa Cruz
Menin	1:1000	——	Menin (B9), Mouse	sc-374371	Santa Cruz
Menin	1:1000	1:100	Menin, Rabbit	PA5-85330	ThermoFisher
p-Menin	1:2000	——	p(Y609)-Menin, Rabbit	Custom	Abclonal
Xpress	1:5000	1:1000	Anti-Xpress, Mouse	46-0528	Invitrogen
SUMO1	1:1000	——	SUMO-1 (D-11), Mouse	sc-5308	Santa Cruz
SUMO-2/3/4	1:2000	——	SUMO-2/3/4 (C-3), Mouse	sc-393144	Santa Cruz
HA	1:1000	——	Anti-HA-HRP	1201381900	Roche
Nanong	1:1000	——	Nanong (5A10)	Sc-134218	Santa Cruz
KLF4	1:1000	——	KLF4, Rabbit	PA5-18058	ThermoFisher
FLAG	1:5000	——	M1 anti-FLAG®	F7425	Millipore-Sigma
HA	——	1:100	Anti-HA.11	901501	BioLegend

Table S4. List of primary antibodies used for immunofluorescence (IF) and immunohistochemistry (IHC)

Antigen	IF/IHC dilutions	Antibody name	Catalog number	Company
SSEA-4	1:100	Anti-HumanSSEA-4, MC-813-70, PE	60062PE	STEMCELL Technologies
TRA-1-60	1:100	Anti-Human TRA-1-60, TRA-1-60R, Alexa Fluor® 488	60064AD	STEMCELL Technologies
Menin	1:200	Menin (D45B1 XP®), Rabbit	6891	Cell Signaling
Fyn	1:50	Fyn (15), Mouse	sc-434	Santa Cruz
Dyskerin	1:100	DKC1, Rabbit	PA5-28922	ThermoFisher
Coilin	1:800	Coilin (D2L3J) XP®, Rabbit	14168	Cell Signaling
SOX2	1:100	Sox-2 (E-4), Mouse	sc-365823	Santa Cruz
KLF4	1:100	KLF4, Rabbit	PA5-18058	ThermoFisher

Table S5. Primer list

Primer Name	Primer Sequences (5'-3')
Telomere, forward	CGGTTTGTTTGGGTTTGGGTTTGGGTTTGGGTTT GGGTT
Telomere, reverse	GGCTTGCCTTACCCTTACCCTTACCCTTACCCTTA CCCT
m36B4, forward	ACTGGTCTAGGACCCGAGAAG
m36B4, reverse	TCAATGGTGCCTCTGGAGATT
h364, forward	CAGCAAGTGGGAAGGTGTAATCC
h364, reverse	CCCATTCTATCATCAACGGGTACAA
hAlu, forward	GACCATCCCGGCTAAAACG
hAlu, reverse	CGGGTTCACGCCATTCTC
Wild type-C57bl/6-genotyping, forward	AGGCCCAAGTTGACTATCCA
Fyn$^{-/-}$-C57bl/6-genotyping, forward	GGGAGGATTGGGAAGACAAT
Common, reverse	GGCAGCCTGTCTCAAAAGTC
MEN1-wt, forward	ACCGCTAGCATGGGGCTGAAGGCCGCCCAGAAG
MEN1-wt, reverse	ATTAAGCTTTTACTTATCGTCATCGTCGTACAGATC GAGGCCTTTGCGCTG
MEN1-Y603F, forward	TGAGGAAAGACAGAATGAAGTCACTAGGGGTGGAC
MEN1-Y603F, reverse	GTCCACCCCTAGTGACTTCATTCTGTCTTTCCTCA
MEN1-Y603D, forward	GAGGAAAGACAGAATGTCGTCACTAGGGGTGGACA
MEN1-Y603D, reverse	TGTCCACCCCTAGTGACGACATTCTGTCTTTCCTC
MEN1-K498R, forward	CTCCTCTGGCCTGGACTCCCGCCG
MEN1- K498R, reverse	CGGCGGGAGTCCAGGCCAGAGGAG

MEN1-K609R, forward	TGCGCTGCCGCCTGAGGAAAGACAGAATGTAGT
MEN1- K609R, reverse	ACTACATTCTGTCTTTCCTCAGGCGGCAGCGCA
hTR-transcription, forward	T7-GGGTTGCGGAGGGTGGGCCT
hTR-transcription, reverse	GCATGTGTGAGCCGAGTCCTGG
mTR-transcription, forward	T7-ACCTAACCCTGATTTTCATTAGC
mTR-transcription, reverse	GGTTGTGAGAACCGAGTTCC
TR-reverse transcription	GCGTCTCAACTGGTGTCGTGGAGTCGGCAATTCAGT TGAGACGCGCATGTGTGAG
U6-reverse transcription	GCGTCTCAACTGGTGTCGTGGAGTCGGCAATTCAGT TGAGACGCAAAATATGGAA
hTR, forward	TTCAGGCCTTTCAGGCCGCAGGAA
hTR, reverse	TGGTGTCGTGGAGTCGGC
mTR, forward	ACCTAACCCTGATTTTCATTAGC
mTR, reverse	GGTTGTGAGAACCGAGTTCC
U6, forward	CGCAAGGATGACACGCAAATTCG
U6, reverse	TGGTGTCGTGGAGTCGGC
MEN1, forward (protein purification)	CG GGATCC TG ATGGGGCTGAAGGCCGCCCAG
MEN1, reverse (protein purification)	TAGAATTCTTAGTGATGGTGATGGTGATGGAGGCCTTTGCGCTG
TERT promoter seq, ChIP assay, forward	5′-ACTTTGGTTGCCCAATGC-3′
TERT promoter seq, ChIP assay, reverse	5′-AAGGAAAGGTCGGCAGGT-3′
hTR, forward (For Fig. 7)	GCGAAGAGTTGGGCTCTGTCA
hTR, reverse (For Fig. 7)	TTCCTCTTCCTGCGGCCTGAAA

Table S6. Fyn CRISPR sequence

Santa Cruz Biotechnology Cat. No	Sequence
sc-400152-NIC Fyn Double Nickase Plasmid (h) - A:	AACAACTTCCACGCAGCCGG
sc-400152-NIC Fyn Double Nickase Plasmid (h) - B:	ATGGAGGTCACACCGAAGCT

Table S7. TR FISH probe set

Probe name	Sequence
FLAP-Y-Cy3	/5Cy3/AATGCATGTCGACGAGGTCCGAGTGTAA/3Cy3Sp/
TRProbe1	GCATGTGTGAGCCGAGTCCTGGGTGCTTACACTCGGACCTCGTCGACATGCATT
TRProbe2	CGCGCGGGGACTCGCTCCGTTCCTTACACTCGGACCTCGTCGACATGCATT
TRProbe3	TTCCTGCGGCCTGAAAGGCCTGAACTTACACTCGGACCTCGTCGACATGCATT
TRProbe4	GGGCCAGCAGCTGACATTTTTTGTTTGCTTTACACTCGGACCTCGTCGACATGCATT
TRProbe5	GGCTTTTCCGCCCGCTGAAAGTCAGCTTACACTCGGACCTCGTCGACATGCATT
TRProbe6	GTCCCACAGCTCAGGGAATCGCGCTTACACTCGGACCTCGTCGACATGCATT
TRProbe7	GCCCAACTCTTCGCGGTGGCAGTGTTACACTCGGACCTCGTCGACATGCATT
TRProbe8	GCGGCCTCCAGGCGGGGTTCGGGTTACACTCGGACCTCGTCGACATGCATT
TRProbe9	CCGCAGGTCCCCGGGAGGGGCGATTACACTCGGACCTCGTCGACATGCATT
TRProbe10	AGAATGAACGGTGGAAGGCGGCAGGCCTTACACTCGGACCTCGTCGACATGCATT
TRProbe11	CGCCTACGCCCTTCTCAGTTAGGGTTTTACACTCGGACCTCGTCGACATGCATT
TRProbe12	CCCCGAGAGACCCGCGGCTGACATTACACTCGGACCTCGTCGACATGCATT
TRProbe13	CCTCCGGAGAAGCCCCGGGCCGATTACACTCGGACCTCGTCGACATGCATT
TRProbe14	GAAAAACAGCGCGCGGGGAGCAAAAGCACTTACACTCGGACCTCGTCGACATGCATT
TRProbe15	ACAAAAAATGGCCACCACCCCTCCCTTACACTCGGACCTCGTCGACATGCATT

Table S8. Material list

Material name	Cat. no	Company
Mitomycin C	11435	Cayman Chemicals
Knockout™ DMEM	10829018	Gibco
Knockout™ Serum replacement	10828028	Gibco
Leukemia Inhibitory Factor	L4501	GenDepot
Alkaline Phosphatase Detection Kit	SCR004	MilliporeSigma
ES-E14TG2a	ATCC® CRL-1821™	ATCC
DMEM, high glucose, pyruvate	11995065	Gibco
Stasis™ Stem Cell Fetal Bovine Serum	100-125	GeminiBio
Gibco™ 2-Mercaptoethanol	21985023	Gibco
L-glutamine	CA009	GenDepot
Non-essential Amino acid	CA012-010	GenDepot
Sh-Fyn pLKO.1 lentiviral vector	TRCN0000023381	UMN genome center
Sh-Menin pLKO.1 lentiviral vector	TRCN0000040138	UMN genome center
psPAX2	12260	Addgene
pMD2.G	12259	Addgene
iMFectin Poly DNA Transfection Reagent	I7200	GenDepot
Polybrene transfection Reagent	TR-1003	GeminiBio
Puromycin dihydrochloride	P8833	MilliporeSigma
TRAPEZE® RT Telomerase Detection Kit	S7710	MilliporeSigma
Colcemid	15364	Cayman Chemicals
Fluoro-Gel II with Dapi	17985-50	Electron Microscopy Sci.
TelC-Alexa488	F1004	PNA Bio Inc
TelG-Cy3	F1006	PNA Bio Inc

CENPB-Cy3	F3002	PNA Bio Inc
Hoechst 33258	16756	Cayman Chemicals
RNase A	T3018L	New England BioLabs Inc.
Blocking reagent	11096176001	MilliporeSigma
DNAzol® reagent	10503027	Invitrogen
SYBR™ Green PCR Master Mix	4344463	Applied Biosystem
Protein G-Agarose	P9202	GenDepot
NE-PER™ Nuclear and Cytoplasmic Extraction Reagents	78835	ThermoFisher Sci.
DAB Substrate	11718096001	MilliporeSigma
Recombinant Human Menin Protein	H00004221-P01	Novus Biologicals
Active Fyn protein	14-441	MilliporeSigma
Recombinant Human beta Catenin protein	ab63175	Abcam
BL21(DE3)-pLysS cells	L1195	Promega
pGEX-5X1	28-9545-53	MilliporeSigma
Lysozyme	50-488-779	Research Product Int.
Ni-NTA agarose	R90110	ThermoFisher Sci.
Men1-pDNR-Dual	HsCD00000838	DNASU
pcDNA3-HA-Sumo1	21154	Addgene
QuikChange II Site-directed mutagenesis kit	200521	Agilent
EpiQuik™ In Vivo Universal Protein Sumoylation Assay Kit	P-8001	EPIGENTEK
One-Day Chromatin Immunoprecipitation Kit	(Magna ChIP G,17-611	MilliporeSigma

Biotin-16-UTP	11388908910	MilliporeSigma
TranscriptAid T7 High Yield Transcription Kit	K0441	Thermo Fisher Sci.
Streptavidin Agarose	69203	MilliporeSigma
TransIT-X2	MIR 6004	Mirus
Lambda Protein Phosphatase	P0753S	New England Biolabs
YOYO®-1 (1mM)	Y3601	Invitrogen
Dextran Sulphate	42867	MilliporeSigma
Ribonucleoside Vanadyl Complex (VRC)	S1402S	New England Biolabs
NEBuffer 3	B7003S	New England Biolabs
Bovine Serum Albumin	B9000S	New England Biolabs
tRNA	10109517001	MilliporeSigma
Xpert Prestained Protein Marker	P8502-050	GenDEPOT
Xpert 2 Prestained Protein Marker	P8503-050	GenDEPOT
Recombinant Human Fibroblast Growth Factor-basic	PHG0266	Gibco
TeSR™-E8™	05990	StemCell Technologies
Matrigel® hESC-qualified Matrix	354277	Corning
Y-27632	72304	StemCell Technologies
G418, Geneticin	10131035	Thermo Fisher Sci.
Xpert Protease Inhibitor Cocktail Solution (100X)	P3100	GenDEPOT
RNase Inhibitor, Murine	M0314L	New England Biolabs.
N-Ethylmaleimide	E3876-5G	MilliporeSigma
SureStart Taq DNA Polymerase	600282	Agilent

3-(4-chlorophenyl)-1-(1,1-dimethylethyl)-1H-pyrazolo[3,4-d]pyrimidin-4-amine	13198	Cayman Chemicals
Dyskeratosis Fibroblast from Skin	AG04646	Coriell Institute
Fyn Double Nickase Plasmid, human	sc-400152-NIC	Santa Cruz Biotechnology
Control Double Nickase Plasmid	sc-437281	Santa Cruz Biotechnology
STEMCCA, Constitutive Polycistronic (OKSM) Lentivirus Reprogramming Kit	SCR510	MilliporeSigma

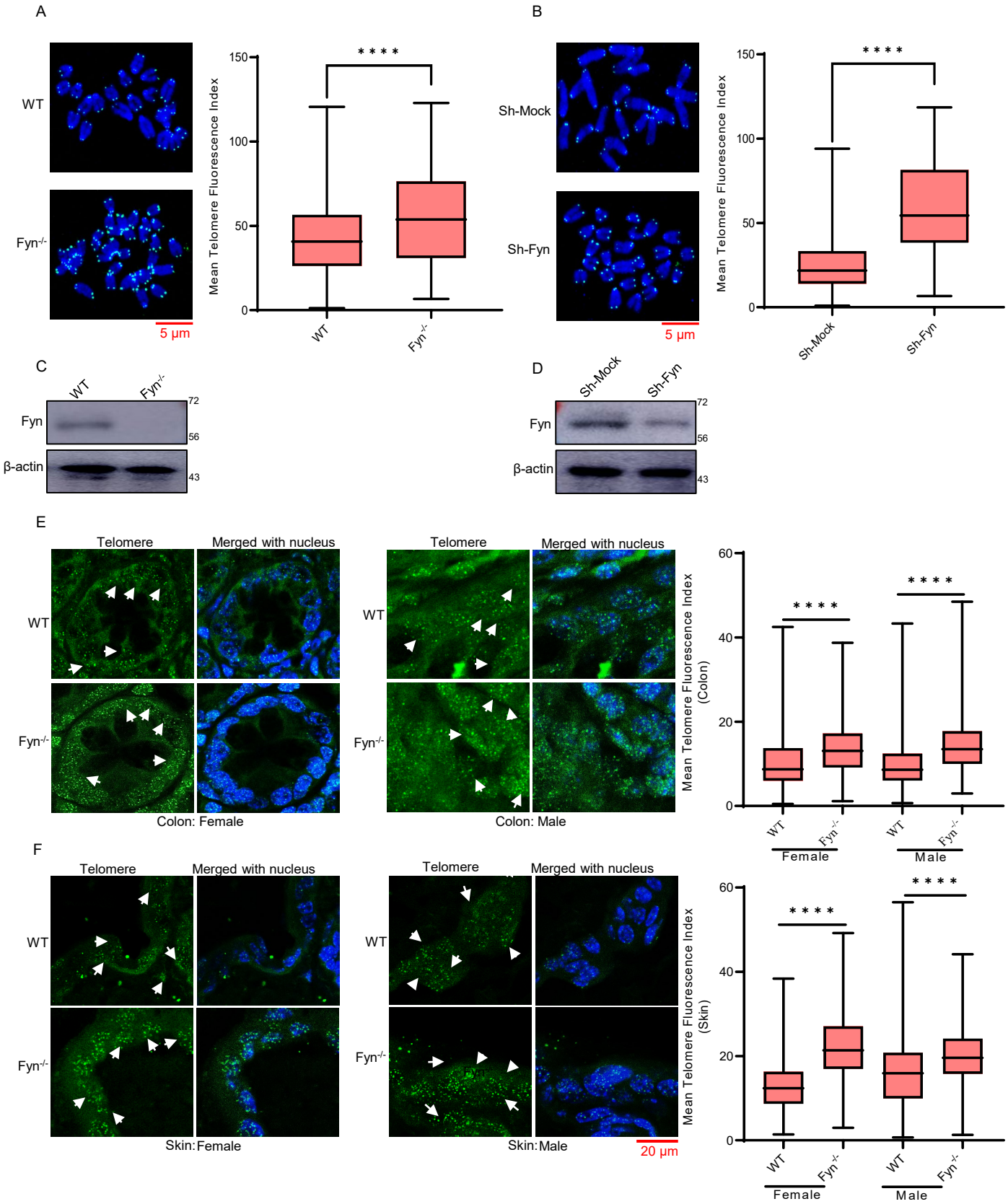
A
WT
Fyn-/-
5 μm
Mean Telomere Fluorescence Index
150
100
50
0
****
WT
Fyn-/-
B
Sh-Mock
Sh-Fyn
5 μm
Mean Telomere Fluorescence Index
150
100
50
0
****
Sh-Mock
Sh-Fyn
C
WT
Fyn-/-
Fyn
β-actin
72
56
43
D
Sh-Mock
Sh-Fyn
Fyn
β-actin
72
56
43
E
Telomere
Merged with nucleus
WT
Fyn-/-
Colon: Female
Telomere
Merged with nucleus
WT
Fyn-/-
Colon: Male
Mean Telomere Fluorescence Index (Colon)
60
40
20
0
****
****
WT
Fyn-/-
WT
Fyn-/-
Female
Male
F
Telomere
Merged with nucleus
WT
Fyn-/-
Skin: Female
Telomere
Merged with nucleus
WT
Fyn-/-
Skin: Male
20 μm
Mean Telomere Fluorescence Index (Skin)
60
40
20
0
****
****
WT
Fyn-/-
WT
Fyn-/-
Female
Male

FIGURE 1

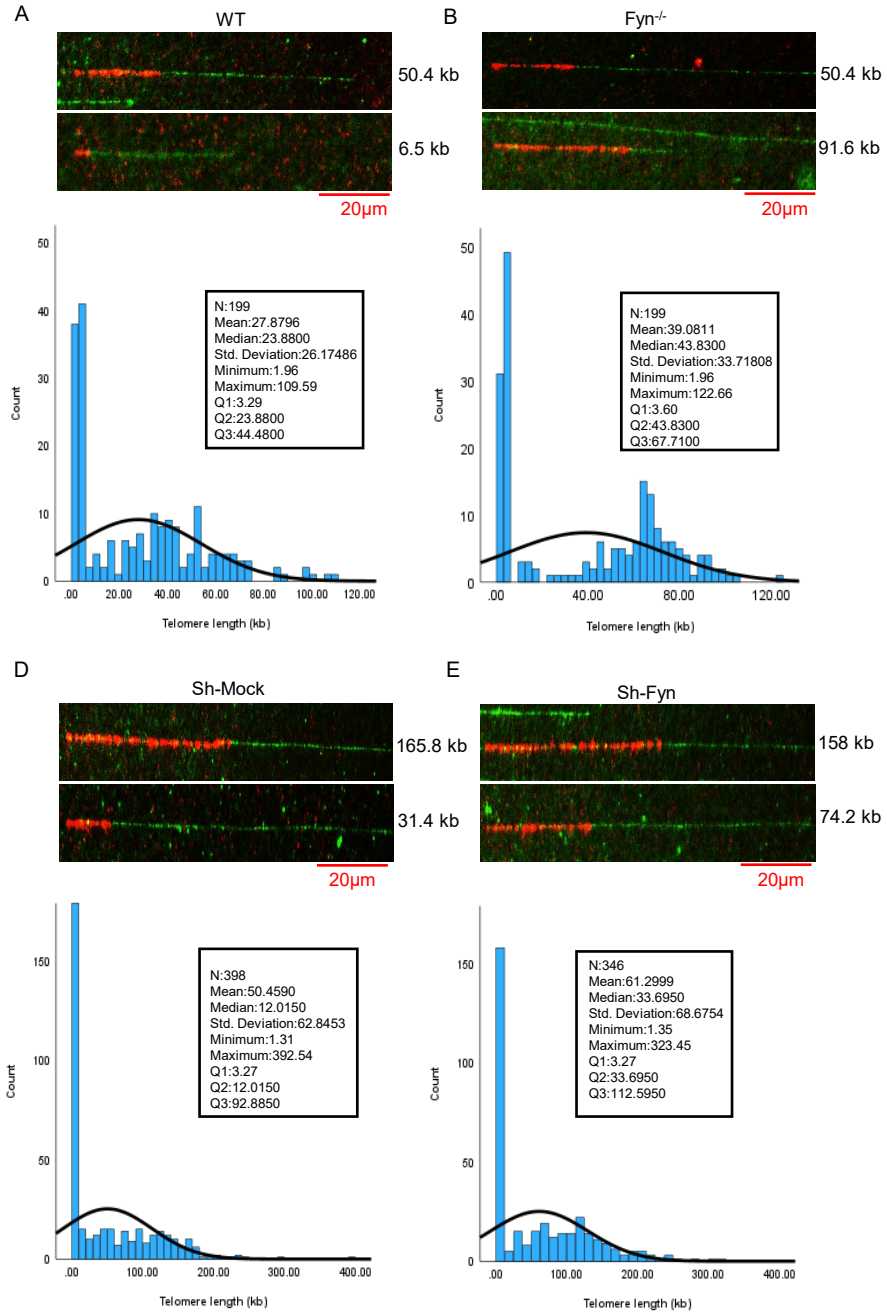
A
WT
50.4 kb
6.5 kb
20µm
N:199
Mean:27.8796
Median:23.8800
Std. Deviation:26.17486
Minimum:1.96
Maximum:109.59
Q1:3.29
Q2:23.8800
Q3:44.4800
Count
Telomere length (kb)
B
Fyn-/-
50.4 kb
91.6 kb
20µm
N:199
Mean:39.0811
Median:43.8300
Std. Deviation:33.71808
Minimum:1.96
Maximum:122.66
Q1:3.60
Q2:43.8300
Q3:67.7100
Count
Telomere length (kb)
D
Sh-Mock
165.8 kb
31.4 kb
20µm
N:398
Mean:50.4590
Median:12.0150
Std. Deviation:62.8453
Minimum:1.31
Maximum:392.54
Q1:3.27
Q2:12.0150
Q3:92.8850
Count
Telomere length (kb)
E
Sh-Fyn
158 kb
74.2 kb
20µm
N:346
Mean:61.2999
Median:33.6950
Std. Deviation:68.6754
Minimum:1.35
Maximum:323.45
Q1:3.27
Q2:33.6950
Q3:112.5950
Count
Telomere length (kb)

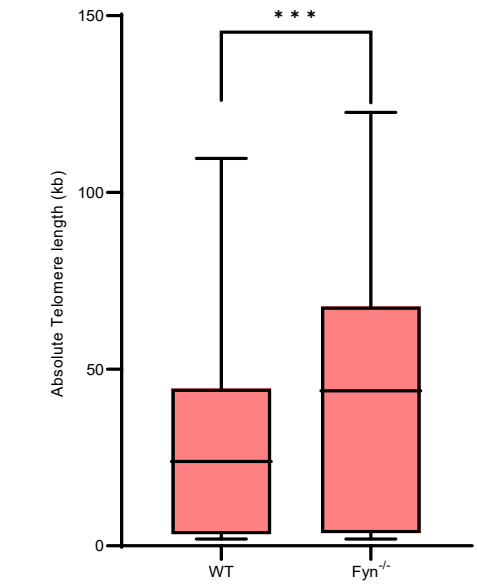
C
* * *
Absolute Telomere length (kb)
WT
Fyn-/-

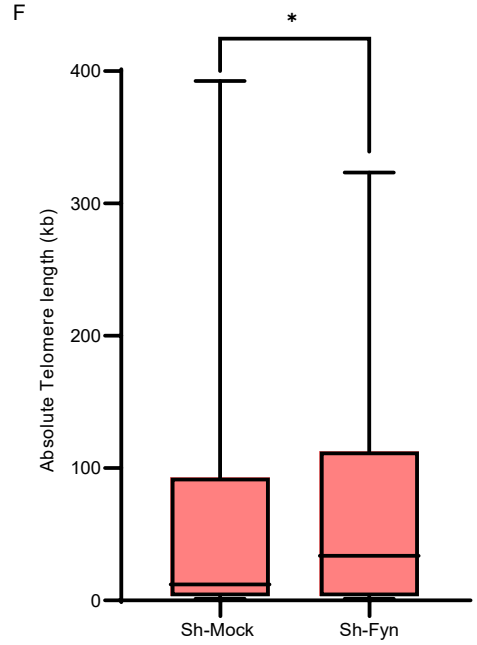
F
*
Absolute Telomere length (kb)
Sh-Mock
Sh-Fyn

FIGURE 2

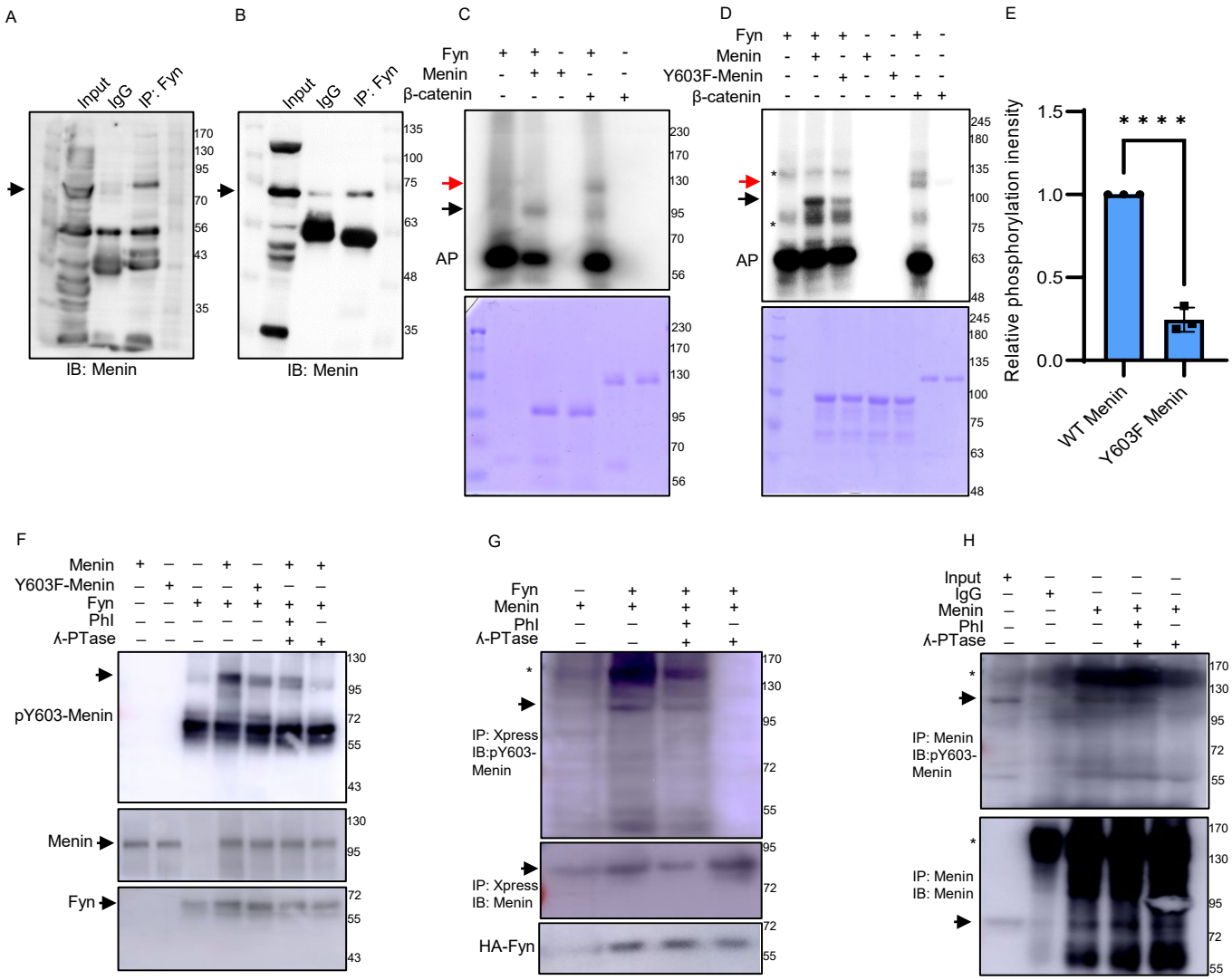
A
Input
IgG
IP: Fyn
170
130
95
70
56
43
35
IB: Menin
B
Input
IgG
IP: Fyn
135
100
75
63
48
35
IB: Menin
C
Fyn + + - + -
Menin - + + - -
β-catenin - - - + +
AP
230
170
130
95
70
56
D
Fyn + + + - - + -
Menin - + - + - - -
Y603F-Menin - - + - + - -
β-catenin - - - - - + +
AP
245
180
135
100
75
63
48
E
Relative phosphorylation inensity
1.5
1.0
0.5
0.0
* * * *
WT Menin
Y603F Menin
F
Menin + – – + – + +
Y603F-Menin – + – – + – –
Fyn – – + + + + +
PhI – – – – – + –
λ-PTase – – – – – + +
pY603-Menin
Menin
Fyn
130
95
72
55
43
G
Fyn – + + +
Menin + + + +
PhI – – + –
λ-PTase – – + +
IP: Xpress
IB:pY603-
Menin
IP: Xpress
IB: Menin
HA-Fyn
170
130
95
72
55
H
Input + – – – –
IgG – + – – –
Menin – – + + +
PhI – – – + –
λ-PTase – – – + +
IP: Menin
IB:pY603-
Menin
IP: Menin
IB: Menin
170
130
95
72
55

FIGURE 3

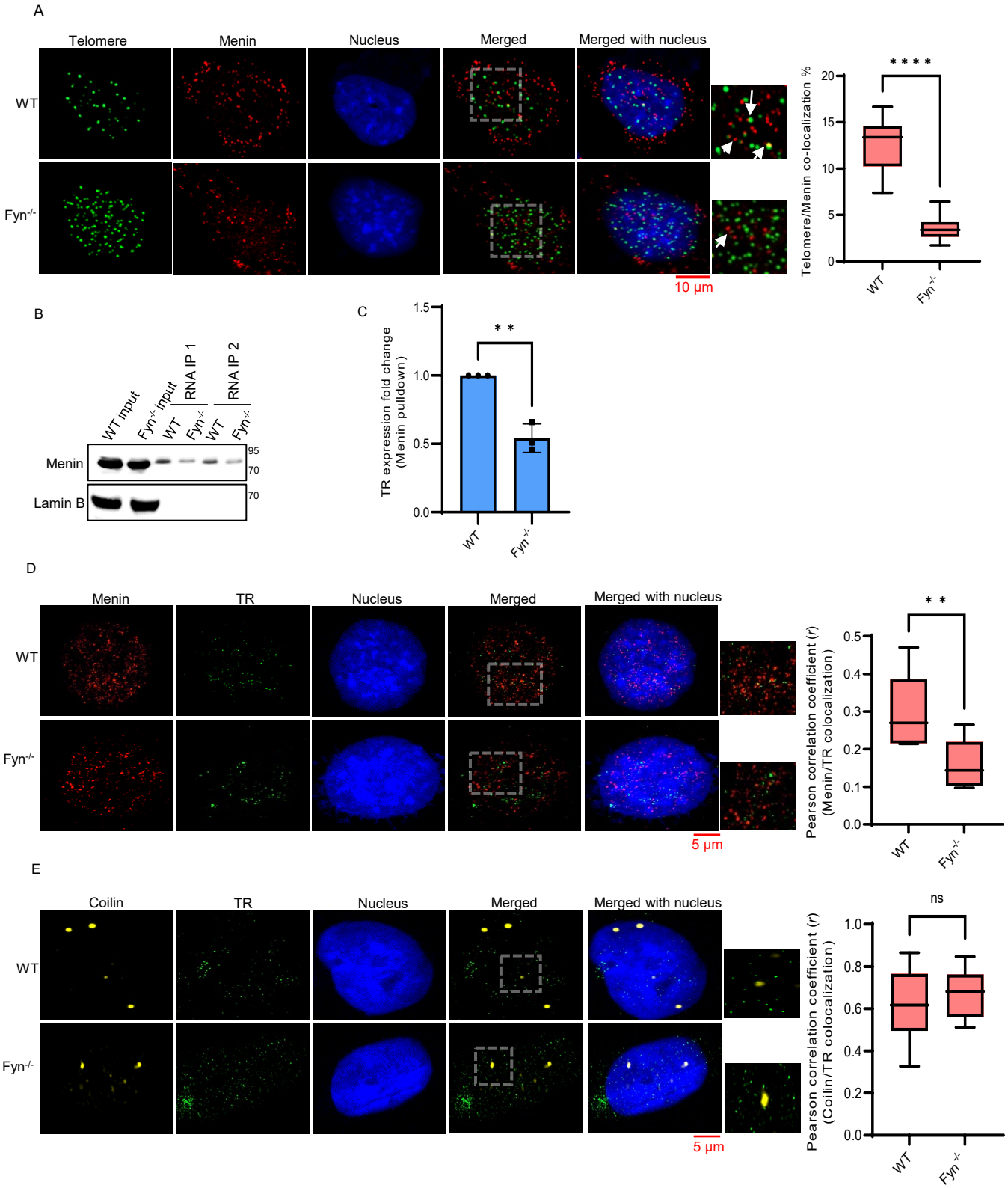
A
Telomere
Menin
Nucleus
Merged
Merged with nucleus
WT
Fyn-/-
10 µm
Telomere/Menin co-localization %
* * * *
WT
Fyn-/-
B
WT input
Fyn-/- input
RNA IP 1
RNA IP 2
WT
Fyn-/-
WT
Fyn-/-
Menin
Lamin B
95
70
70
C
TR expression fold change (Menin pulldown)
* *
WT
Fyn-/-
D
Menin
TR
Nucleus
Merged
Merged with nucleus
WT
Fyn-/-
5 µm
Pearson correlation coefficient (r) (Menin/TR colocalization)
* *
WT
Fyn-/-
E
Coilin
TR
Nucleus
Merged
Merged with nucleus
WT
Fyn-/-
5 µm
Pearson correlation coefficient (r) (Coilin/TR colocalization)
ns
WT
Fyn-/-

FIGURE 4

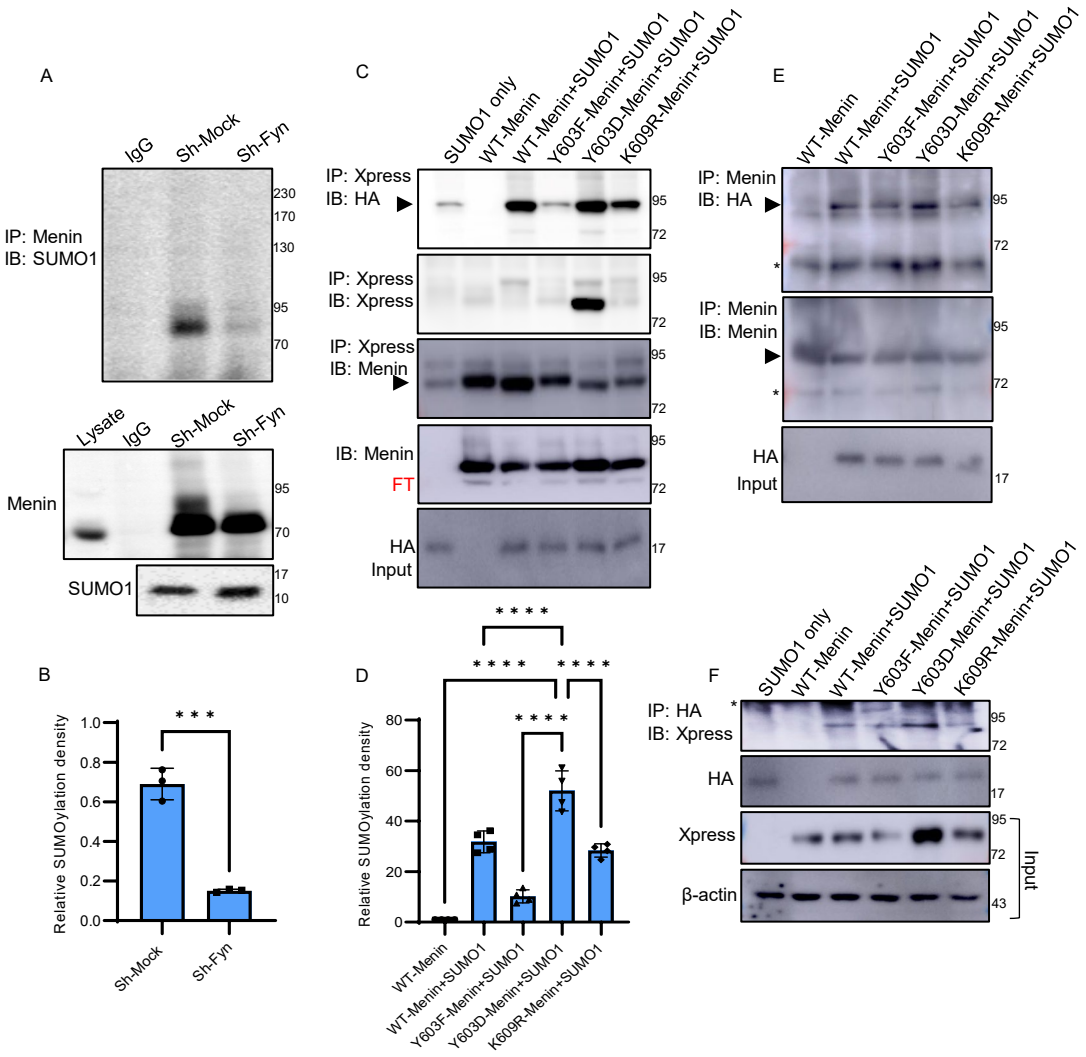
A
IgG
Sh-Mock
Sh-Fyn
IP: Menin
IB: SUMO1
230
170
130
95
70
Lysate
IgG
Sh-Mock
Sh-Fyn
Menin
95
70
SUMO1
17
10
B
Relative SUMOylation density
1.0
0.8
0.6
0.4
0.2
0.0
* * *
Sh-Mock
Sh-Fyn
C
SUMO1 only
WT-Menin
WT-Menin+SUMO1
Y603F-Menin+SUMO1
Y603D-Menin+SUMO1
K609R-Menin+SUMO1
IP: Xpress
IB: HA
IP: Xpress
IB: Xpress
IP: Xpress
IB: Menin
IB: Menin
FT
HA
Input
95
72
17
D
Relative SUMOylation density
80
60
40
20
0
* * * *
* * * *
* * * *
WT-Menin
WT-Menin+SUMO1
Y603F-Menin+SUMO1
Y603D-Menin+SUMO1
K609R-Menin+SUMO1
E
WT-Menin
WT-Menin+SUMO1
Y603F-Menin+SUMO1
Y603D-Menin+SUMO1
K609R-Menin+SUMO1
IP: Menin
IB: HA
IP: Menin
IB: Menin
HA
Input
95
72
17
F
SUMO1 only
WT-Menin
WT-Menin+SUMO1
Y603F-Menin+SUMO1
Y603D-Menin+SUMO1
K609R-Menin+SUMO1
IP: HA
IB: Xpress
HA
Xpress
β-actin
95
72
17
43
Input

FIGURE 5

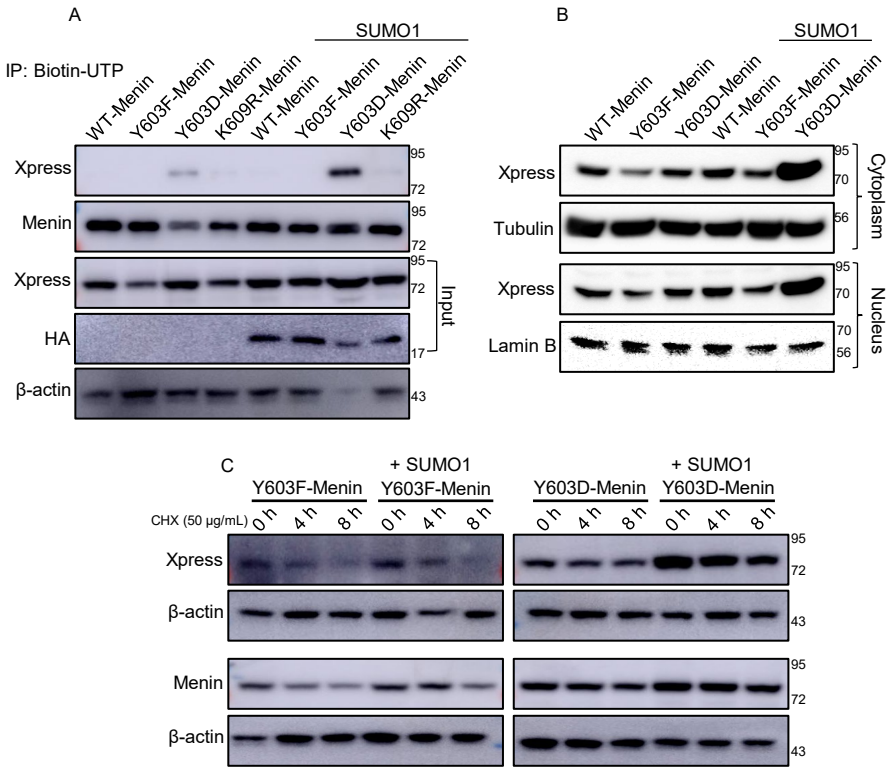
A
SUMO1
IP: Biotin-UTP
WT-Menin
Y603F-Menin
Y603D-Menin
K609R-Menin
WT-Menin
Y603F-Menin
Y603D-Menin
K609R-Menin
Xpress
Menin
Xpress
HA
β-actin
95
72
95
72
95
72
17
43
Input
B
SUMO1
WT-Menin
Y603F-Menin
Y603D-Menin
WT-Menin
Y603F-Menin
Y603D-Menin
Xpress
Tubulin
Xpress
Lamin B
95
70
56
95
70
70
56
Cytoplasm
Nucleus
C
Y603F-Menin
+ SUMO1
Y603F-Menin
Y603D-Menin
+ SUMO1
Y603D-Menin
CHX (50 μg/mL)
0 h
4 h
8 h
0 h
4 h
8 h
0 h
4 h
8 h
0 h
4 h
8 h
Xpress
β-actin
Menin
β-actin
95
72
43
95
72
43

FIGURE 6

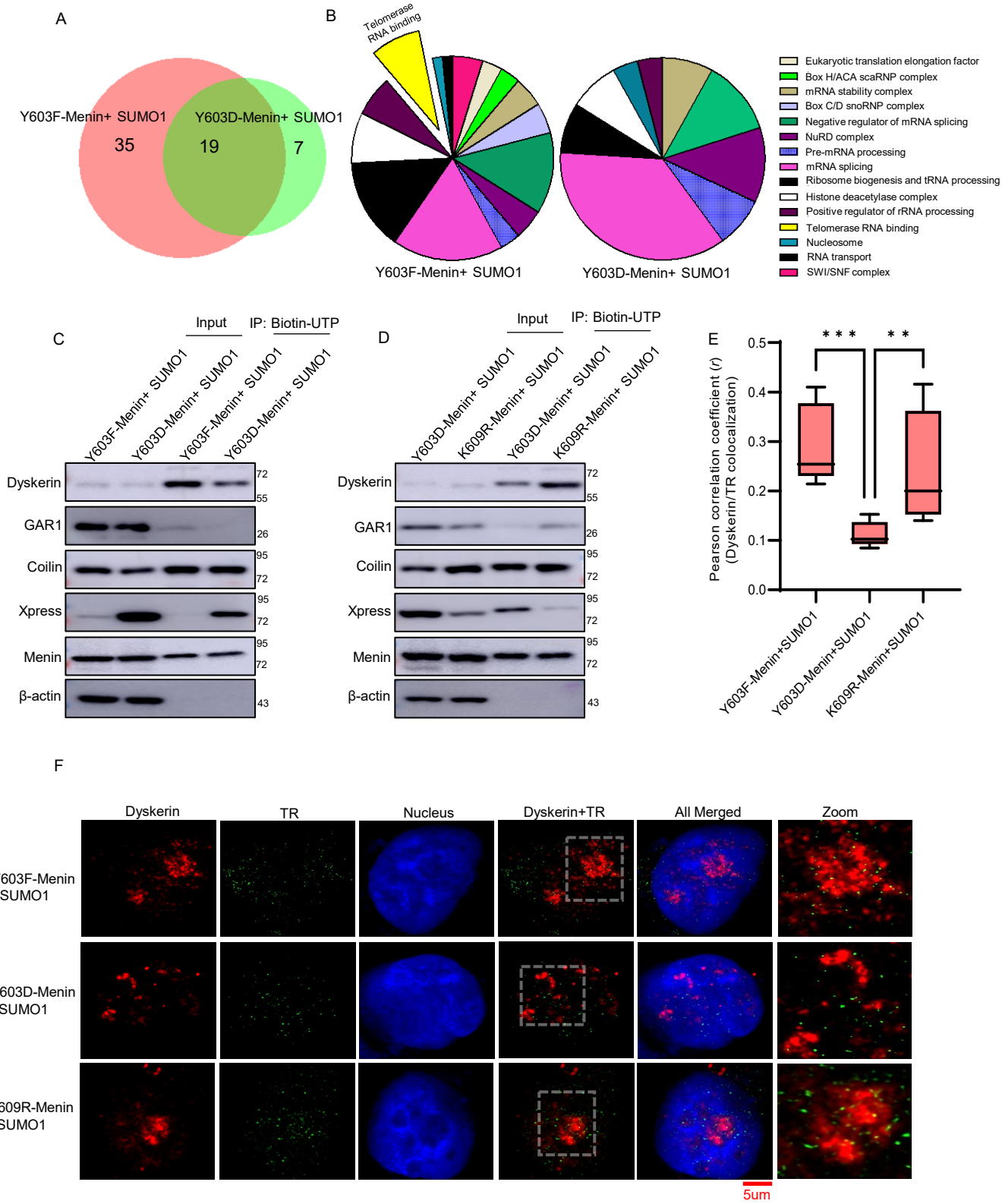
A
Y603F-Menin+ SUMO1
Y603D-Menin+ SUMO1
35
19
7
B
Telomerase RNA binding
Y603F-Menin+ SUMO1
Y603D-Menin+ SUMO1
Eukaryotic translation elongation factor
Box H/ACA scaRNP complex
mRNA stability complex
Box C/D snoRNP complex
Negative regulator of mRNA splicing
NuRD complex
Pre-mRNA processing
mRNA splicing
Ribosome biogenesis and tRNA processing
Histone deacetylase complex
Positive regulator of rRNA processing
Telomerase RNA binding
Nucleosome
RNA transport
SWI/SNF complex
C
Input
IP: Biotin-UTP
Y603F-Menin+ SUMO1
Y603D-Menin+ SUMO1
Y603F-Menin+ SUMO1
Y603D-Menin+ SUMO1
Dyskerin
GAR1
Coilin
Xpress
Menin
β-actin
72
55
26
95
72
95
72
95
72
43
D
Input
IP: Biotin-UTP
Y603D-Menin+ SUMO1
K609R-Menin+ SUMO1
Y603D-Menin+ SUMO1
K609R-Menin+ SUMO1
Dyskerin
GAR1
Coilin
Xpress
Menin
β-actin
72
55
26
95
72
95
72
95
72
43
E
Pearson correlation coefficient (r)
(Dyskerin/TR colocalization)
0.5
0.4
0.3
0.2
0.1
0.0
* * *
* *
Y603F-Menin+SUMO1
Y603D-Menin+SUMO1
K609R-Menin+SUMO1
F
Dyskerin
TR
Nucleus
Dyskerin+TR
All Merged
Zoom
Y603F-Menin +SUMO1
Y603D-Menin +SUMO1
K609R-Menin +SUMO1
5um

FIGURE 7

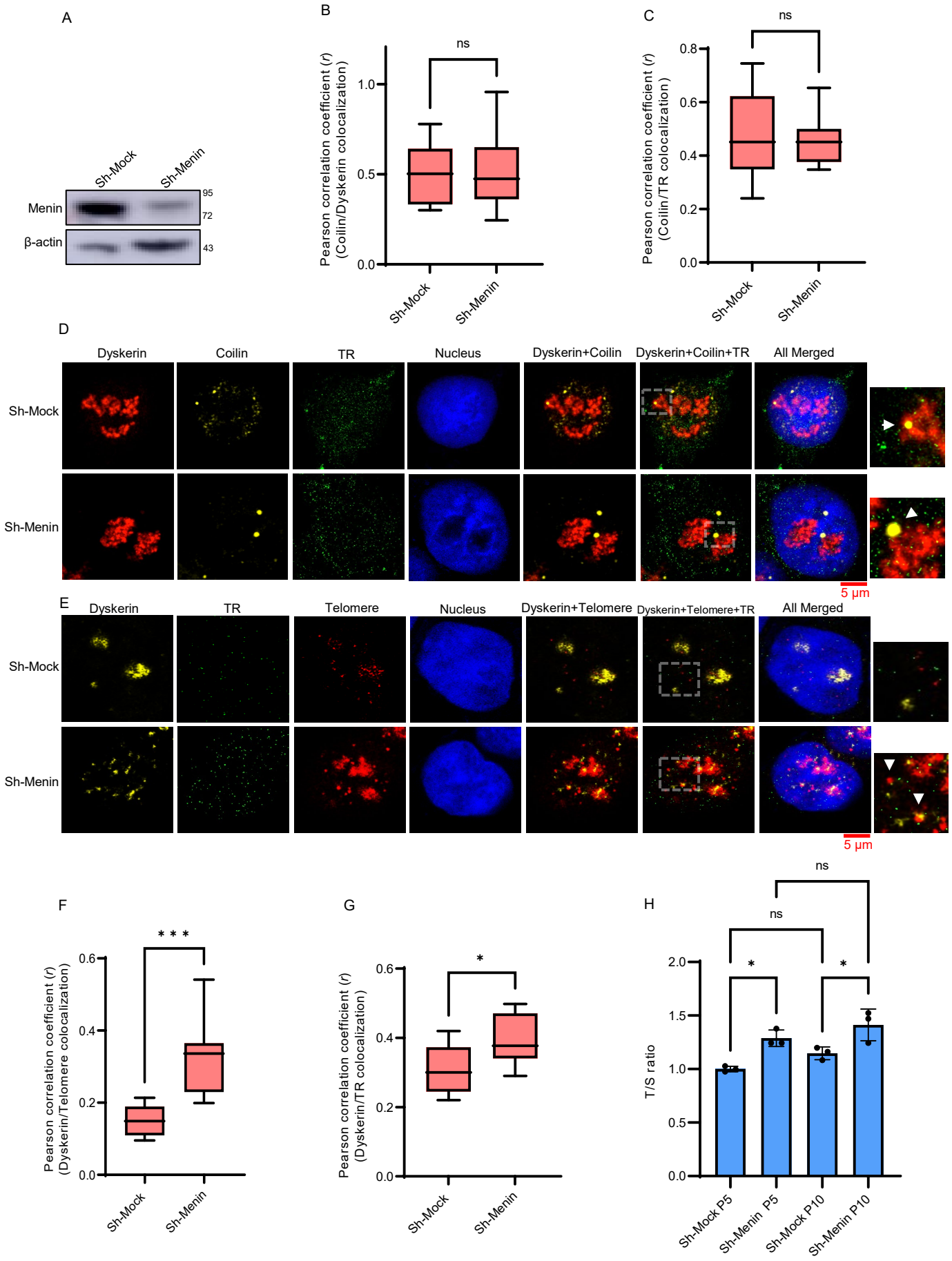
A
Sh-Mock
Sh-Menin
Menin
β-actin
95
72
43
B
ns
Pearson correlation coefficient (r)
(Coilin/Dyskerin colocalization)
1.0
0.5
0.0
Sh-Mock
Sh-Menin
C
ns
Pearson correlation coefficient (r)
(Coilin/TR colocalization)
0.8
0.6
0.4
0.2
0.0
Sh-Mock
Sh-Menin
D
Dyskerin
Coilin
TR
Nucleus
Dyskerin+Coilin
Dyskerin+Coilin+TR
All Merged
Sh-Mock
Sh-Menin
5 µm
E
Dyskerin
TR
Telomere
Nucleus
Dyskerin+Telomere
Dyskerin+Telomere+TR
All Merged
Sh-Mock
Sh-Menin
5 µm
F
* * *
Pearson correlation coefficient (r)
(Dyskerin/Telomere colocalization)
0.6
0.4
0.2
0.0
Sh-Mock
Sh-Menin
G
*
Pearson correlation coefficient (r)
(Dyskerin/TR colocalization)
0.6
0.4
0.2
0.0
Sh-Mock
Sh-Menin
H
ns
ns
*
*
T/S ratio
2.0
1.5
1.0
0.5
0.0
Sh-Mock P5
Sh-Menin P5
Sh-Mock P10
Sh-Menin P10

FIGURE 8

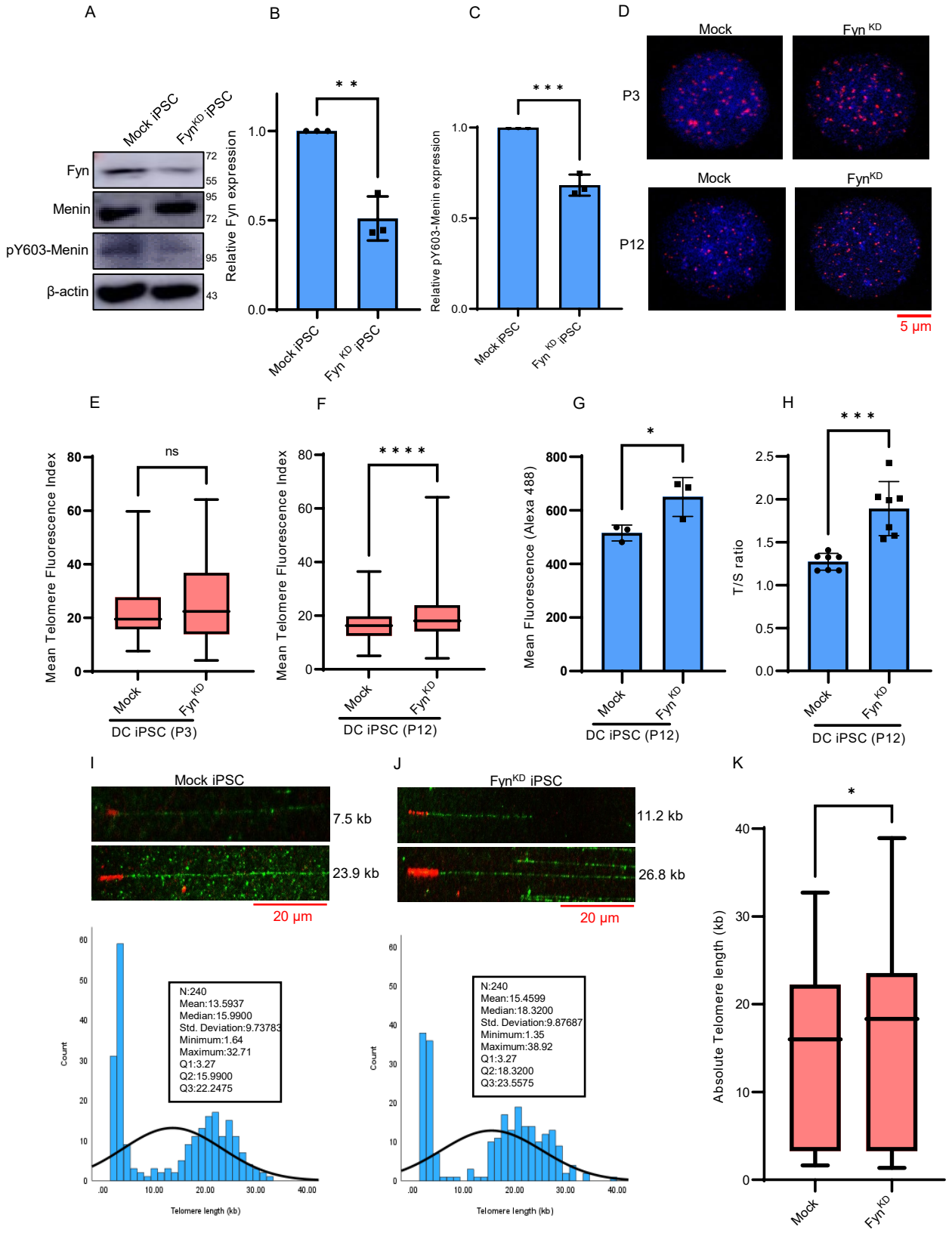
A
Mock iPSC
FynKD iPSC
Fyn
Menin
pY603-Menin
β-actin
72
55
95
72
95
43
B
Relative Fyn expression
1.0
0.5
0.0
* *
Mock iPSC
Fyn KD iPSC
C
Relative pY603-Menin expression
* * *
D
Mock
Fyn KD
P3
P12
5 μm
E
Mean Telomere Fluorescence Index
ns
DC iPSC (P3)
F
* * * *
DC iPSC (P12)
G
Mean Fluorescence (Alexa 488)
*
H
T/S ratio
* * *
I
Mock iPSC
7.5 kb
23.9 kb
20 μm
N:240
Mean:13.5937
Median:15.9900
Std. Deviation:9.73783
Minimum:1.64
Maximum:32.71
Q1:3.27
Q2:15.9900
Q3:22.2475
Count
Telomere length (kb)
J
FynKD iPSC
11.2 kb
26.8 kb
N:240
Mean:15.4599
Median:18.3200
Std. Deviation:9.87687
Minimum:1.35
Maximum:38.92
Q1:3.27
Q2:18.3200
Q3:23.5575
K
Absolute Telomere length (kb)

FIGURE 9

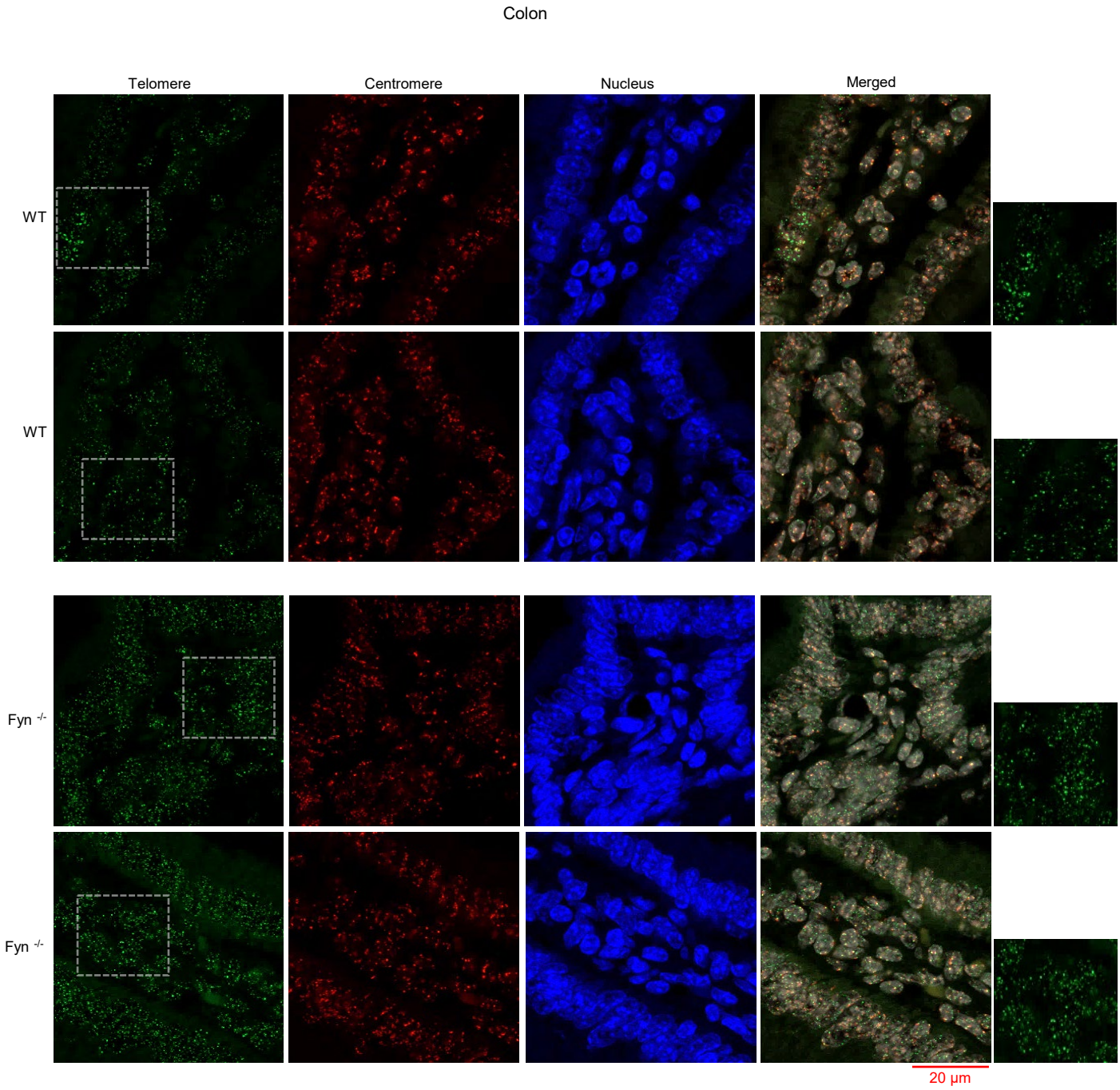
Colon
Telomere
Centromere
Nucleus
Merged
WT
WT
Fyn -/-
Fyn -/-
20 µm

Fig. EV1

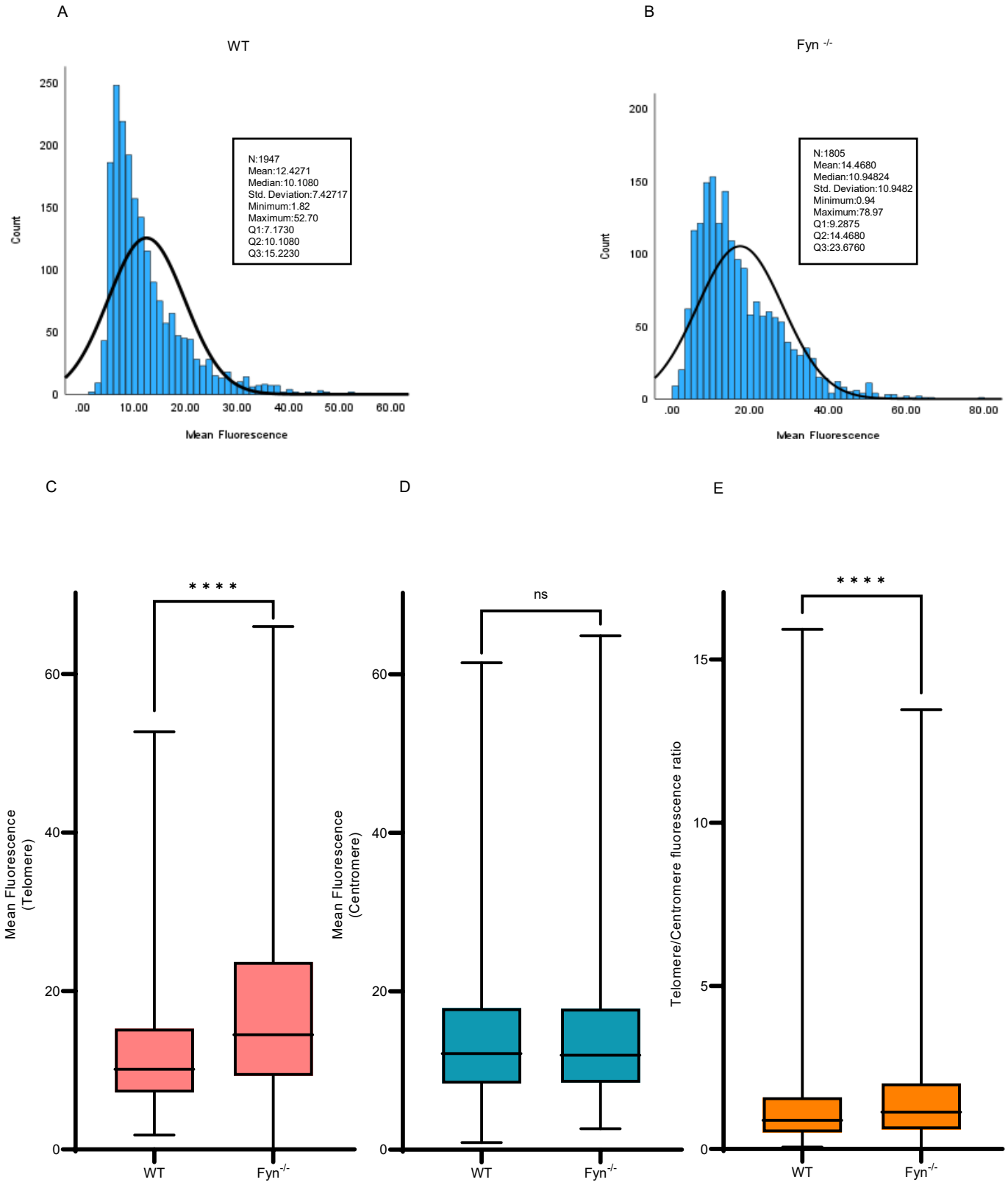
A
WT
N:1947
Mean:12.4271
Median:10.1080
Std. Deviation:7.42717
Minimum:1.82
Maximum:52.70
Q1:7.1730
Q2:10.1080
Q3:15.2230
Count
Mean Fluorescence
B
Fyn -/-
N:1805
Mean:14.4680
Median:10.94824
Std. Deviation:10.9482
Minimum:0.94
Maximum:78.97
Q1:9.2875
Q2:14.4680
Q3:23.6760
Count
Mean Fluorescence
C
* * * *
Mean Fluorescence (Telomere)
WT
Fyn-/-
D
ns
Mean Fluorescence (Centromere)
WT
Fyn-/-
E
* * * *
Telomere/Centromere fluorescence ratio
WT
Fyn-/-

Fig. EV2

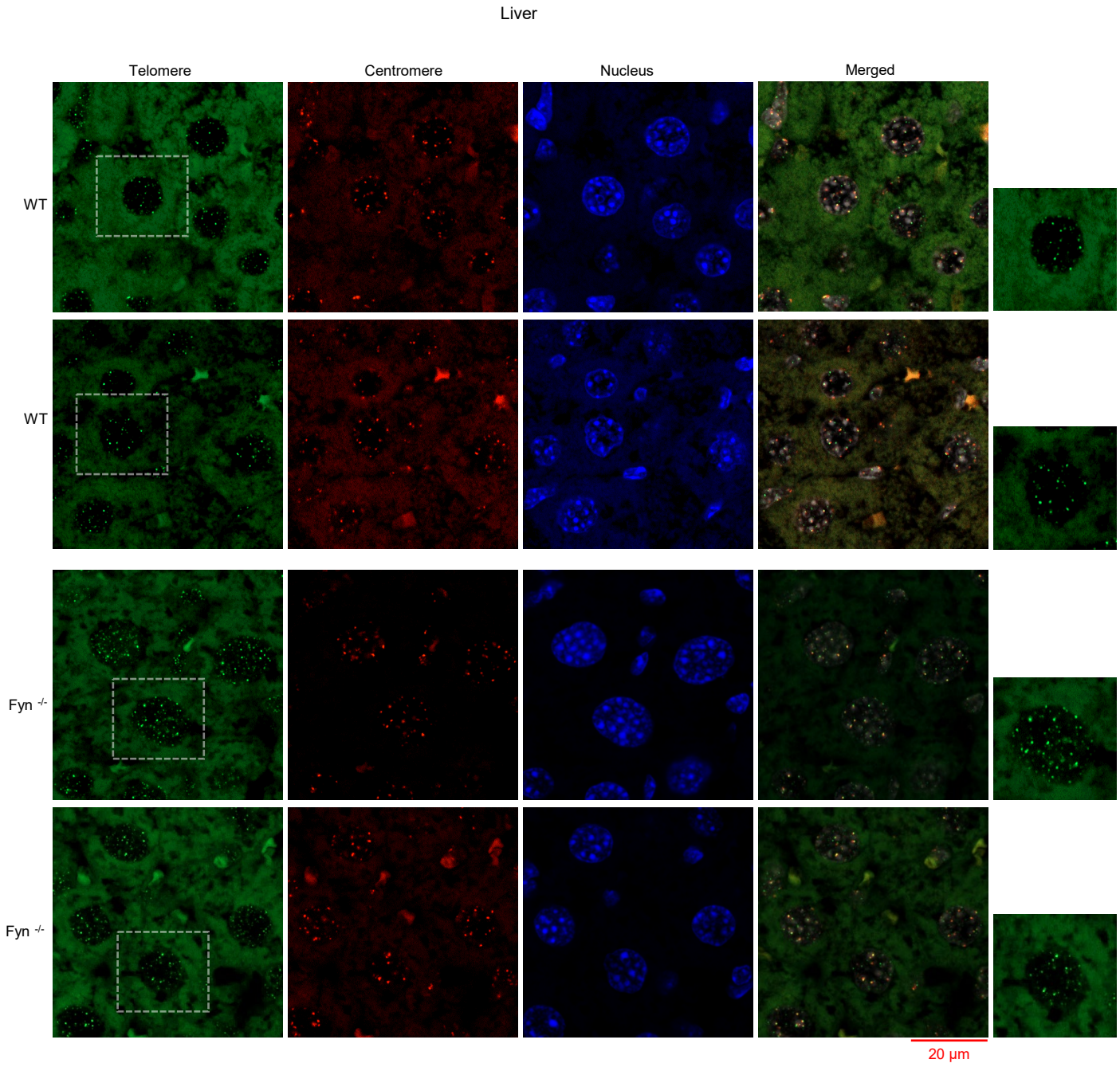
Liver
Telomere
Centromere
Nucleus
Merged
WT
WT
Fyn -/-
Fyn -/-
20 µm

Fig. EV3

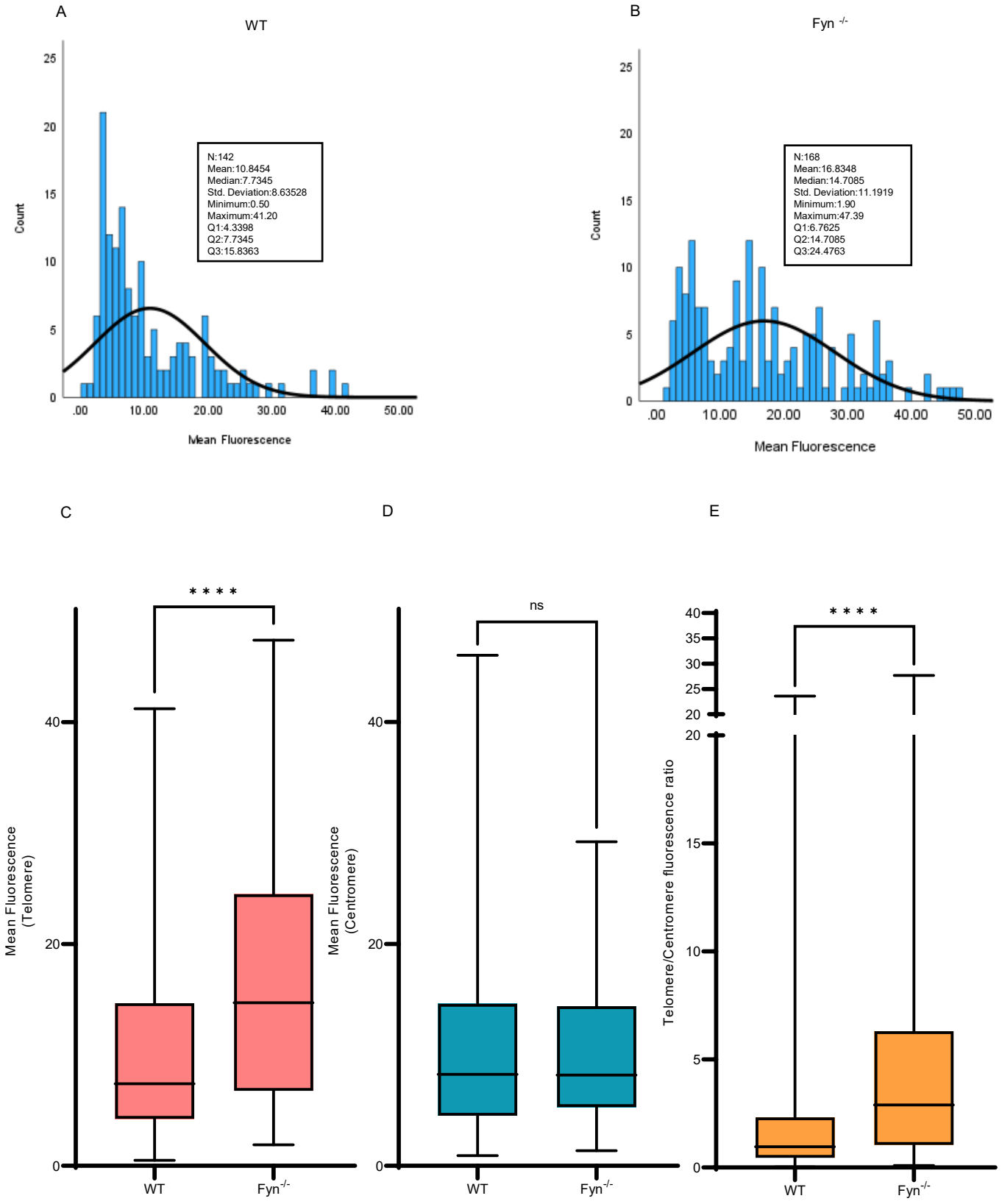
A
WT
N:142
Mean:10.8454
Median:7.7345
Std. Deviation:8.63528
Minimum:0.50
Maximum:41.20
Q1:4.3398
Q2:7.7345
Q3:15.8363
Count
Mean Fluorescence
B
Fyn -/-
N:168
Mean:16.8348
Median:14.7085
Std. Deviation:11.1919
Minimum:1.90
Maximum:47.39
Q1:6.7625
Q2:14.7085
Q3:24.4763
Count
Mean Fluorescence
C
* * * *
Mean Fluorescence (Telomere)
WT
Fyn-/-
D
ns
Mean Fluorescence (Centromere)
WT
Fyn-/-
E
* * * *
Telomere/Centromere fluorescence ratio
WT
Fyn-/-

Fig. EV4

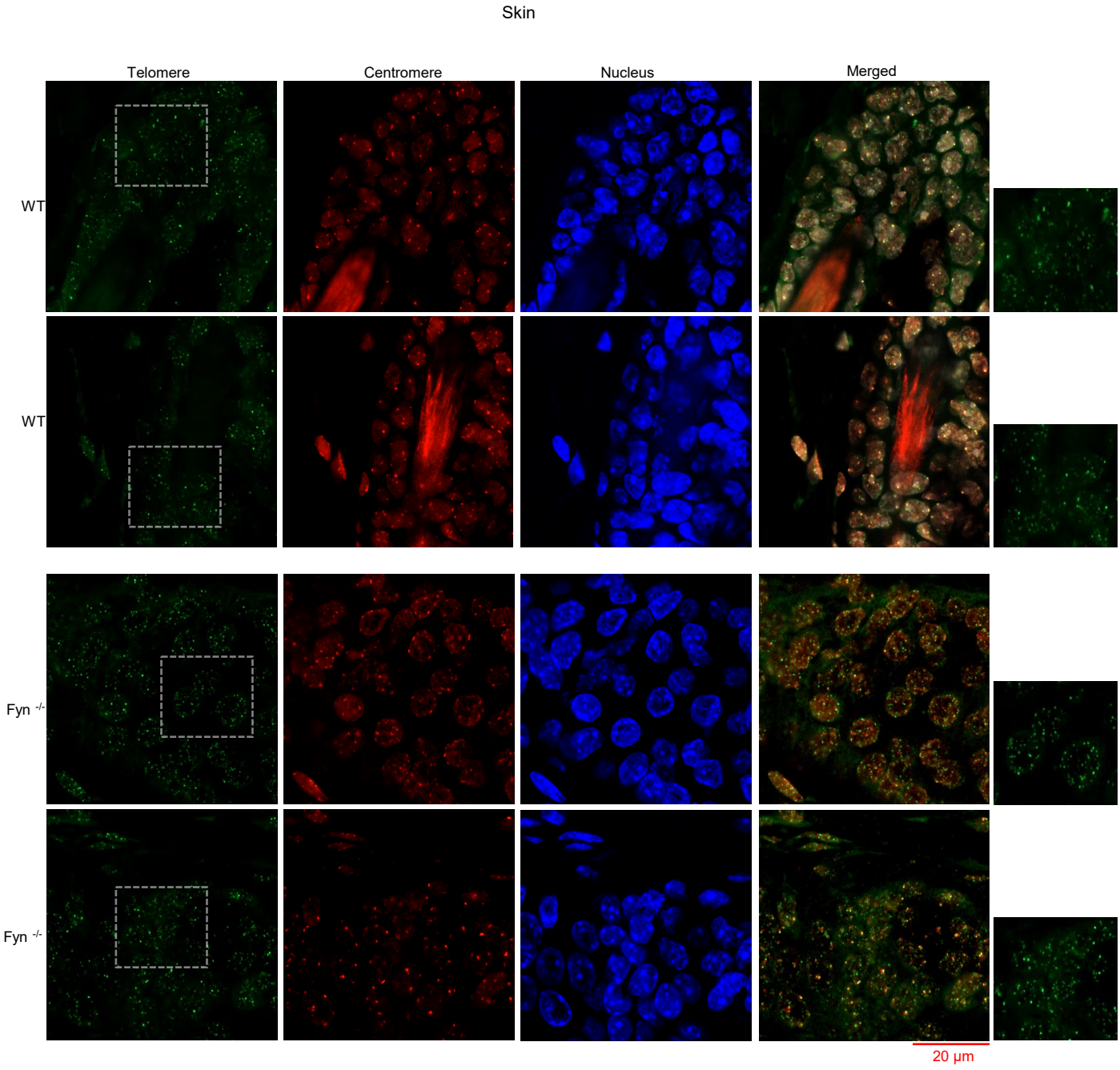

Fig. EV5

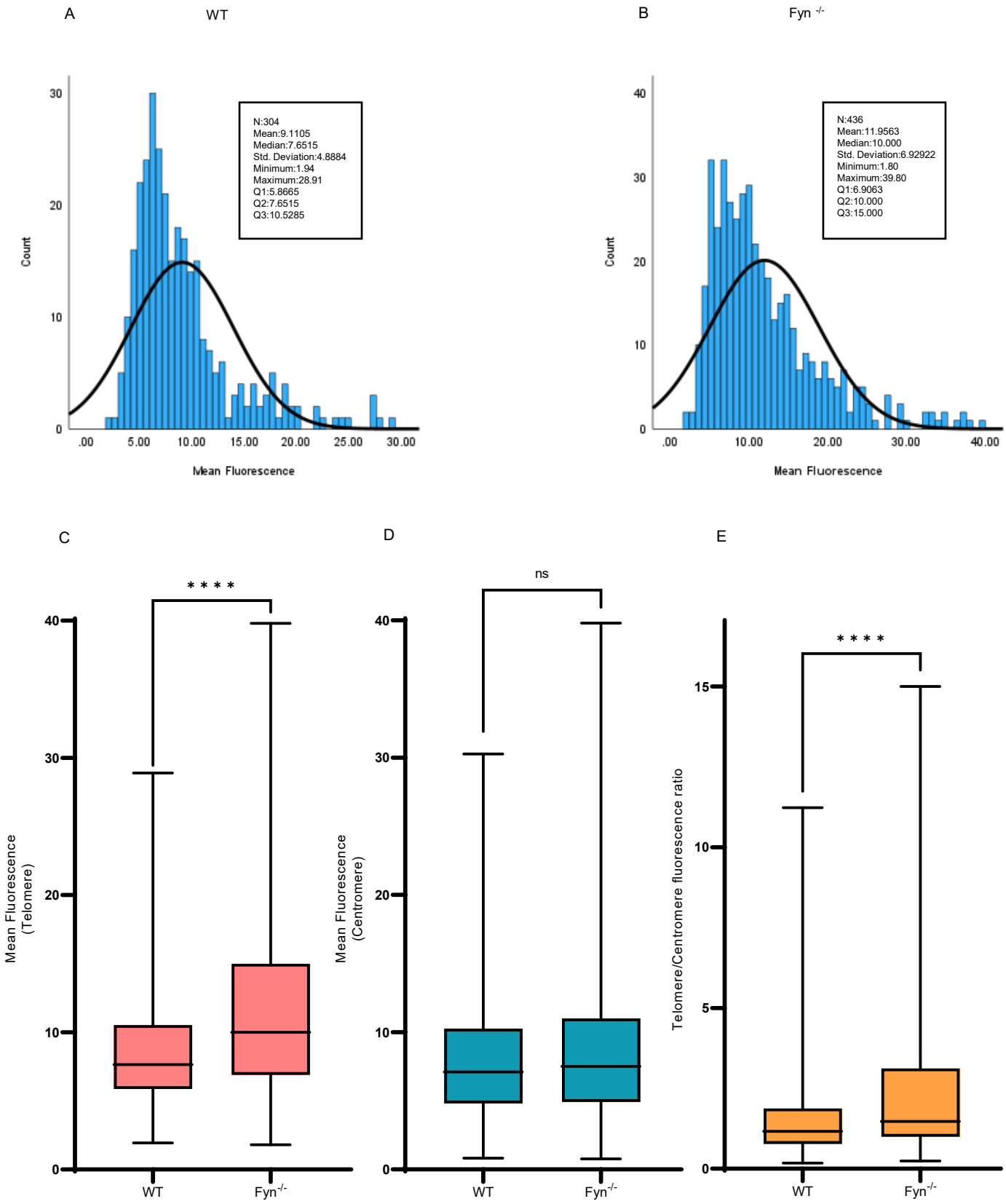
A
WT
N:304
Mean:9.1105
Median:7.6515
Std. Deviation:4.8884
Minimum:1.94
Maximum:28.91
Q1:5.8665
Q2:7.6515
Q3:10.5285
Count
Mean Fluorescence
B
Fyn -/-
N:436
Mean:11.9563
Median:10.000
Std. Deviation:6.92922
Minimum:1.80
Maximum:39.80
Q1:6.9063
Q2:10.000
Q3:15.000
Count
Mean Fluorescence
C
* * * *
Mean Fluorescence (Telomere)
WT
Fyn-/-
D
ns
Mean Fluorescence (Centromere)
WT
Fyn-/-
E
* * * *
Telomere/Centromere fluorescence ratio
WT
Fyn-/-

Fig. EV6

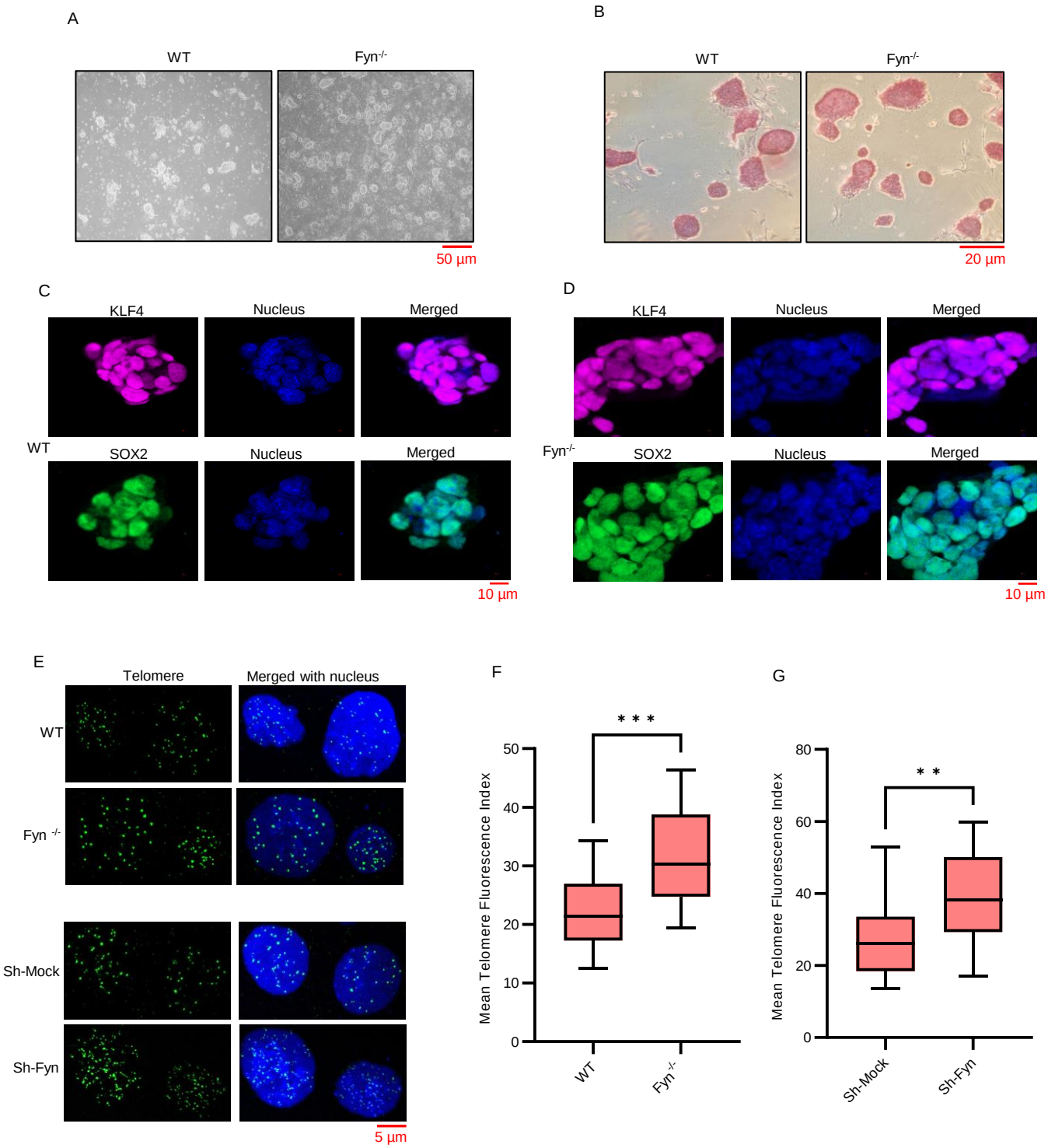
A
WT
Fyn-/-
50 μm
B
WT
Fyn-/-
20 μm
C
KLF4
Nucleus
Merged
WT
SOX2
Nucleus
Merged
10 μm
D
KLF4
Nucleus
Merged
Fyn-/-
SOX2
Nucleus
Merged
10 μm
E
Telomere
Merged with nucleus
WT
Fyn -/-
Sh-Mock
Sh-Fyn
5 μm
F
* * *
Mean Telomere Fluorescence Index
0
10
20
30
40
50
WT
Fyn -/-
G
* *
Mean Telomere Fluorescence Index
0
20
40
60
80
Sh-Mock
Sh-Fyn

Fig. EV7

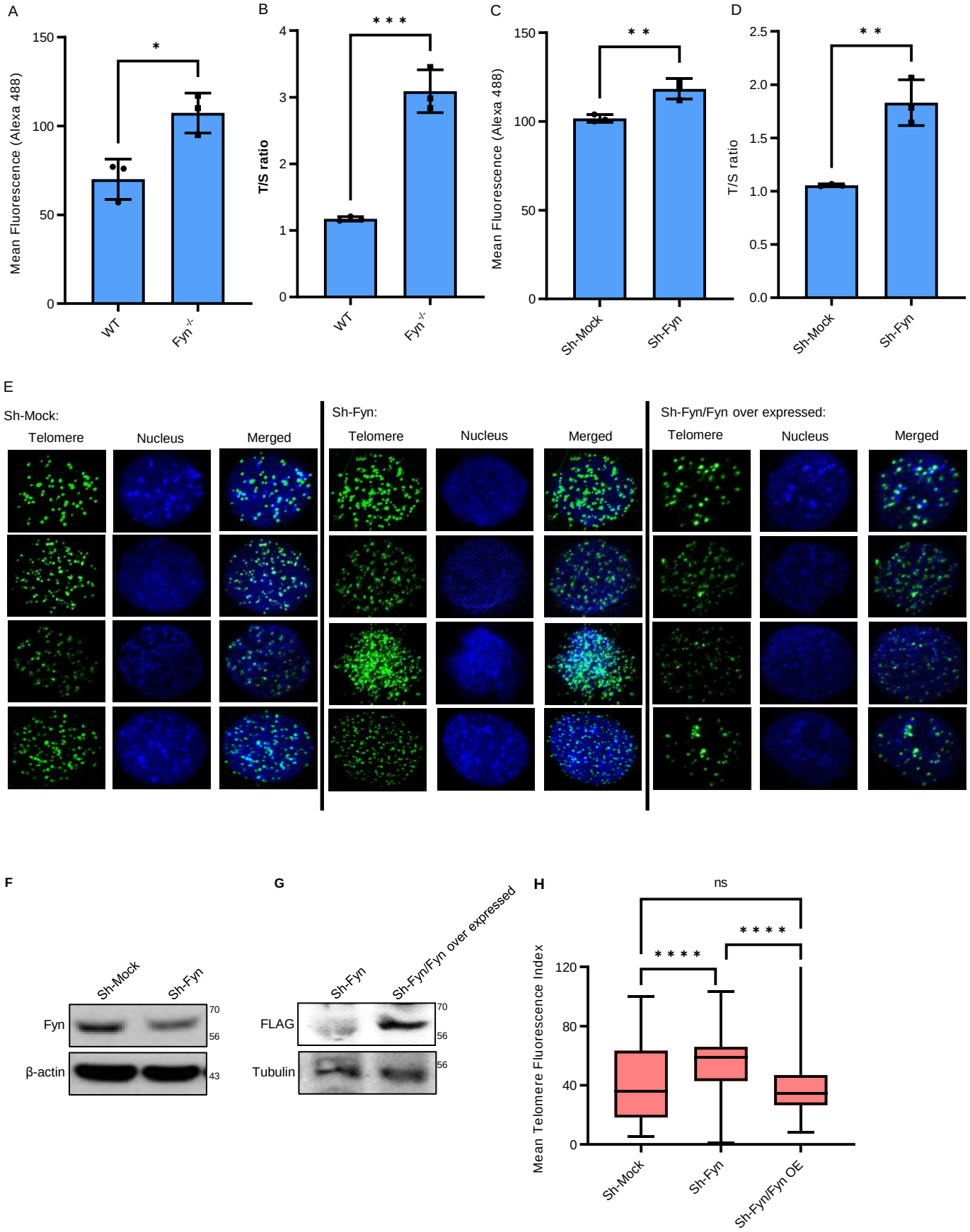
A
Mean Fluorescence (Alexa 488)
150
100
50
0
*
WT
Fyn -/-
B
T/S ratio
4
3
2
1
0
* * *
WT
Fyn -/-
C
Mean Fluorescence (Alexa 488)
150
100
50
0
* *
Sh-Mock
Sh-Fyn
D
T/S ratio
2.5
2.0
1.5
1.0
0.5
0.0
* *
Sh-Mock
Sh-Fyn
E
Sh-Mock:
Telomere
Nucleus
Merged
Sh-Fyn:
Telomere
Nucleus
Merged
Sh-Fyn/Fyn over expressed:
Telomere
Nucleus
Merged
F
Sh-Mock
Sh-Fyn
Fyn
β-actin
70
56
43
G
Sh-Fyn
Sh-Fyn/Fyn over expressed
FLAG
Tubulin
70
56
56
H
ns
* * * *
* * * *
Mean Telomere Fluorescence Index
120
80
40
0
Sh-Mock
Sh-Fyn
Sh-Fyn/Fyn OE

Fig. EV8

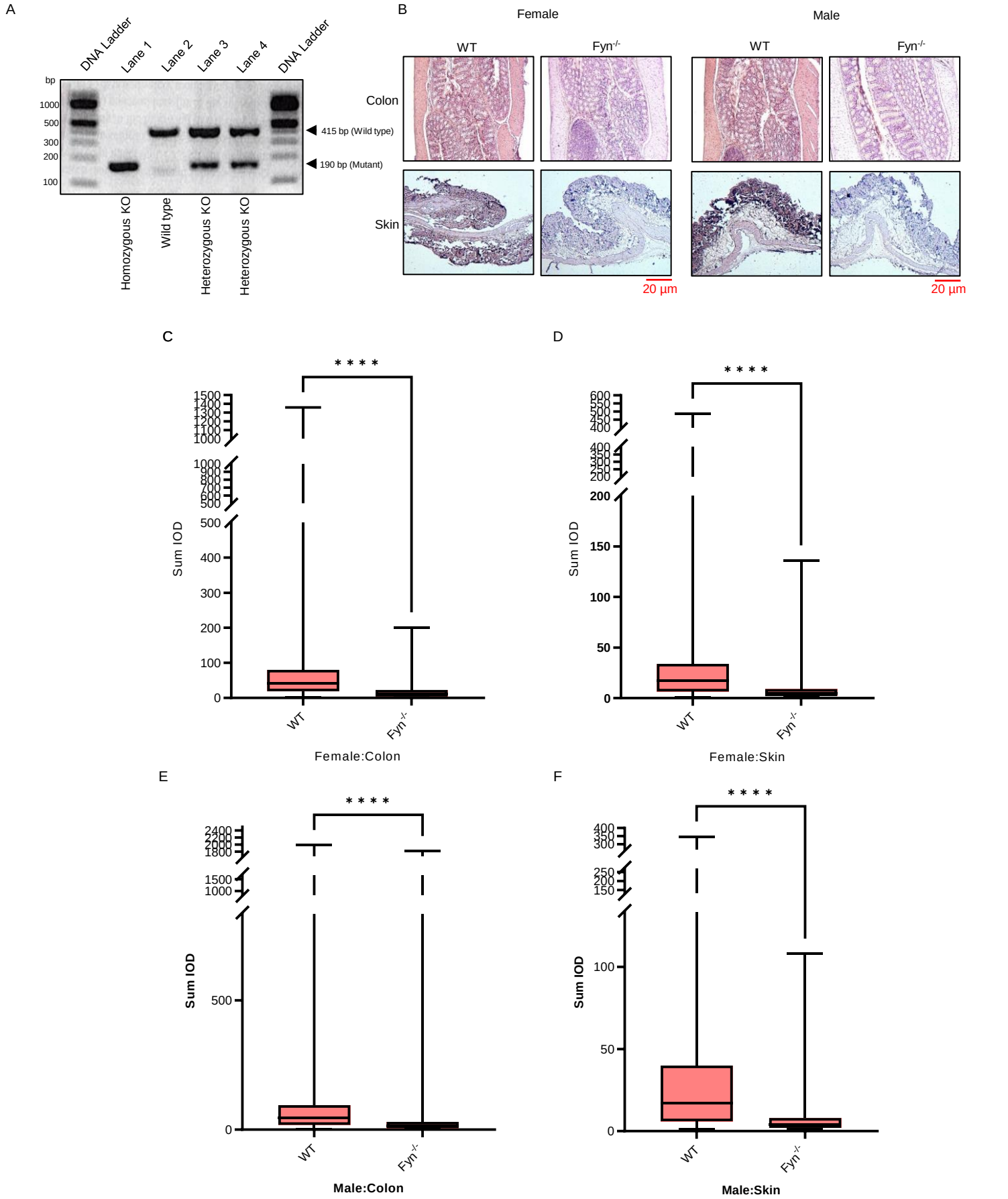
A
DNA Ladder
Lane 1
Lane 2
Lane 3
Lane 4
DNA Ladder
bp
1000
500
300
200
100
415 bp (Wild type)
190 bp (Mutant)
Homozygous KO
Wild type
Heterozygous KO
Heterozygous KO
B
Female
Male
WT
Fyn-/-
WT
Fyn-/-
Colon
Skin
20 µm
20 µm
C
D
E
F
* * * *
Sum IOD
WT
Fyn-/-
Female:Colon
Female:Skin
Male:Colon
Male:Skin

Fig. EV9

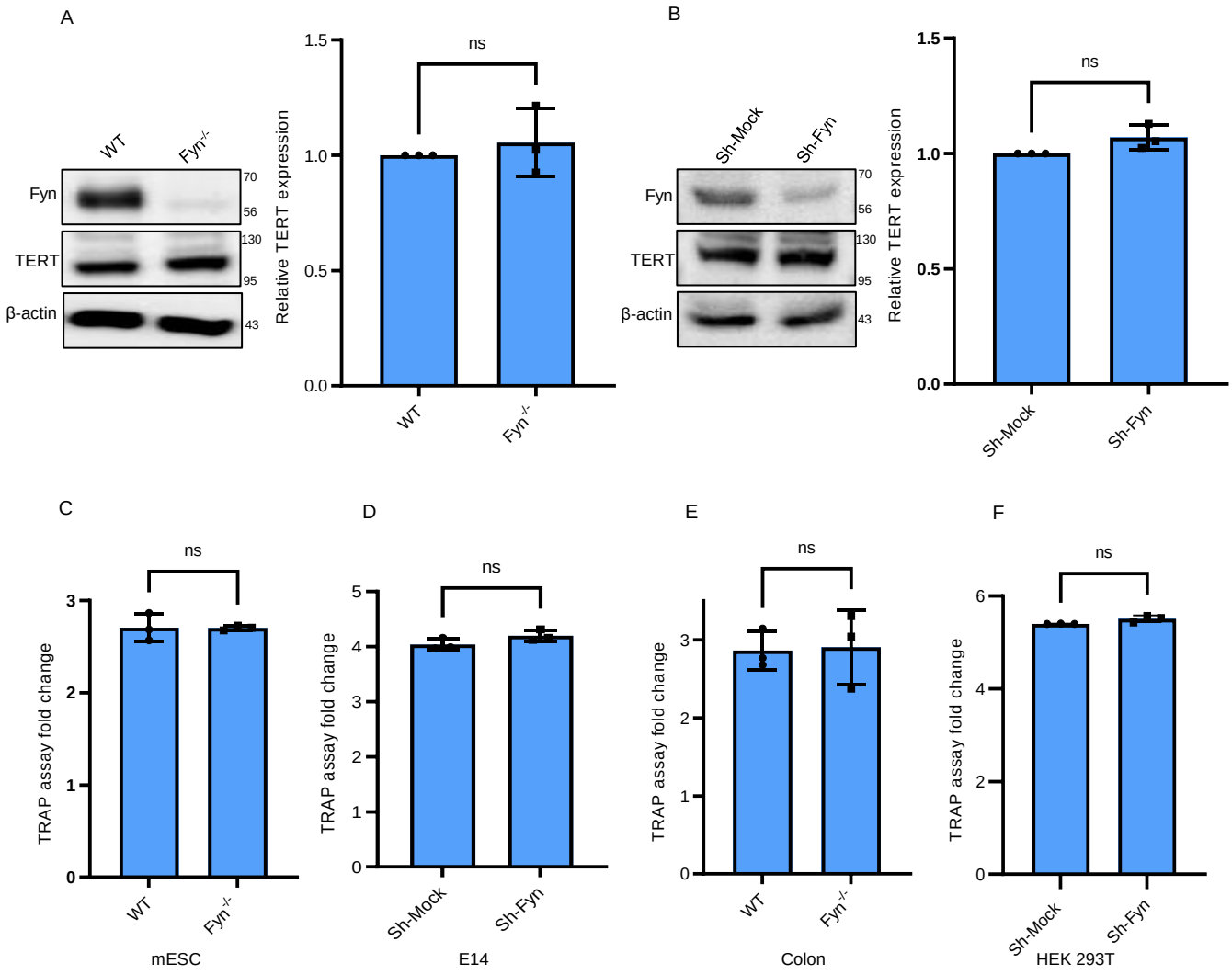
A
WT
Fyn-/-
Fyn
TERT
β-actin
70
56
130
95
43
Relative TERT expression
ns
1.5
1.0
0.5
0.0
WT
Fyn-/-
B
Sh-Mock
Sh-Fyn
Fyn
TERT
β-actin
70
56
130
95
43
Relative TERT expression
ns
1.5
1.0
0.5
0.0
Sh-Mock
Sh-Fyn
C
ns
TRAP assay fold change
3
2
1
0
WT
Fyn-/-
mESC
D
ns
TRAP assay fold change
5
4
3
2
1
0
Sh-Mock
Sh-Fyn
E14
E
ns
TRAP assay fold change
3
2
1
0
WT
Fyn-/-
Colon
F
ns
TRAP assay fold change
6
4
2
0
Sh-Mock
Sh-Fyn
HEK 293T

Fig. EV10

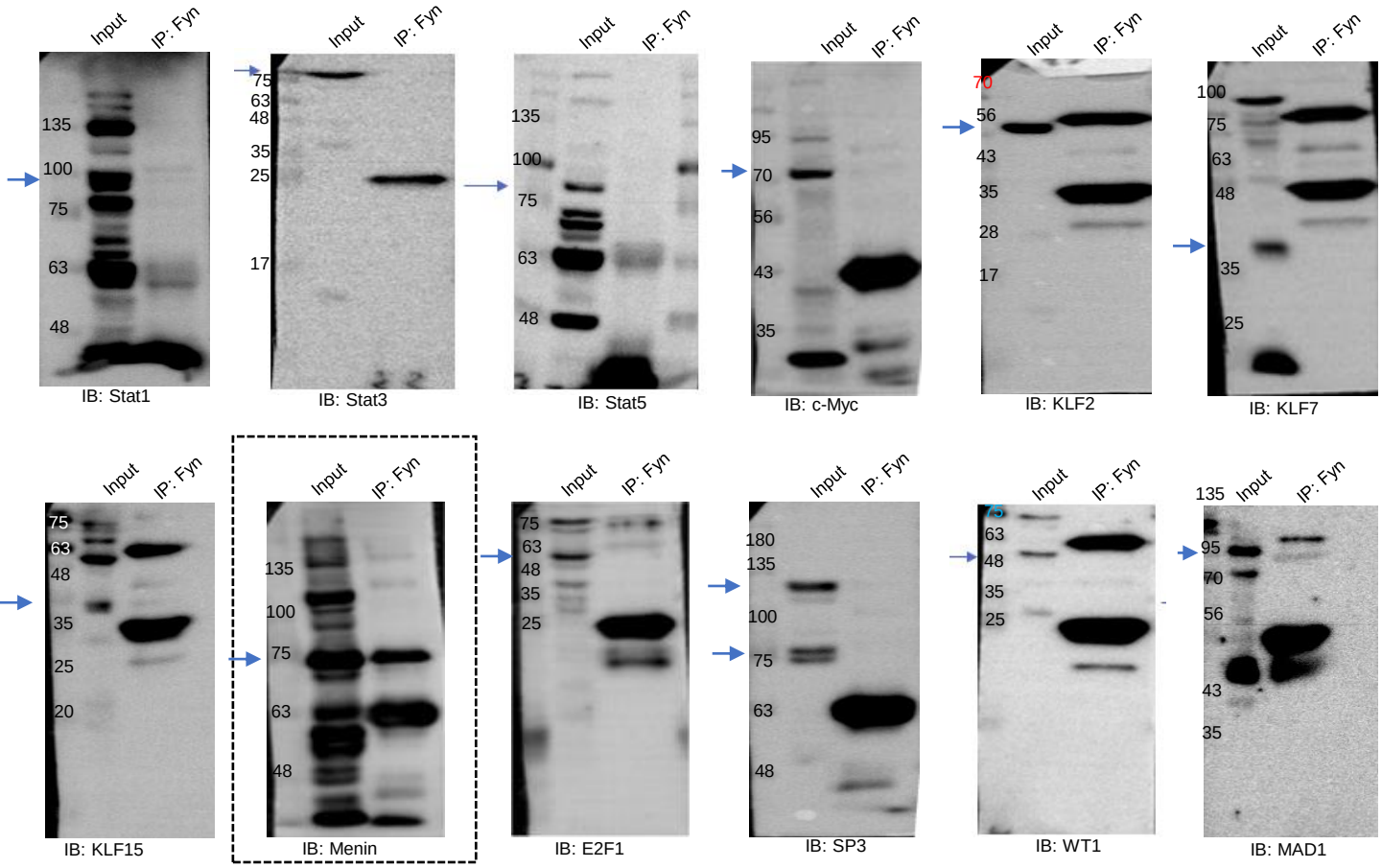
Input
IP: Fyn
135
100
75
63
48
IB: Stat1
75
63
48
35
25
17
IB: Stat3
135
100
75
63
48
IB: Stat5
95
70
56
43
35
IB: c-Myc
70
56
43
35
28
17
IB: KLF2
100
75
63
48
35
25
IB: KLF7
75
63
48
35
25
20
IB: KLF15
135
100
75
63
48
IB: Menin
75
63
48
35
25
IB: E2F1
180
135
100
75
63
48
IB: SP3
75
63
48
35
25
IB: WT1
135
95
70
56
43
35
IB: MAD1

Fig. EV11

A

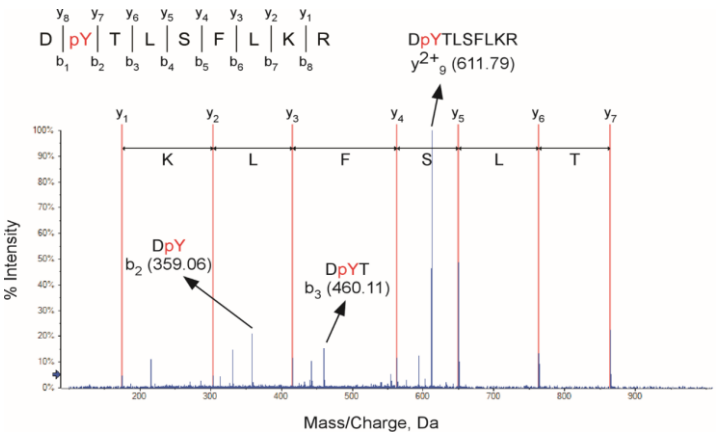

B

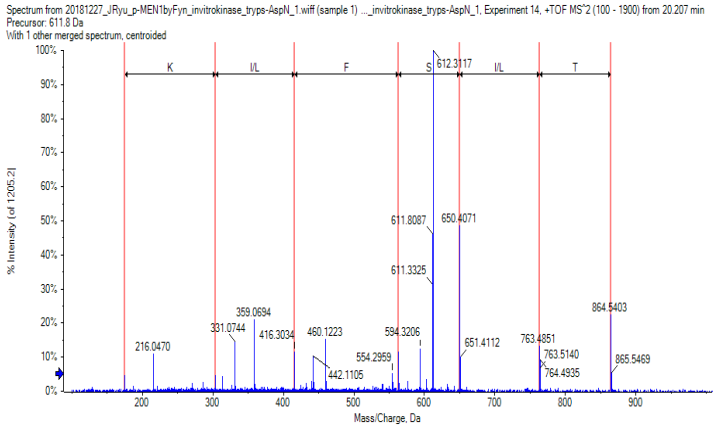

Conf.[1]	Sc[2]	Prec m/z[3]	z[4]	Sequence	Theor m/z[5]	ΔMass[6]	Site
99	12	611.7975	2	DpYTLSFLKR	611.7970	0.0009	Y603

1, the confidence for the peptide identification; 2, the score for the peptide; 3, precursor mass/charge; 4, the charge for the fragmented ion; 5, theoretical precursor mass/charge; 6, the difference between theoretical molecular weight and experimental molecular weight of the matching peptide sequence

C

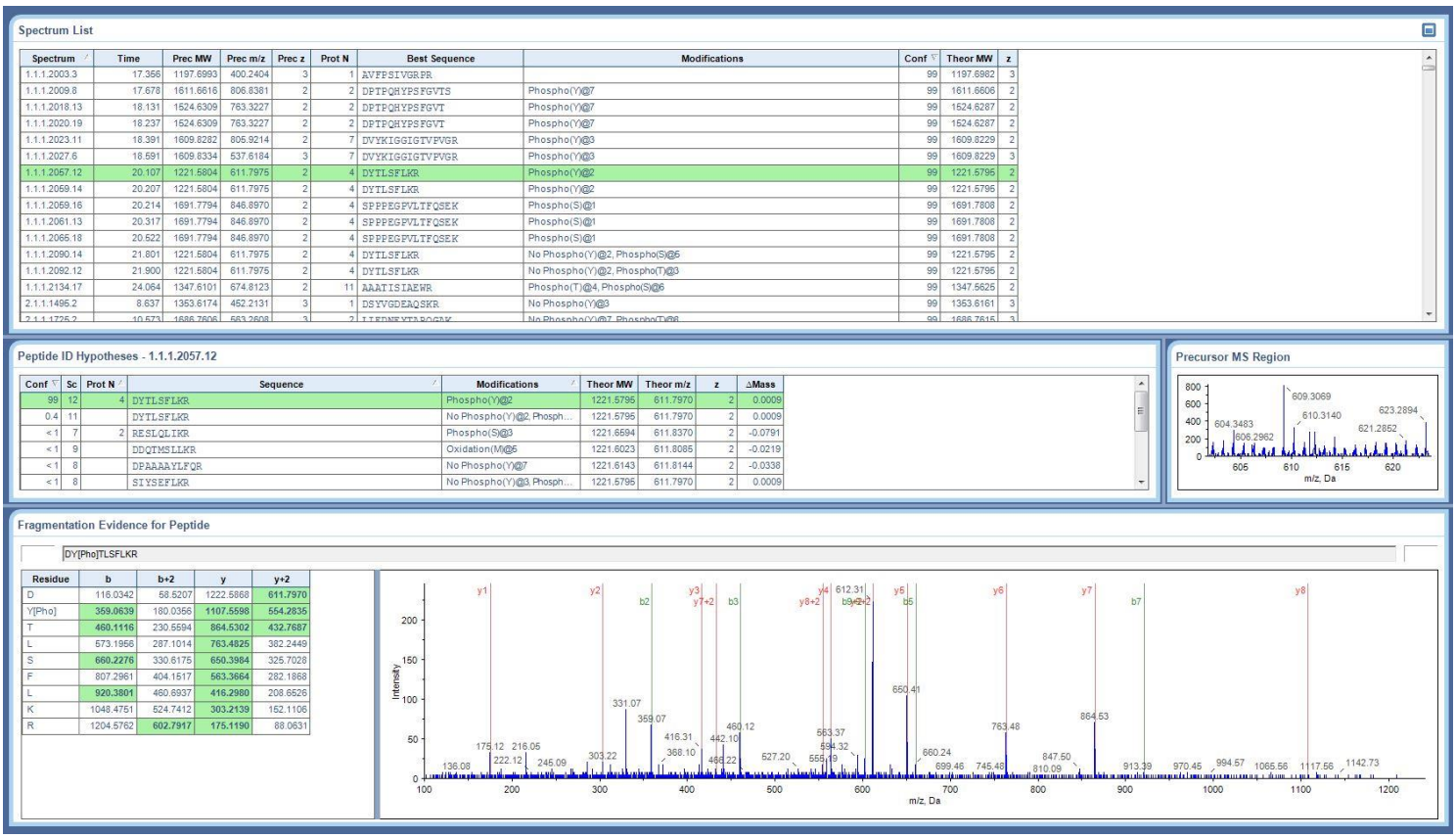

Fig. EV12

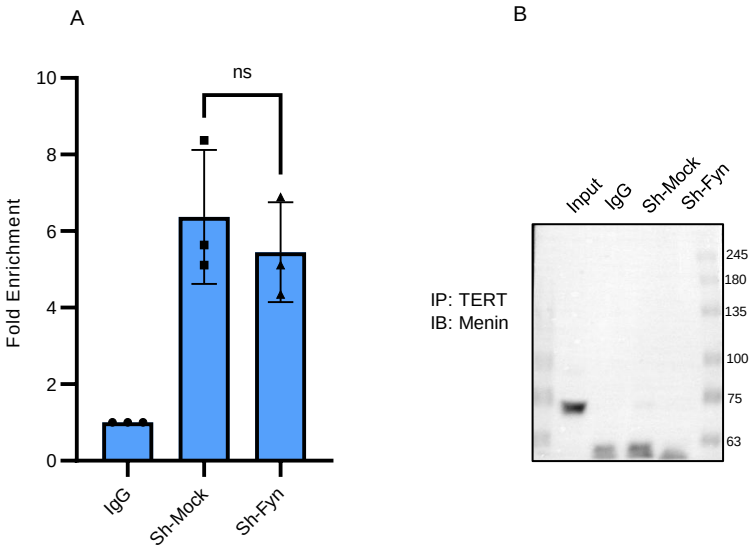
A
B
ns
Fold Enrichment
10
8
6
4
2
0
IgG
Sh-Mock
Sh-Fyn
Input
IgG
Sh-Mock
Sh-Fyn
IP: TERT
IB: Menin
245
180
135
100
75
63

Fig. EV13

A

Position	Peptide	Score	Cutoff	P-Value
156	GWSPVGTKLDSSGVA	2.919	2.592	0.26
238	SYMRCDRKMEVAFMV	2.847	2.592	0.182
427	RFYDGICKWEEGSPT	2.608	2.592	0.398
493	RGPRRESKPEEPPPP	4.31	2.592	0.053
609	DYTLSFLKRQRKGL*	2.697	2.592	0.052
613	SFLKRQRKGL*****	3.328	2.592	0.056

B

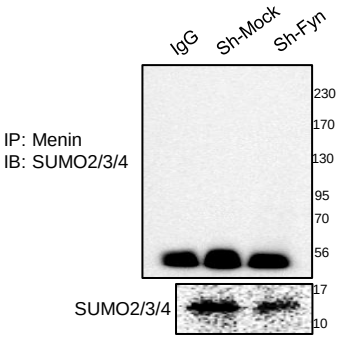

C

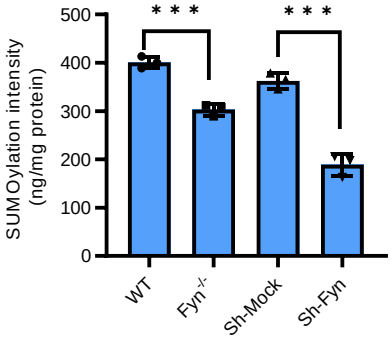

Fig. EV14

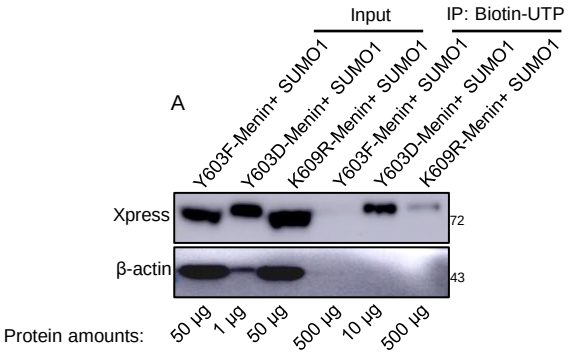
A
Input
IP: Biotin-UTP
Y603F-Menin+ SUMO1
Y603D-Menin+ SUMO1
K609R-Menin+ SUMO1
Y603F-Menin+ SUMO1
Y603D-Menin+ SUMO1
K609R-Menin+ SUMO1
Xpress
β-actin
72
43
Protein amounts:
50 µg
1 µg
50 µg
500 µg
10 µg
500 µg

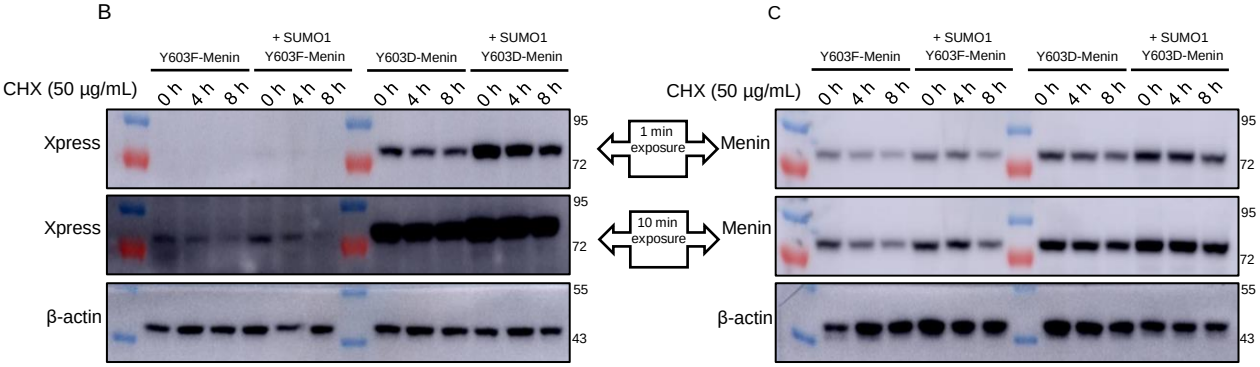
B
C
Y603F-Menin
+ SUMO1 Y603F-Menin
Y603D-Menin
+ SUMO1 Y603D-Menin
CHX (50 µg/mL)
0 h
4 h
8 h
Xpress
β-actin
Menin
1 min exposure
10 min exposure
95
72
55
43

Fig. EV15

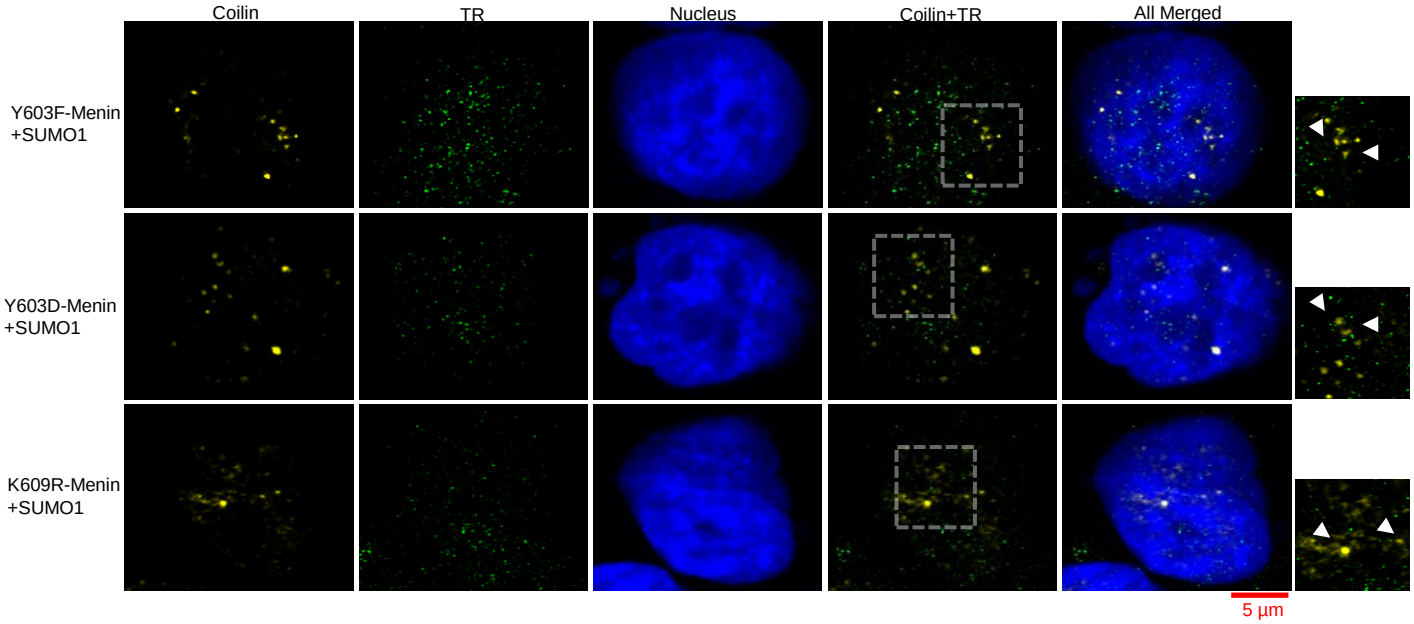
Coilin
TR
Nucleus
Coilin+TR
All Merged
Y603F-Menin
+SUMO1
Y603D-Menin
+SUMO1
K609R-Menin
+SUMO1
5 µm

Fig. EV16

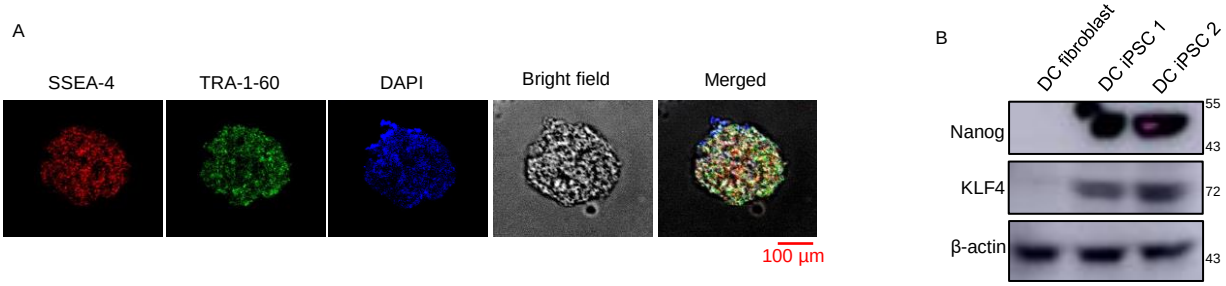
A
SSEA-4
TRA-1-60
DAPI
Bright field
Merged
100 µm
B
DC fibroblast
DC iPSC 1
DC iPSC 2
Nanog
KLF4
β-actin
55
43
72
43

Fig. EV17